

NATIONAL BUREAU OF STANDARDS  
MICROCOPY RESOLUTION TEST CHART

*Br* ①

AD-A155 471



NITROGEN DOPED SILICON

THESIS

Mary A. O'Leary  
Captain, USAF

AFIT/CE/ENG/BSA-2

DTIC FILE COPY

DTIC  
SELECTED  
JUL 03 1985

DEPARTMENT OF THE AIR FORCE  
AIR UNIVERSITY  
**AIR FORCE INSTITUTE OF TECHNOLOGY**

Wright-Patterson Air Force Base, Ohio

85 5 21 081

AFIT/GE/ENG/85M-3

ELECTRICAL PROPERTIES OF BULK GROWN  
NITROGEN DOPED SILICON

THESIS

Mary A. O'Leary  
Captain USAF

AFIT/GE/ENG/85M-3

Accession For	
NTIS GRA&I	<input checked="" type="checkbox"/>
DTIC TAB	<input type="checkbox"/>
Unannounced	<input type="checkbox"/>
Justification	
By _____	
Distribution/	
Availability Codes	
Dist	Avail and/or Special
A/1	

DTIC  
S  
JUN 2 1985  
D

G

AFIT/GE/ENG/85M-3

AFIT/GE/ENG/85M-3

ELECTRICAL PROPERTIES OF BULK GROWN  
NITROGEN DOPED SILICON

THESIS

Presented to the Faculty of the School of Engineering  
of the Air Force Institute of Technology  
Air University

In Partial Fulfillment of the  
Requirements for the Degree of  
Master of Science in Electrical Engineering

Mary A. O'Leary, B.S.E.E.  
Captain, USAF

March 1985

Approved for public release; distribution unlimited

## Preface

The idea that nitrogen doping strengthens a silicon lattice is intriguing in light of the continuous search for better semiconductor materials. A review of the literature showed that strengthening effect of nitrogen has been studied, but the electrical parameters had not. This work is an effort to fill that gap.

Dr. W. C. Mitchel of the Materials Laboratory (AFWAL) proposed this project. He supplied the material and provided the Hall effect system on which the experiments were performed. I am grateful for his suggestions on how to proceed with the experiments and his advice in analyzing the data. I would like to thank Lynnette Brown who gave me much needed help with the day to day operation of the equipment.

I would like to thank CAPT D. Kitchen, my advisor, for his guidance and encouragement and also MAJ W. Sutton, my reader, for his suggestions in editing this work.

Finally, I express my gratitude to my husband, Michael, for his patience and help in putting together the final.

Mary A. O'Leary

## Table of Contents

	Page
Preface.....	ii
List of Figures.....	v
List of Tables.....	viii
Abstract.....	ix
I. Introduction.....	1
Approach.....	5
Experiments Performed.....	6
Results.....	8
Organization of Thesis Chapters.....	8
II. Background.....	10
Lattice Defects.....	10
Single Crystal Manufacturing.....	16
Controlling Defects.....	20
Previous Nitrogen Studies.....	23
III. The Hall Effect.....	29
The Hall Effect.....	29
The Curve Fitting Function to Determine Carrier Concentration and Activation Energy.....	33
Computer Generated Curve Fitting.....	37
IV. Experimental Procedure.....	40
Sample Geometry and Configuration.....	40
Hall Effect Systems.....	43
Sample Preparation.....	49
V. Results.....	52
Electrical Data at 300 K.....	52
Comparison of Electrical Data from 20 to 380 K.....	58
Temperature Dependence of $R_1/R_2$ .....	78
Curve Fitting of Experimental Data.....	93
VI. Analysis.....	104
VII. Conclusions and Recommendations.....	109
Findings.....	109
Recommendations.....	112

Appendix A: Hall Effect Experiment with Bulk  
Grown Nitrogen Doped Silicon Ion  
Implant with Gallium.....114

Appendix B: Graphs of Experiments FZ0004-A and FZ0005..118

Bibliography.....124

Vita.....128



## List of Figures

Figure	Title	Page
1.	Effects of Nitrogen on Dislocation Nucleation and Movement in Silicon.....	4
2.	Minority Carrier Lifetime Distribution.....	12
3.	Schematic Illustration of Point Defects.....	14
4.	Edge Dislocation.....	14
5.	Screw Dislocation.....	15
6.	Stacking Fault.....	15
7.	Schematic of Czochralski Puller Method.....	17
8.	Axial Distribution of Oxygen in Three Cz Processes..	18
9.	Resistivity and Oxygen Concentration Distribution...	18
10.	Schematic of Float Process.....	19
11.	Float Zone with Needle-Eye Coil.....	19
12.	Denuded Zone in the Cross Section of a Wafer.....	20
13.	Warpage Due to Stress Cycles at 1050 °C.....	22
14.	The Hall Effect.....	29
15.	Phosphorus Doped CZ Silicon Annealed at 900 °C.....	36
16.	Van der Pauw Configurations for Hall Measurements...	42
17.	Schematic Diagram of Guarded Hall System.....	45
18.	Schematic Diagram of Hall Effect System.....	46
19.	Schematic Diagram of Sample Probe.....	48
20.	Resistivity versus Impurity Concentration for Silicon at 300 K.....	56
21.	Drift Mobility versus Impurity Concentration at 300 K.....	56

22. Hall Coefficient of Three Si:N Samples versus Inverse Temperature.....	59
23. Resistivity of Three Si:N Samples versus Inverse Temperature.....	60
24. Carrier Concentration of Three Si:N Samples versus Inverse Temperature.....	61
25. Hall Mobility of Three Si:N Samples versus Inverse Temperature.....	62
26. Hall Mobility of Three Si:N Samples versus Temperature.....	63
27. Hall Coefficient of CZ and Si:N Samples Annealed at 900 °C.....	66
28. Resistivity of CZ and Si:N Samples Annealed at 900 °C.....	67
29. Carrier Concentration of CZ and Si:N Samples Annealed at 900 °C.....	68
30. Hall Mobility of CZ and Si:N Samples Annealed at 900 °C versus Inverse Temperature.....	69
31. Hall Mobility of CZ and Si:N Samples Annealed at 900 °C versus Temperature.....	70
32. Hall Coefficient of Si:N NTD and High Purity FZ NTD Samples.....	73
33. Resistivity of Si:N NTD and High Purity FZ NTD Samples.....	74
34. Carrier Concentration of Si:N NTD and High Purity FZ NTD Samples.....	75
35. Hall Mobility of Si:N NTD and High Purity FZ NTD Samples versus Inverse Temperature.....	76
36. Hall Mobility of Si:N NTD and High Purity FZ NTD Samples versus Temperature.....	77
37. $R_1/R_2$ Ratio of CZ-AN-001.....	79
38. Hall Coefficient of CZ-AN-001 from 20 - 380 K.....	80
39. Resistivity of CZ-AN-001 from 20 - 380 K.....	81
40. Carrier Concentration of CZ-AN-001 from 20 - 380 K...	82
41. $R_1/R_2$ Ratio of Si:N Sample Annealed at 800 °C.....	84

42. $R_1/R_2$ Ratio of Si:N Sample Annealed at 830 °C.....	85
43. $R_1/R_2$ Ratio of Unannealed Si:N Sample.....	86
44. $R_1/R_2$ Ratio of Si:N Sample Annealed at 800 °C (SI-N800C).....	87
45. $R_1/R_2$ Ratio of Si:N Sample Annealed at 900 °C.....	89
46. $R_1/R_2$ Ratio of High Purity FZ NTD Sample.....	90
47. $R_1/R_2$ Ratio of Si:N NTD Sample (FZ0002).....	91
48. $R_1/R_2$ Ratio of Si:N NTD Sample (FZ0003).....	92
49. Least Squares Fit of Carrier Concentration of High Purity FZ NTD Samples.....	95
50. Least Squares Fit of Carrier Concentration of Si:N NTD Sample (FZ0002).....	96
51. Least Squares Fit of Carrier Concentration of Si:N NTD Sample (FZ0003).....	97
52. Two Level Least Squares Fit of Carrier Concentration of Unannealed Si:N Sample.....	99
53. One Level Least Squares Fit of Carrier Concentration of Si:N Annealed at 900 °C.....	101
54. Three Level Least Squares Fit of Carrier Concentration of Si:N Annealed at 900 °C.....	102
55. Photoluminescence Plot of Si:N.....	106
56. Schematic of the Hall Effect System Modified for an Ion Implanted Sample.....	116
57. Hall Coefficient of FZ0004-A and FZ0005 versus Inverse Temperature.....	119
58. Resistivity of FZ0004-A and FZ0005 versus Inverse Temperature.....	120
59. Carrier Concentration of FZ0004-A and FZ0005 verses Inverse Temperature.....	121
60. Hall Mobility of FZ0004-A and FZ0005 versus Inverse Temperature.....	122
61. Hall Mobility of FZ0004-A and FZ0005 versus Temperature.....	123

List of Tables

Table	Page
I. Comparison of Activation Energies and Techniques Used.....	28
II. List of Samples on Which Experiments Were Performed.....	53
III. Electrical Parameters at 300 K.....	54
IV. Comparison of Experimental Data with Values from Figures 20 and 21.....	57
V. Results of Curve Fitting NTD Samples.....	98

## Abstract

The electrical parameters of a boule of nitrogen doped float zone silicon were studied by Hall effect analysis. Samples were annealed at temperatures ranging from 800 to 900 °C. In addition, a section of this boule was neutron transmuted (NTD) to increase the n-type doping. Samples from the NTD section were annealed at 800 °C.

Resistivity and mobility varied considerably from sample to sample, but the variation is not a function of annealing temperature. The annealed Si:N samples were found to be inhomogeneous; however, the Si:N NTD samples were homogeneous. In addition, annealing activated deep energy levels. The shallow energy levels reported in studies on ion implanted nitrogen in silicon were not found. The only shallow energy level found was phosphorus.

The conclusion is nitrogen does not go into substitutional sites in silicon to any great extent. Although what happens to nitrogen in silicon is unknown it is suggested that nitrogen may form silicon-nitride complexes and precipitates. This could be the mechanism for strengthening the lattice.

# ELECTRICAL PROPERTIES OF BULK GROWN NITROGEN DOPED SILICON

## I. Introduction

Single crystal silicon is by far the most widely used semiconductor material in the world today. The dominance of silicon over other materials is mostly due to its material properties but probably equally important is the fact that high quality single crystal silicon is cheaper and easier to grow than any other semiconductor material. As the demand for higher device density and faster performance increases, manufacturers are pushed to produce silicon with fewer lattice defects. The control of defects in a semiconductor substrate is important since defects directly effect device characteristics and can cause device failure. If device manufacturers could make their product as small as they liked without regard to the limits of lithography and other processes:

..... localized defect clusters in an otherwise well controlled silicon wafer may well become the limiting factor for improved device/circuit performance and product yield. This may especially be the case for VLSI circuitry as the probability of a defect occurring within a die increases as the die size increases (for constant defect density) while concurrently, the probability of a defect resulting in the occurrence of a

circuit malfunction increases as the minimum lithographic dimension decreases (16:90).

Lithographic techniques are improving, making smaller geometries possible. However, a clear, sharp image relies on a flat surface. "Today's technology produces a flatness of less than 6 microns; however, flatness as low as 2 microns or less will be required by 1985, and less than 1 micron by 1990" (35:101). Many device processing steps require high temperatures (up to 1200 °C) which can result in wafer warpage due to residual lattice strain.

Furthermore, in order to maximize charge carrier mobility, which is the parameter that ultimately limits device speed, the crystal lattice must be as defect free as possible. That is, the crystal needs to be free of unwanted impurity atoms and other irregularities which disrupt the periodicity of the lattice, such as dislocation defects. The dilemma facing very large scale integrated circuit (VLSI) and very high speed integrated circuit (VHSIC) device manufacturers is that high purity, dislocation free silicon warps badly during device processing at elevated temperatures. It has recently been discovered that the oxygen that contaminates electronic grade commercial silicon is responsible for strengthening the wafers (30:L51). Oxygen contamination is a consequence of the Czochralski (CZ) method of growing a single silicon crystal. Ninety percent of the silicon substrates in use today are manufactured by the CZ method. The other ten

percent of the single crystal silicon is manufactured by the float zone (FZ) method, usually for applications requiring high purity silicon. Typically, FZ silicon has 1000 times less oxygen than CZ silicon. FZ grown silicon has been rejected as a substrate for nearly all scales of integration because of its poor resistance to warping during processing. Although the oxygen has the beneficial effect of strengthening the wafer by pinning the dislocation faults, it is at the expense of creating stacking faults and decreasing carrier mobilities.

In response to this, new ideas are being explored to either control or exploit crystal defects. The intrinsic gettering approach exploits the oxygen in CZ silicon by precipitating this element onto defects in the bulk of the wafer. This leaves a defect free zone on the surface for device processing. The intrinsic gettering process adds extra processing steps to device fabrication. It is a complex process requiring several high temperature cycles, and results in a wafer with altered characteristics (10). In addition to this, oxygen is difficult to control during crystal growth (11).

In 1981 a group of Japanese researchers doped a boule of FZ grown silicon with nitrogen. They reported that this material had fewer dislocations defects than ordinary FZ silicon and slightly less than CZ silicon after two heat treatments (1:63). A reproduction of the X-ray topographs of the wafers is shown in Figure 1.







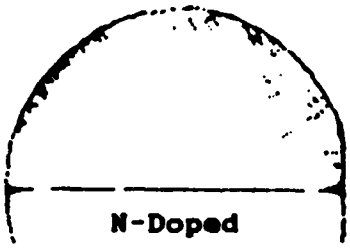
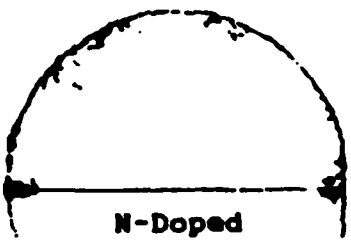
	1st Heat Treatment	2nd Heat Treatment
CZ		
FZ		
FZ	 N-Doped	 N-Doped

Figure 1. Effect of Nitrogen on Dislocation Nucleation and Movement in Silicon (1:71)

The nitrogen concentration of the boule was  $1.5 \times 10^{15} \text{ cm}^{-3}$ . This is 1000 times less than the oxygen doped CZ wafer at  $1.7 \times 10^{18} \text{ cm}^{-3}$ . The conversion efficiency of donors by nitrogen is 2 to 5%, thus nitrogen is essentially electrically inert. This suggests that the carrier mobilities could be higher than CZ silicon and that nitrogen doped wafers will survive thermal processing. Nitrogen doped silicon (Si:N) would then be suitable for VLSI and VHSIC applications.

#### Approach

While the mechanical properties of FZ Si:N have been reported in the literature, the electrical properties have not. Matsato Imai and Koji Sumino reported in their X-ray topographic studies of dislocation mobility in silicon that

"Nitrogen atoms are concluded to have a strong immobilization effect for dislocations in silicon crystal since the cessation of motion occurs at a concentration as low as  $5.4 \times 10^{15} \text{ cm}^{-3}$  (13:619)."

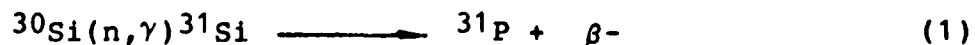
Photoluminescence (PL) studies have been undertaken by various other groups (38,39,40). These studies have produced data about the activation energy of nitrogen in silicon, deep level trap states, and the conversion efficiency, that is, the ratio of electrically active nitrogen to the total concentration of nitrogen in the material. The electrical parameters of ion implanted nitrogen in p-type silicon have been studied. Unfortunately, there are disagreements as to what the

activation energy is, what the deep level activation energy is, and whether the shallow level is caused by substitutional nitrogen or silicon nitride complexes.

In this study, the electrical parameters of bulk grown Si:N were studied using the Hall Effect technique. This technique is frequently used to characterize semiconductor materials. The Hall Effect technique gives a wealth of data about the material being studied. Resistivity, carrier concentration, and carrier mobility are determined from room temperature data. If the experiment is performed over a wide range of temperatures, such as liquid helium temperature (4 Kelvin) to room temperature (approximately 300 Kelvin), the activation energy levels and doping concentration can be determined.

#### Experiments Performed

Samples of Si:N were annealed at various temperatures from 800 to 900 °C and compared an unannealed sample and a CZ sample annealed at 900 °C. In addition, a two inch chunk of Si:N was sent to the University of Missouri Nuclear Reactor for neutron transmutation doping (NTD). This technique increased the n-type doping of the Si:N material by the nuclear reaction (22:1):



where n = neutron  
γ = gamma  
β- = beta

"....and the fact that the  ${}^{30}\text{Si}$  isotope, with an

abundance of 3.1%, is uniformly distributed throughout the crystal lattice (17:139)".

The data from the NTD Si:N was compared to the data from a previous experiment performed by W.C. Mitchel of AFWAL/MLPO on a high purity FZ sample that was also neutron transmuted (23).

The Hall effect experiments were performed at the Materials Laboratory (AFWAL) on the Hall effect systems owned by the Laser and Optical Materials Branch. The resulting data was analyzed by a computer program written specifically for use with the Hall experiment. The program resides on the Prime computer at the Materials Laboratory.

The Hall Effect experiments only give mobility data on the majority carrier. Because nitrogen is a donor in silicon, the mobilities obtained were for electrons only. In order to study the mobility of holes the material would have to be p-type. It is possible to ion implant n-type substrate with a p-type ion. By reverse biasing the pn-junction formed by the p-type ion implanted layer and the n-type substrate, the p-type layer is electrically isolated from the substrate so that the Hall effect experiment can be performed. However, in order to study an ion implanted layer, the system has to be modified to include an extra power supply and ammeter. A detailed discussion of this is provided in Appendix A.

## Results

The results of the Hall experiments on these samples of Si:N showed that the material is not homogeneous. The electrical parameters varied widely from sample to sample. The electrical parameters do not appear to change as a function of the annealing temperature. Although, annealing does activate deep energy levels in the material. In addition, annealing can cause a reasonably homogeneous sample to become inhomogeneous. The NTD Si:N samples were dominated by the phosphorus doping. Annealing did not result in inhomogeneity. The energy levels reported in the previously published PL studies were not found in these experiments. A PL study of samples from the same boule of Si:N used in the Hall experiments did confirm the presence of nitrogen (6).

This series of experiments showed that the electrical properties of Si:N are not consistent due to the inhomogeneous nature of the material. Thus, without further study on how to overcome this problem Si:N cannot be recommended as a VLSI or VHSIC substrate.

## Organization of Thesis Chapters

In order to understand how these conclusions were reached the remaining chapters give an overview of silicon and current issues in manufacturing an explanation of the Hall experiment, and a detailed discussion of the results. Specifically Chapter II has a discussion on the silicon

crystal lattice and defects, methods of manufacturing, and previous work on nitrogen in silicon. Chapter III explains the Hall effect, how the electrical parameters are derived from the experimental data, and an explanation of the computer analysis of the data. Chapter IV describes the experimental procedure and the Hall effect system. The results of the experiments are given in Chapter V, while Chapter VI gives an analysis of the results. Chapter VII, the last chapter, gives the conclusions and recommendations.

## II. Background

Since crystal defects affect device performance, the various types of defects and how they occur need to be explained. Certain defects occur when the crystal is grown, others occur during device processing. The various types of defects will be described first, then the methods of manufacturing single crystal silicon. With this background the implications of intrinsic gettering and nitrogen doped FZ Si can be understood. From this, previous work on the effect of nitrogen in silicon is more easily explained.

### Lattice Defects

Solid state semiconductor theory is based on taking advantage of defects in a lattice. Doping atoms, such as phosphorus or boron, add extra charge carriers to the material. Phosphorus adds extra electrons (negative charge carriers), while boron atoms create a deficiency of electrons, called holes (positively charge carriers). When a material is doped to have excess negative carriers (n-doped) the electrons are referred to as majority carriers while the holes are minority carriers. For p-doped material (excess holes) the holes are the majority carriers while the electrons are the minority carriers. The electrical characteristics of devices are described by

the behavior of the carriers. The flow of the charged carriers through the material is an electrical current. When an electron recombines with a hole, the current decreases. Unfortunately, unintentional impurities, such as oxygen, and lattice deformations provide extra generation/recombination sites. Since they are unwanted they are called a traps. Traps reduce minority carrier lifetime and diffusion length. The equations governing minority carrier lifetime and diffusion length are (8:124,134):

$$t_m = 1/(s \times v_{th} \times N_t) \quad (\text{seconds}) \quad (2)$$

$$L_m = (D \times t_m)^{-1/2} \quad (\text{cm}) \quad (3)$$

where

- $t_m$  = minority carrier lifetime (sec)
- $v_{th}$  = thermal velocity =  $(3KT/M)^{1/2}$  (cm/sec)
- $s$  = effective trap cross section ( $\text{cm}^2$ )
- $N_t$  = concentration of traps ( $\text{cm}^{-3}$ )
- $L_m$  = diffusion length of minority carriers (cm)
- $D$  = diffusion coefficient of minority carriers ( $\text{cm}^2/\text{sec}$ )

Mobility is mainly dependent on charged center scattering. Traps are charged, so they scatter electrons which reduces mobility (29:97-102,253-263). Defects are not uniformly distributed; therefore, minority carrier lifetime is not constant within the wafer (Figure 2). This lack of homogeneity can result in differences in the the electrical parameters of the individual devices in an integrated circuit chip.

Defects occur as the crystal is grown or during device processing. Grown-in, or intrinsic, defects include the



various types of point defects, dislocations, and stacking faults. Process induced, or extrinsic, defects include surface impurities, dielectric definition, design related faults, and process generated dislocation and stacking faults. Extrinsic defects are controlled by following procedures for cleanliness and using proper design rules. Issues in dielectric definition are beyond the scope of this paper. Process induced dislocation and stacking faults are directly related to the quality of the starting material.

Defects disrupt the periodicity of the lattice and produce stresses in the immediate vicinity, producing traps and scattering centers. Point defects disrupt one lattice site, but dislocations and stacking faults disrupt whole sections.

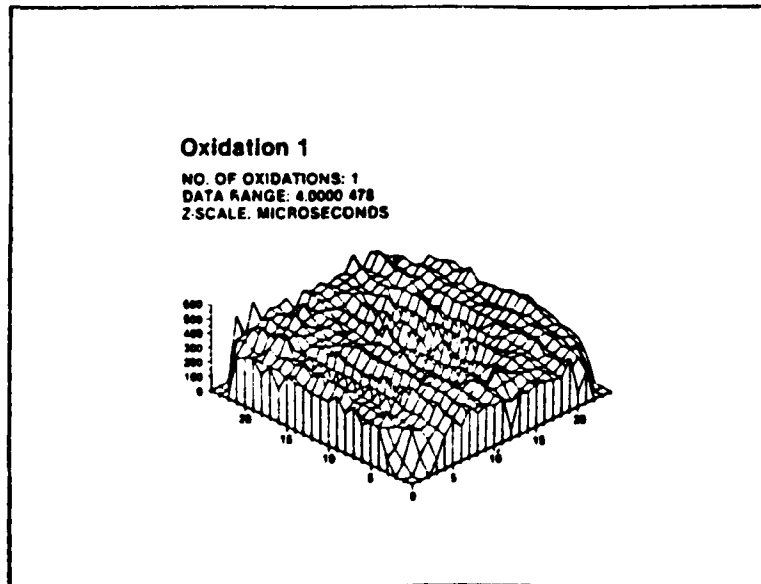


Figure 2. Minority Carrier Lifetime Distribution (28:331)

The diamond structure of crystalline silicon is rather open, so impurity atoms can occur interstitially as well as substitutionally. Figure 3 gives examples of each of the point defects. Note that silicon atoms can also occur between lattice sites, which is referred to as a self-interstitial. The oxygen in silicon is primarily interstitial. When an atom of silicon is missing from the lattice its called a Schottky defect or a vacancy, but if an atom leaves its lattice site and becomes interstitial the combination of a vacancy and an interstitial is called a Frenkel defect.

Dislocation and stacking faults are extra planes of atoms in the lattice. Figure 4 illustrates an edge dislocation. The lattice is in compression above the the edge and in tension below it. A screw dislocation occurs when an entire block of atom slips out of place as shown in Figure 5. This produces a twisting stress on the lattice. A stacking fault, Figure 6, can be any combination of edge and screw faults.

Point defects and dislocations can slip and move within the lattice, especially when heated. In fact, Frenkel and Schottky defects have an activation energy. Dislocation faults are particularly troublesome. If an epitaxial layer is grown over a dislocation fault, the dislocation will grow into the new layer. Dislocations can be generated during high temperature processing and will move and grow when stressed.

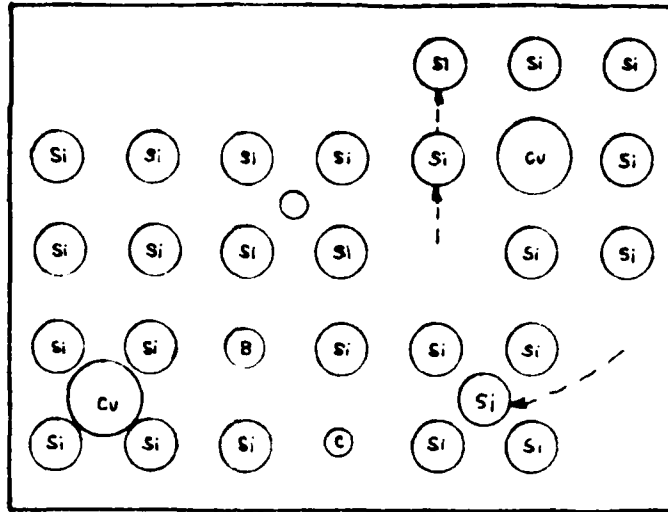


Figure 3. Schematic Illustration of Point Defects: Substitutional Boron, Substitutional Carbon, Interstitial Oxygen, Silicon Self-Interstitial, Vacancy or Schottky, Substitutional and Interstitial Copper, and Frenkel. Note the surface steps of silicon atoms. (11:212)

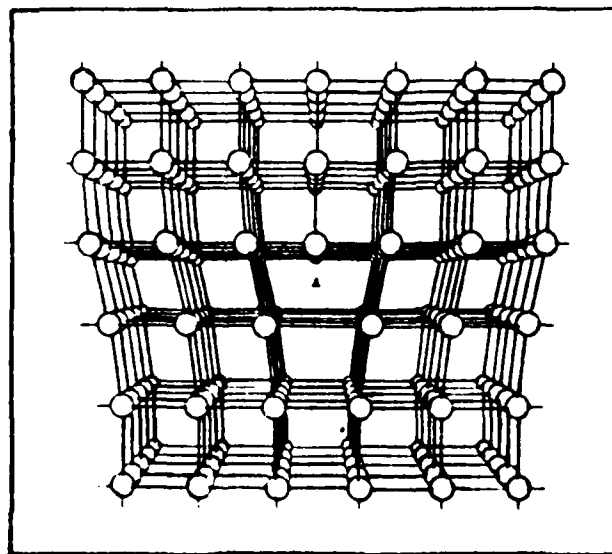


Figure 4. Edge Dislocation (23:212)

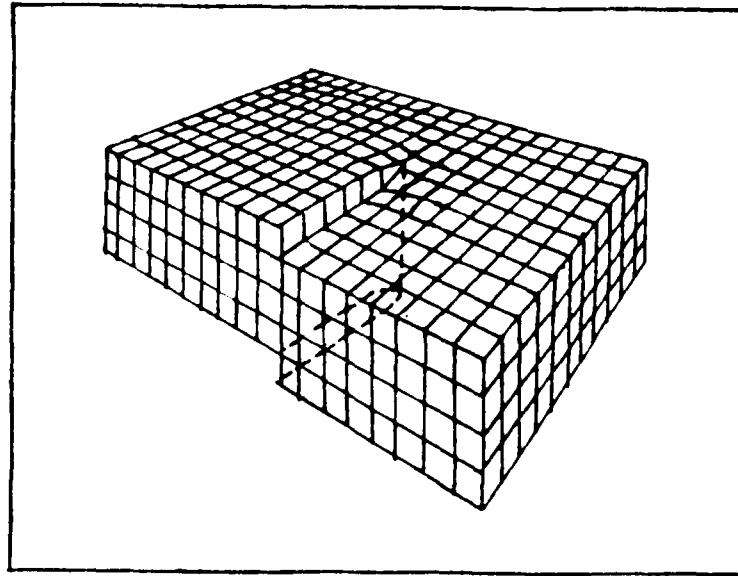


Figure 5. Screw Dislocation (16:154)

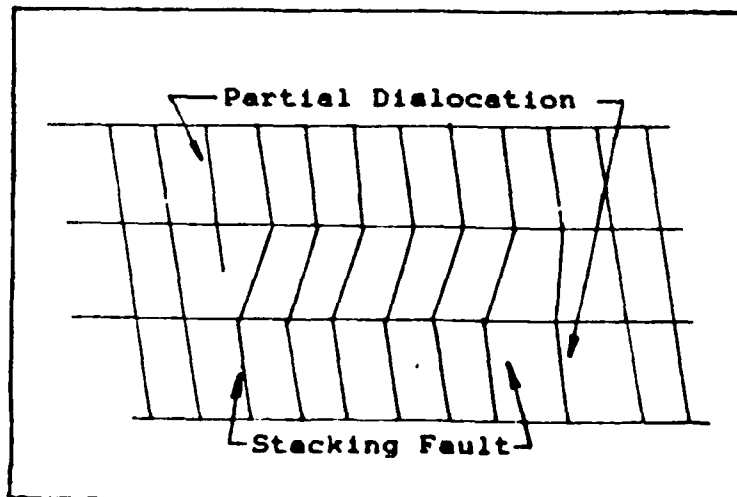


Figure 6. Stacking Fault

The dislocation density on the surface of a wafer is revealed by X-ray topography. Dislocation areas are more susceptible to etching because the region is stressed. Illuminating the surface with X-rays shows the dislocations as spots. Typically, electronic grade silicon has less than 100 dislocations/cm<sup>2</sup>, although less than 10/cm<sup>2</sup> is possible (23). Thus, most single crystal silicon is called dislocation free. Even so, any dislocations are becoming worrisome to device manufacturers, because of ever decreasing component size and the simultaneous increase in chip size.

#### Single Crystal Manufacturing

Commercially available single crystal silicon is made by the Czochralski Puller method or the float zone method. Although FZ crystals are purer than CZ crystals, CZ crystals account for 90% of the world's production, while FZ is 10%.

In the CZ method polycrystalline silicon is melted in a quartz crucible. The crucible is placed in a graphite susceptor. A small seed crystal of the proper crystal orientation is introduced to the surface of the melt, then is slowly pulled out. As the seed crystal is pulled out of the melt, new material is deposited which continues the same lattice configuration. Figure 7 shows this arrangement schematically. The pull rate is in the range of 2 to 5 x 10<sup>-13</sup> cm/sec. The diameter of the boule is

determined by the temperature and the pull rate. The largest boule reported is 12 inches in diameter (23).

Besides the doping atoms which are intentionally added, the melt is contaminated by oxygen and carbon atoms. The hot melt slowly dissolves the crucible, then breaks the silicon dioxide down into silicon and oxygen. Carbon atoms from the susceptor contaminate the atmosphere surrounding the melt. A few of these atoms dissolve into the melt. Carbon contamination varies between 0.1 to 3 parts per million atoms (ppma) or equivalently  $0.05$  to  $1.5 \times 10^{17}$

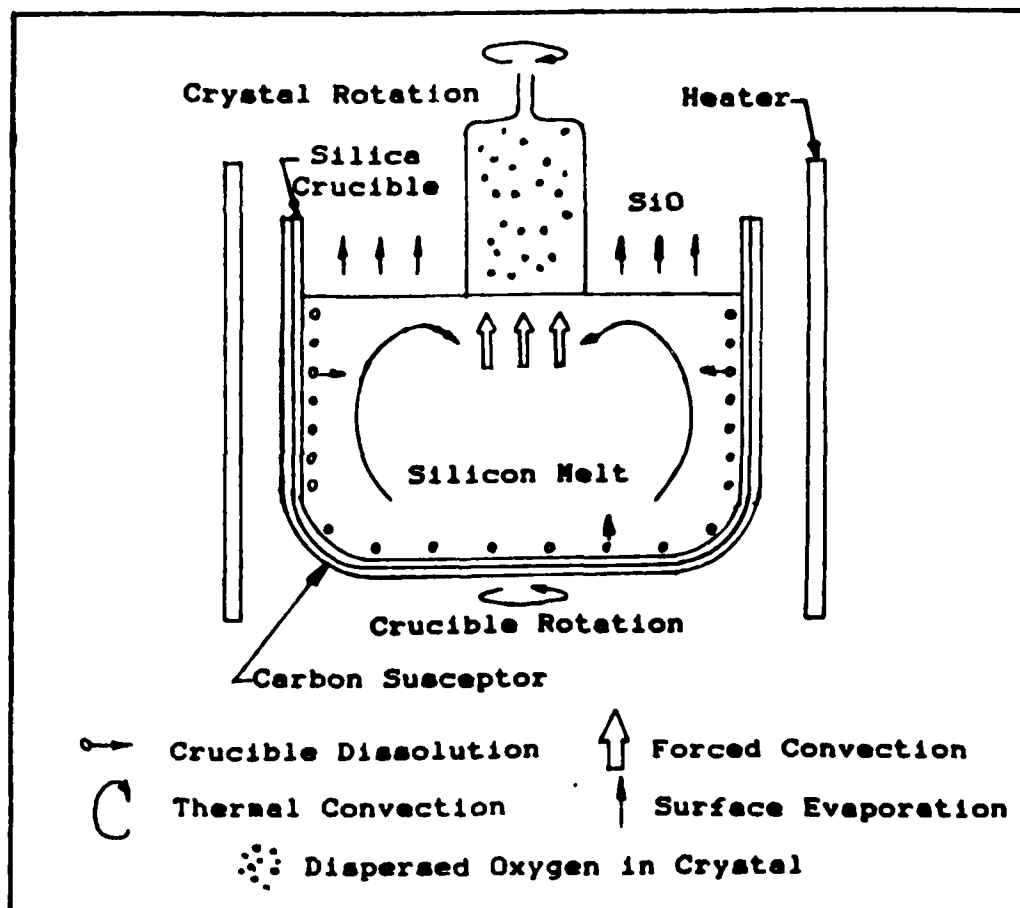


Figure 7. Schematic of Czochralski Puller Method (11:92)

atoms/cm (34:113). The role of carbon is uncertain, but seems to aid in the precipitation of oxygen.

Typically oxygen concentration in Cz crystal varies from 18 to 40 ppma ( $0.9$  to  $2 \times 10^{17}$  atoms/cm<sup>3</sup>) along the length of the boule (34:112-113). Efforts to control the oxygen concentration can reduce axial variation to between 24 to 38 ppma ( $1.2$  to  $2 \times 10^{18}$  atoms/cm<sup>3</sup>). Applying a magnetic field across the melt to dampen out convection currents reduces the oxygen variation and concentration to 10 to 14 ppma ( $5$  to  $7 \times 10^{17}$  atoms/cm<sup>3</sup>). Figure 8 shows the oxygen distribution from top to bottom of the boule for three different types of CZ silicon. The distribution of oxygen across a wafer is also

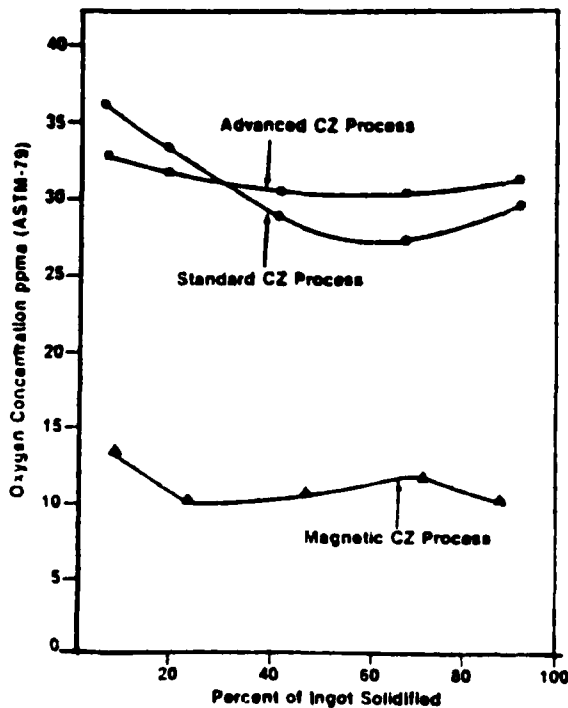


Figure 8. Axial Distribution of Oxygen in Three CZ Processes (34:112)

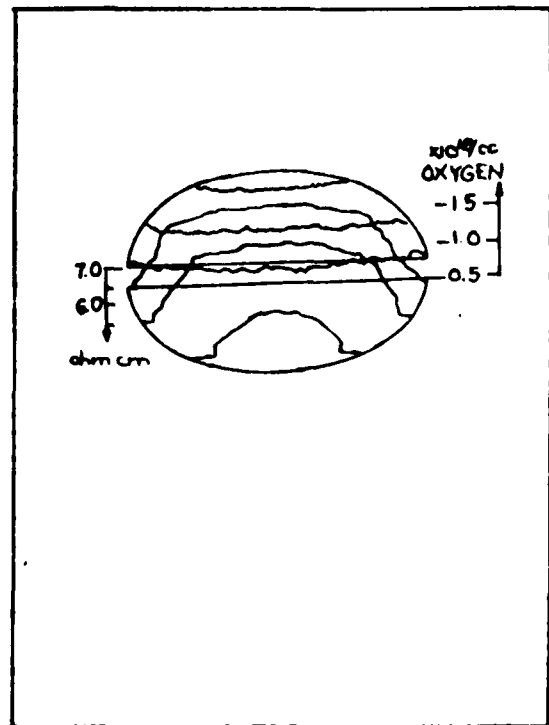


Figure 9. Resistivity (Dotted) and Oxygen Concentration Distribution (Solid) (1:67)

not constant. Figure 9 shows the oxygen distribution and resistivity across the surface of three different wafers.

Single crystal silicon of very high purity is made by the Float Zone method. Most FZ silicon is made for applications where high resistivity, 9 to 30 K ohms-cm, is necessary, such as infrared detectors. Examples where very pure crystals, but not necessarily high resistivity, are needed are power devices and devices such as discrete transistors and diodes. Most FZ silicon is grown for these applications.

The polycrystalline boule is held vertically as schematically illustrated in Figure 10. An RF heating source heats the bottom while a seed crystal is brought up from underneath. The heat source is slowly moved upward

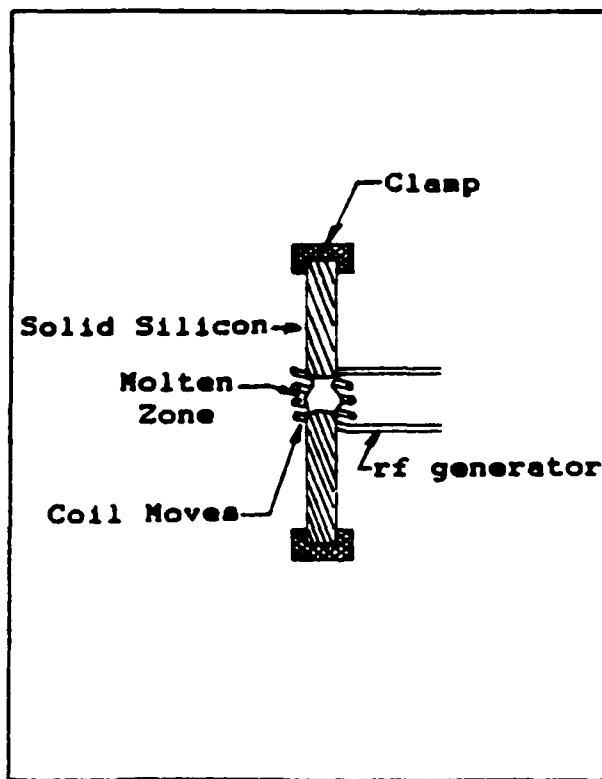


Figure 10. Schematic of Float Process (21:376)

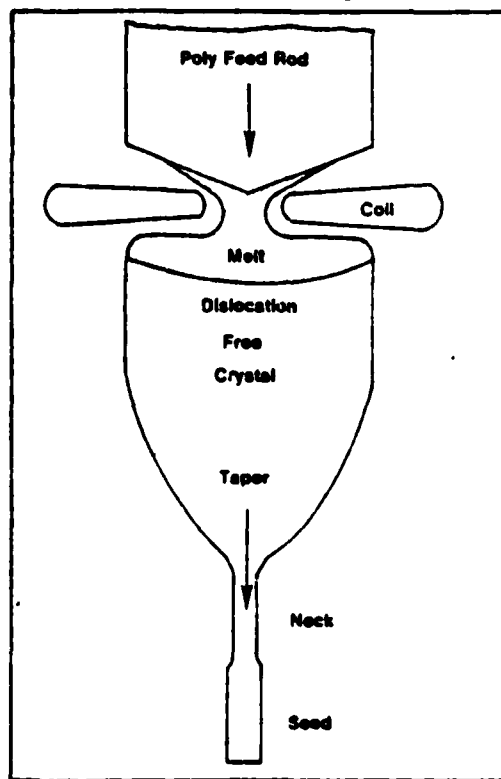


Figure 11. Float Zone with Needle-Eye Coil (17:138)



and, as it goes, the polycrystalline material takes on the lattice structure of the seed crystal. The surface tension of the liquid keeps the melted silicon from flowing away. Figure 11 is a schematic the current FZ process with a small "needle-eye" RF induction coil.

Since there is no crucible to contaminate the melt, the oxygen content of FZ silicon can be as low as 0.01 to 0.06 ppma ( $0.5$  to  $3 \times 10^{15}$  atoms/cm<sup>3</sup>). Because there is no graphite susceptor, the carbon concentration in FZ silicon is less than 0.01 ppma ( $5 \times 10^{14}$  atoms/cm<sup>3</sup>).

#### Controlling Defects

Controlling defects is of great concern to the semiconductor industry. The role of oxygen has been studied extensively as it is a major contaminant. Until recently, oxygen was thought of as an unfortunate consequence of the CZ process. Efforts have been made to

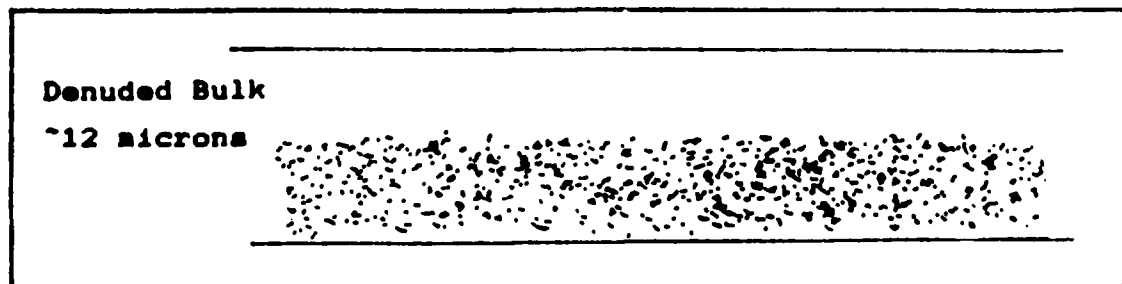


Figure 12. Denuded Zone in the Cross Section of a Wafer (35:98)

reduce the oxygen concentration in the CZ silicon; however, it is now realized that oxygen hardens the wafer by pinning dislocation faults and keeping them from multiplying.

The silicon industry is now making efforts to exploit the benefits of oxygen. Although oxygen pins dislocation faults, it does so by forming stacking faults. Thus, faults are not eliminated but controlled. If the concentration of oxygen is greater than 38 ppm (1.9 x 10<sup>18</sup> atoms/cm<sup>3</sup>), Si<sub>y</sub>O<sub>x</sub> precipitates form, leading to wafer warpage during thermal processing.

If a defect free zone is produced on the surface of a wafer and active electronic devices are confined to this region, then it would not matter if the bulk has defects. This new idea is called intrinsic gettering. Basically it consists of three temperature cycles ranging from 650 to 1200 °C for 6 to 36 hours. This produces a defect free or denuded layer 10 to 40 microns deep (Figure 12).

However, care must be taken when planning the thermal cycles for intrinsic gettering. D. Huber and J. Reffle caution that intrinsic gettering introduces a new parameter to device processing (10:139). They carried out experiments which show that if the oxygen has precipitated, the wafer is subject to warping during subsequent processing (Figure 13). As an aid to designing the appropriate temperature cycles for the intrinsic gettering process, Huber and Reffle processed a group of wafers at 1100 °C for 10 hours then, exposed to different

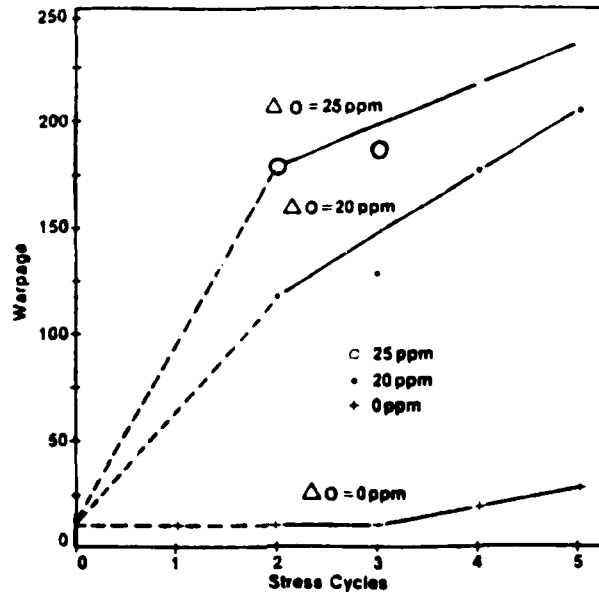


Figure 13. Warpage Due to Stress Cycles at 1050 °C  
(10:140)

nucleation (pre-anneal) and precipitation/gettering (out-diffusion) cycles. Subsequently, bipolar transistors were made. "After initial oxidation no defects are delineated; however, minority carrier diffusion length measurements show a drop from the initial values of 250 to 500 microns down to values between 50 and 100 microns" (10:141). The beneficial effects of intrinsic gettering may be negated if wafers are not properly processed.

The group of Japanese researchers (T. Abe et al.) that reported that nitrogen also pins dislocation faults are continuing their investigations (2,13,31,32,33). When it was discovered that oxygen, a contaminant, strengthened C<sub>z</sub> silicon wafers, the Japanese investigated other dopants that have the same effect. Matsato Imai and Koji Sumino reported that oxygen, nitrogen, and phosphorus have a locking effect, but carbon does not (13:618-619). Imai and Sumino used in-situ x-ray topography to study the propagation and movement of the dislocations on the surface of silicon.

Apparently this group of researchers are looking for a material that has a strong locking effect on silicon that is either electrically inert or doped in such low concentration that it does not affect the silicon. This is a new area of investigation. Literature on the strengthening effect of nitrogen starts around 1980. Although nitrogen does seem to have good properties in silicon, it is primarily used for discrete devices and power devices (26:66).

#### Previous Nitrogen Studies

All group V elements in the periodic table are donors in silicon (group IV); however, the behavior of nitrogen is the least understood. Early attempts to dope silicon with nitrogen using conventional doping techniques were unsuccessful. Nitrogen reacts with molten silicon to give

silicon nitride ( $\text{Si}_3\text{N}_4$ ) which readily dissolves into the melt (15:431). In 1973, Yatsurgai determined the phase diagram of N-Si in extremely low nitrogen concentrations. He discovered that a small amount of nitrogen can be present in silicon and reported that the solubility limit of nitrogen in silicon is  $4.5 \pm 1.0 \times 10^{15} \text{ cm}^{-3}$  in solid silicon and about  $6 \times 10^{18} \text{ cm}^{-3}$  in liquid silicon (43:978), making nitrogen the least soluble group V element in silicon. Further, from his infrared absorption studies he reported that less than 1% of the nitrogen goes into the lattice substitutionally, and concluded that most of the nitrogen remains un-ionized (43:978).

The difficulties of introducing nitrogen into silicon was well known before Yatsurgai's results were published. Other groups got around this difficulty by ion implanting nitrogen into p-type silicon substrate. One of the earliest studies of ion implanted nitrogen was performed in 1968 by Zorin et al. of the USSR (44). They were able to isolate the n-type nitrogen layer by reverse biasing the pn-junction formed by the n-type ion implanted layer and the p-type substrate, and performed the Hall experiment on it. They reported the activation energy of nitrogen to be 0.045 eV below the conduction band, that ion implanted nitrogen occupies substitutional sites, and the nitrogen behaves like a normal donor (44:111,112). This result is remarkable in that the activation energy of phosphorus is also 0.045 eV below the conduction band, and the donor

concentration measured was less than 1% of the implanted nitrogen ions.

A similar Hall experiment was repeated on ion implanted nitrogen in 1975 by J. B. Mitchell et al. (25). In this experiment FZ and CZ samples were ion implanted. Mitchell reported an activation energy of  $0.017 \pm 0.002$  eV. In this study the temperature range of the Hall experiment was much greater, from 20 K to 300 K, while Zorin's data was taken from 125 K to 250 K. From a previous paper of atom-site location measurements (24), Mitchell found that greater than 95% of the implanted nitrogen was located on interstitial sites, leaving an undetectable amount on possible substitutional sites.

The existence of a unique ionization energy which is independent of anneal time and implantation temperature (and consequently, the initial amount of damage) suggests a substitutional position for the donor-active nitrogen. The shallowness of the level ( $0.17 \pm 0.002$  eV) below the conduction band also suggests a substitutional site, as all known defect centers in silicon give rise to deeper states in the band gap (25:341).

However, he also suggests that there may be a defect conduction mechanism since the data does not fit the usual curve for a single donor level. This indicates that there may be some form of defect centers.

In a later study (1980), Keith Brower ion implanted nitrogen into intrinsic FZ silicon (4). The implanted layer was laser annealed to restore the crystal lattice. Brower used electron paramagnetic resonance (EPR) to study the structure of nitrogen in silicon. He concluded that

substitutional nitrogen and neighboring silicon atoms are "Jahn Teller distorted off their tetrahedral substitutional sites along directions which preserve axial symmetry about the  $\langle 111 \rangle$  axis (4:1628)." Associated with the distorted substitutional nitrogen is an activation energy of 0.58 eV below the conduction band. Thermal annealing above 430 °C appears to modify the structure of the distortion, and "might be the beginning of the formation of silicon nitride complexes with shallow donor levels which have been observed in electrical measurements by others (4:1629)."

Since the discovery of the strengthening effect of nitrogen in silicon, other studies have been undertaken to characterize nitrogen in bulk grown silicon rather than ion implanted layers. The nitrogen is introduced into the boule during the growth phase either by adding nitrogen gas to the argon ambient or adding silicon nitride to the melt. A photoluminescence (PL) study by Tajima et al. in 1981, revealed the presence of a PL line at  $1.1223 \pm 0.0001$  eV which increases in amplitude with nitrogen doping (38:L423). This same PL line was also found in ion implanted nitrogen, which is further evidence that this defect is associated with nitrogen (3:426). PL can be used to determine the impurity concentration of shallow impurities in bulk material. The nitrogen concentration in this study was determined by activation analysis. Tajima considers the 1.1223 eV line to be due to the radiative recombination of an exciton bound to a deep nitrogen center (38:L425).

that there is some electrically active nitrogen in the crystal, but not necessarily substitutional nitrogen. The discovery of the 1.1223 eV line defines a non-destructive test for the presence of nitrogen in a sample.

Another experiment, performed a year later by Tokumaru et al., studied the material using deep level transient spectroscopy (DLTS) in an effort to find the 0.58 eV deep level reported by Brower (40). Instead of the 0.58 eV level, two other deep levels were found: 0.19 eV at 0.1% of the nitrogen doping concentration, and 0.28 eV at 0.01% of the nitrogen concentration. However, the material Brower used was ion implanted and annealed at about 450 °C. The nitrogen doped FZ crystals used in this study were grown at a much higher temperature, thus isolated substitutional nitrogen atoms may not exist in this material and that the energy levels may be due to different types of nitrogen related complexes (40:L444). The shallow donor of 0.017 eV may exist in the crystal, but is too shallow to be measured by DLTS.

In summary, nitrogen doped silicon has been studied a number of different ways, each reporting a different activation energy and theory for nitrogen's effect on silicon. Although, there is evidence for substitutional nitrogen in ion implanted silicon, there is no clear cut evidence for it in bulk grown silicon or that the activation energies are the same. Hall effect analysis of this material has not been published, which is the most



sensitive method of determining electrical parameters in a semiconductor. The experiments undertaken in this thesis used the previous work as a starting point to determine the activation energies. The results of previous studies are summarized in Table I.

Table I  
Comparison of Activation Energies and Techniques Used

Researcher Year	Material	Energy Level	Method/Limitation
Zorin et al. 1968	Ion Implanted	0.045 eV	Hall: temperature range 100 -250 K too limited to find much shallower or deeper levels
Mitchell et al. 1974	Ion Implanted	0.017 eV	Hall: temperature range 20-250 K, not high enough to find deep levels
Brower 1980	Ion Implanted	0.58 eV	EPM: cannot detect shallow levels
Tokumaru et al. 1982	Bulk	0.19 eV 0.28 eV	DLTS: cannot detect shallow levels

### III. The Hall Effect

The Hall effect experiments were performed at the Laser and Optical Materials Branch, Materials Laboratory on equipment developed by P. Hemenger specifically for testing semiconductor material (9). However, before describing the equipment in detail, the Hall effect will be explained. This will give the reader an understanding of the principles involved in the experiment and the wealth of information that results. After the principles are explained the computer program used to resolve the raw data will be discussed.

#### The Hall Effect

When a magnetic field is applied to moving charges, a force is induced on the charges that is mutually perpendicular to the magnetic field and the direction of charge travel. Thus, charge is deflected toward the edges

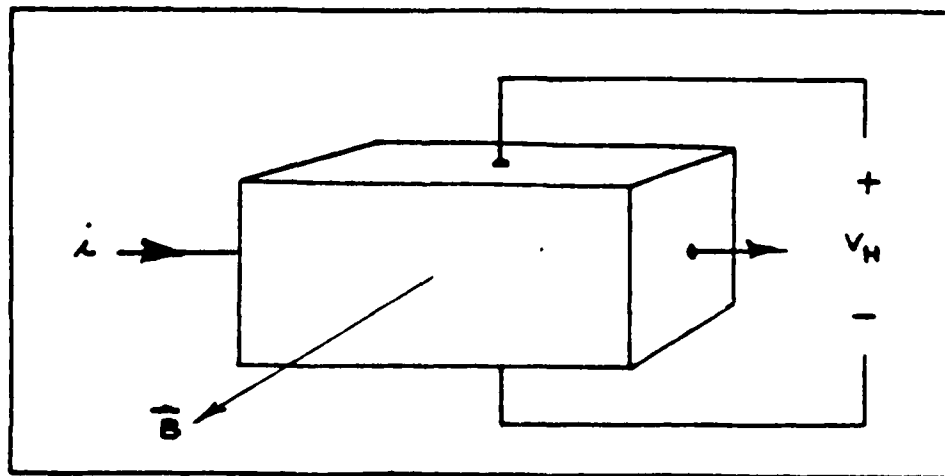


Figure 14. The Hall Effect

of the material with opposite polarities building up on opposite sides (Fig. 14). The charge builds up until an electric field is generated that balances the deflecting force (27:2). (This phenomenon was discovered in 1879 by E. H. Hall). The voltage induced between the sides of the material is called the Hall Voltage ( $V_H$ ).

For a constant magnetic field and constant current, the Hall Coefficient is defined by:

$$V_H = R_H IB/t \quad (\text{volts}) \quad (4)$$

where  $I$  = current (amps)  
 $B$  = magnetic field (gauss)  
 $t$  = thickness of sample (cm)  
 $R_H$  = Hall coefficient ( $\text{cm}^3/\text{coul}$ ) (7:12)

The Hall coefficient,  $R_H$ , is a material parameter that is related to the carrier concentrations and the mobilities.

It is computed directly from Equation 4:

$$R_H = V_H t / (IB) \quad (\text{cm}^3/\text{coul}) \quad (5)$$

When conduction is dominated by one type of charge carrier,  $R_H$  is given by:

$$\text{or} \quad R_H = -u_{Hn} / (enu_n) \quad \text{for electron conduction} \quad (6)$$

$$R_H = u_{Hp} / (epu_p) \quad \text{for hole conduction} \quad (7)$$

where

$u_{Hn}$  = Hall mobility of electrons ( $\text{cm}^2/\text{V-sec}$ )  
 $u_{Hp}$  = Hall mobility of holes ( $\text{cm}^2/\text{V-sec}$ )  
 $u_n$  = conductivity mobility of electrons ( $\text{cm}^2/\text{V-sec}$ )  
 $u_p$  = conductivity mobility of holes ( $\text{cm}^2/\text{V-sec}$ )  
 $n$  = concentration of electrons ( $\text{cm}^{-3}$ )  
 $p$  = concentration of holes ( $\text{cm}^{-3}$ )  
 $e$  = charge of an electron (coul) (19:2)

The ratio of the Hall mobility to the conductivity mobility,  $u_{Hn}/u_n$ , is called the Hall scattering factor,

$r_e$  or r-factor, for electrons. (A similar scattering factor is defined for holes,  $r_p$ .) The scattering factor is a function of the band structure of the material, temperature, magnetic field strength, and the scattering mechanisms (7:12-14). All material related effects are contained in  $r_e$ . Usually, the r-factor can only be measured over a limited range. It can be calculated or estimated, but in most cases it is close to unity and this is often the value used in analysis. In this work the r-factor is assumed to be unity, thus,  $R_H$  for n-type material is reduced to:

$$R_H = r/en = 1/en \quad (\text{cm}^3/\text{coul}) \quad (8)$$

By re-arranging Equation 8, the carrier concentration is simply:

$$n = r/eR_H = 1/eR_H \quad (\text{cm}^{-3}) \quad (9)$$

The resistivity is determined directly from measured voltage current characteristics of the material. Again, when one type of conduction dominates, resistivity is related to the carrier concentration and conductivity mobility by:

$$\rho_r = 1/enu_n \quad (\text{ohm-cm}) \quad (10)$$

where  $\rho_r$  is defined as resistivity in this work. Only  $R_H$  and  $\rho_r$  are directly measured. The Hall electron mobility is defined by:

$$u_{Hn} = R_H/\rho_r \quad (\text{cm}^2/\text{V-sec}) \quad (11)$$

If the scattering factor, that is, the r-factor can be

determined or assumed to be unity, as it is in this work, then the conductivity mobility is given by:

$$u_n = u_{Hn}/r \text{ (cm}^2\text{/V-sec)} \quad (12)$$

or

$$u_n = u_{Hn} \text{ (cm}^2\text{/V-sec)} \quad (13)$$

If the Hall coefficient,  $R_H$ , and resistivity,  $\rho_r$  of a material is measured over a wide temperature range, then the carrier concentration data derived from these measurements can be used to determine the electrically active impurities and their concentrations. At very low temperatures, for example near 20 K, there is not enough thermal energy to ionize the impurities. Thus, carrier concentration is negligible and resistivity is high. As the temperature is increased impurities start to ionize, giving up carriers to the conduction or valence band. Finally when all of the impurities of an atomic species become ionized, an increase in temperature does not increase the carrier concentration and the sample is said to be saturated. In silicon most shallow dopants are completely ionized at room temperature (300 K). The rate at which a species ionizes with temperature is related to the activation energy. The activation energy is determined from the slope of the logarithm of the carrier concentration versus inverse temperature. The equation for this curve is derived from the charge balance equation and Fermi-Dirac statistics (19:12-17). This equation contains the species concentration and the activation energy. A

computer program can use this complex expression to generate a least squares fit curve and determine the concentrations and activation energies for a number of levels. Thus, Hall effect experiments can be used to determine the impurities and the concentrations in a semiconductor.

The Curve Fitting Function to Determine Carrier Concentration and Activation Energy

The fitting function used to generate a least squares fit curve to the carrier concentration points versus inverse temperature is derived from the charge balance equation:

$$n + \sum_k N_{Ak} = p + \sum_i N_{Di} \quad (14)$$

where

- n = number of electrons in the conduction band
- p = number of holes in the valence band
- $N_{Di}$  = number of ionized donors (positively charged)
- $N_{Ak}$  = number of ionized acceptors (negatively charged) (19:12)

Sums are over all donor and acceptor species. If the number of donors greatly exceeds acceptors, which is the case for n-type silicon, then the number of holes in the valence band is negligible and equation 14 reduces to:

$$n + \sum_k N_{Ak} = \sum_i N_{Di} \quad (15)$$

The sum over the acceptors can be replaced by the total number of acceptors,  $N_A$ , because the number of holes is negligible at room temperature and below and all of the

acceptors end up negatively charged (19:12). If Fermi-Dirac statistics are applied to the donors and Boltzmann statistics are applied to the electrons in the conduction band as discussed by Putley (27:122-137) and Lang and Hemenger (19:13-18,50-54), the charge balance equation becomes:

$$n + N_A = \sum_i \frac{N_{Di}}{1 + n/Q_i} \quad (16)$$

$$Q_i = \frac{N_C}{\sum_j g_{ij} \exp(E_{Aij}/kT)} \quad (17)$$

where

- $N_C$  = density of states in the conduction band
- $g_{ij}$  = degeneracy of the excited energy states
- $E_{Aij}$  = activation or ionization energy (eV)
- $k$  = Boltzmann's constant (eV/Kelvin)
- $T$  = temperature (Kelvin) (19:13;27:132)

The density of states,  $N_C$ , is roughly dependent on temperature raised to 3/2 power (19:17;20:4646). Unless the sample is very heavily doped or the activation energy is very small, the excited states contribute very little to the sum in Equation 16, so that  $Q_i$  becomes:

$$Q_i = [N_C \exp(-E_{Ai}/kT)]/g \quad (18)$$

where

- $g$  = degeneracy of the ground state (19:14)

For donors in silicon,  $g$  is taken to be two (27:123;18).

By fitting Equation 16 to the experimentally measured temperature dependent carrier concentration,  $n(T)$ , the total concentration of all the acceptors, concentration of each donor, and the activation energy of each donor are determined variables of the fit. As an example, a typical

Hall experiment performed on a phosphorus doped silicon is shown in Figure 15. At high temperatures all of the donors are ionized thus,  $n = N_D - N_A$ . In the high temperature "exhaustion" (or saturation) region the carrier concentration is independent of temperature as there are no more electrons to be given up by the donors. This can be seen at the left side of Figure 15. At the lowest temperatures none of the donors are ionized. This is seen at the right side of Figure 15. The electron concentration is given by:

$$n = (N_D - N_A)Q/N_A \text{ (cm}^{-3}\text{)} \quad (19)$$

but because  $Q$  is exponentially dependent on temperature,  $n$  is proportional to the exponent of  $-E_A/kT$  (19:16). By taking the logarithm of equation 19 a linear equation results. Plotting the logarithm of the carrier concentration versus the inverse of the temperature (multiplied by 1000 as shown in Fig. 15) as the dependent variable gives the activation energy as the slope of the graph. In the example, the donor concentration is  $3.19 \times 10^{15} \text{ cm}^{-3}$ , the activation energy is 0.04445 eV, and the number of acceptors is  $1.33 \times 10^{12} \text{ cm}^{-3}$ . The activation energy of phosphorus given by Sze (37:21) is 0.045 eV which is close enough to identify phosphorus as the donor species.

If there is more than one donor species, the shape of the curve is more complex and is more difficult to resolve. The plot of carrier concentration versus inverse



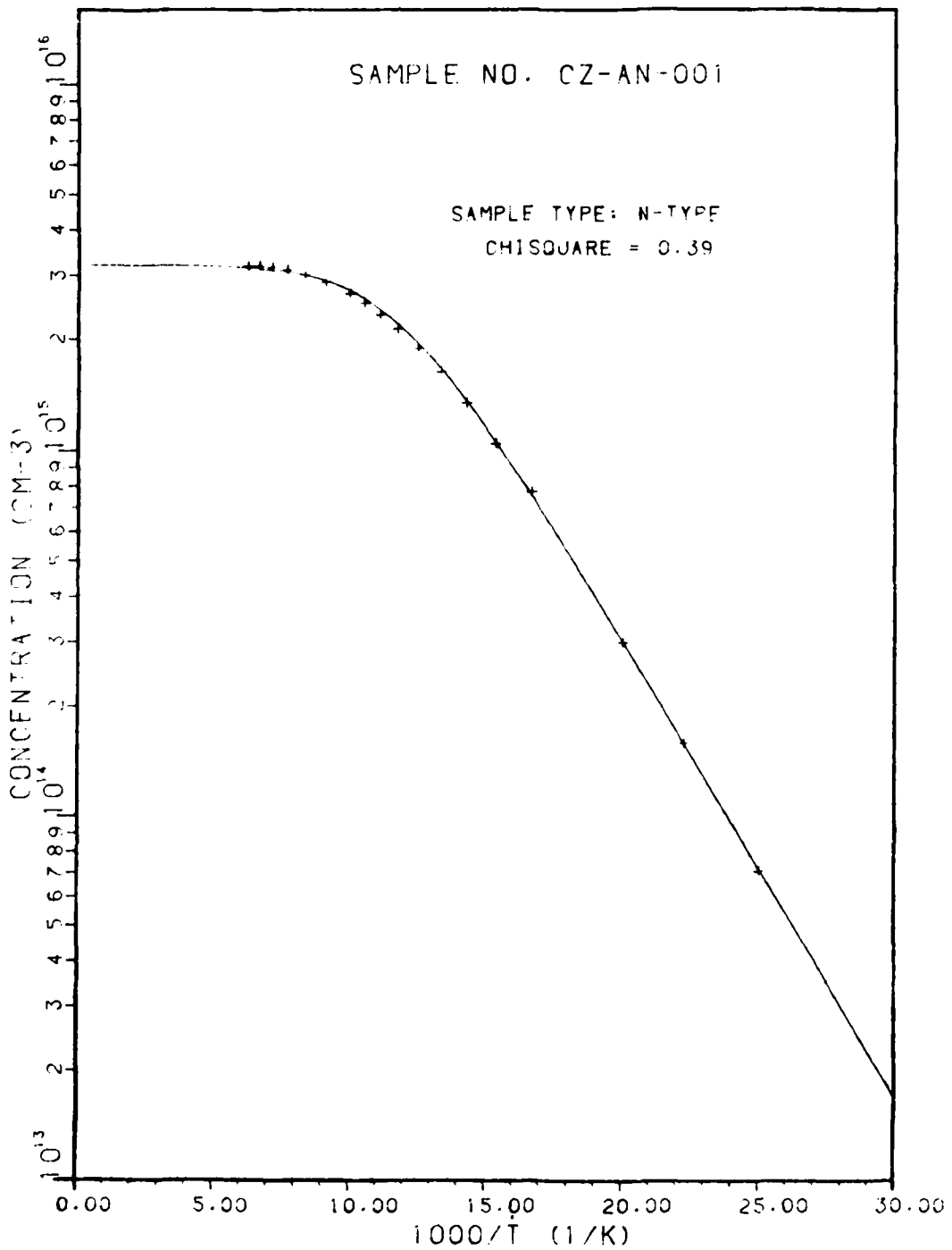


Figure 15. Phosphorus Doped CZ Silicon  
Annealed at 900°C

temperature will still have an exhaustion region on the left if the temperature range of the experiment was high enough to ionize all donors, but the analysis of the lower temperature range will depend on the number of acceptors. The shallowest donors will not be seen in the data if they are overcompensated by the acceptors, that is, the number of acceptors exceeds the shallow donors. If the number of acceptors equals the number shallow donors, the middle temperature range will be the same as a single donor plot, but the low temperature range slope will be equal to average of the activation energies of the donors. Only if the shallowest donor is undercompensated will its activation energy be given by the slope. In all cases only the deeper donors, which are activated at higher temperatures, are unambiguous. The concentration of the donor species are found directly from the inflection points on the curve (19:18-27).

#### Computer Generated Curve Fitting

Generating a fitting function to the carrier concentration data is an iterative process. The parameters, acceptor concentration, donor concentrations, donor energy levels, and degeneracy, are specified by the user. The computer generates the fitting function and compares the value of the function to each data point. It then adjusts the parameters, generates another fitting function, and compares the new values. This process continues until the

user is satisfied that the best fit has been obtained. The computer reports the final values of the parameters: degeneracy, the activation energy, the concentration of donors at each energy level, and the acceptor concentration. The parameters may be specified as fixed or variable. The degeneracy was fixed at two for each donor level in these samples. The computer draws the fitting function on the carrier concentration graph and gives the percent error between the function and the data at each point.

The quality of the fit is determined by the error between the data and the fitting function. It is expected that if there are  $n$  free parameters, the function should go through  $n$  points and miss the rest by one standard deviation (19:28-29). A number value for the quality of the fit is called Chi-squared ( $\chi^2$ ):

$$\chi^2 = \sum^N [Y_i - f(x_i)]^2 / (\sigma_i)^2 \quad (20)$$

where

- $N$  = number of data points
- $Y_i$  =  $i$ th data point
- $\sigma_i$  = standard deviation at the  $i$ th point
- $f(x_i)$  = value of the fitting function at  $x_i$  (19:30)

The standard deviation is assumed to be  $0.03Y_i$  (19:30).

An estimate of the minimum value of Chi-squared depends on the number of data points,  $N$ , and the number of free parameters,  $n$ , so that Chi-squared is approximately equal to  $N$  minus  $n$ . The quality of the fit is then determined by

the reduced Chi-squared (19:30):

$$\chi^2_{\nu} = \chi^2 / (N-n) \quad (21)$$

The reduced Chi-squared is used so that the quality of a one level fit can be compared to a multi-level fit (23). A multi-level fit has more free parameters than a one level fit, making the value of Chi-squared even smaller for the same data points.

When curve fitting, it is important to be aware that the program can settle on unrealistic values. This may be due to several factors such as: systematic errors in the experiment, not taking enough data points, or an r-factor problem. If the parameter values are unrealistic, the user can try again with different starting parameters.

#### IV. Experimental Procedure

A boule of two inch diameter nitrogen doped  $\langle 100 \rangle$  FZ silicon manufactured by the Shin-etsu Company was given to the United States Air Force by T. Abe. Photoluminescence studies were performed by David Brown of University of Dayton Research Institute for the Materials Laboratory (AFWAL), while the Hall effect analysis was undertaken in this thesis. Samples cut from bulk material were annealed at different temperatures for one hour then subjected to the Hall experiment to determine the effect of annealing. Further, to show the effect of Si:N as a substrate material with increased n-type doping, a section of the boule was neutron transmutation doped. The Hall effect experiment was performed on samples from the NTD section of Si:N.

##### Sample Geometry and Configuration

In order to accurately compute the Hall coefficient and resistivity, the sample must be homogeneous, of uniform thickness, and contain no holes. All the samples in these experiments were square in shape with contacts at each corner. This configuration was suggested by L. J. van der Pauw (41). Van der Pauw showed that resistivity can be accurately measured for an arbitrarily shaped sample with four point contacts on the periphery if the above conditions hold and that the contacts are small compared to

the periphery (41:2).

In this configuration each contact plays a role as voltage probe or a current connection as illustrated in Fig. 16. Measurements are required for only three of the six configurations. Resistivity measurements are taken over two of the four resistivity configurations, 1 and 2 or 3 and 4. In each configuration two voltage measurements are taken with the current reversed for the second measurement. Thermoelectric effects result from the dissimilar metals used in lead materials and are independent of current direction. Averaging the resistance measurements eliminates the thermoelectric effects (7:17;27:29-31). The resistivity equation given by van der Pauw is (42:221):

$$\rho_r = \frac{\pi t (R_1 + R_2)}{(\ln 2)} \frac{f(R_1/R_2)}{2} \text{ (ohm-cm)} \quad (22)$$

where

$$\begin{aligned} t &= \text{thickness (cm)} \\ R_1 &= V_1/I \text{ ohms} \\ R_2 &= V_2/I \text{ ohms} \end{aligned}$$

The function,  $f(R_1/R_2)$ , is a dimensionless function of the ratio of the resistances of the two separate configurations. If the difference between  $R_1$  and  $R_2$  is small then the function can be approximated (41:6):

$$\begin{aligned} x &= R_1/R_2 \\ f(x) &= 1 - \frac{(x-1)^2 \ln(2)}{(x+1)^2} \\ &\quad - \frac{(x-1)^4}{(x+1)^4} \left\{ [\ln(2)]^2/4 - [\ln(2)]^3/12 \right\} \end{aligned} \quad (23)$$

For a symmetrical sample, such as a square,  $R_1/R_2$

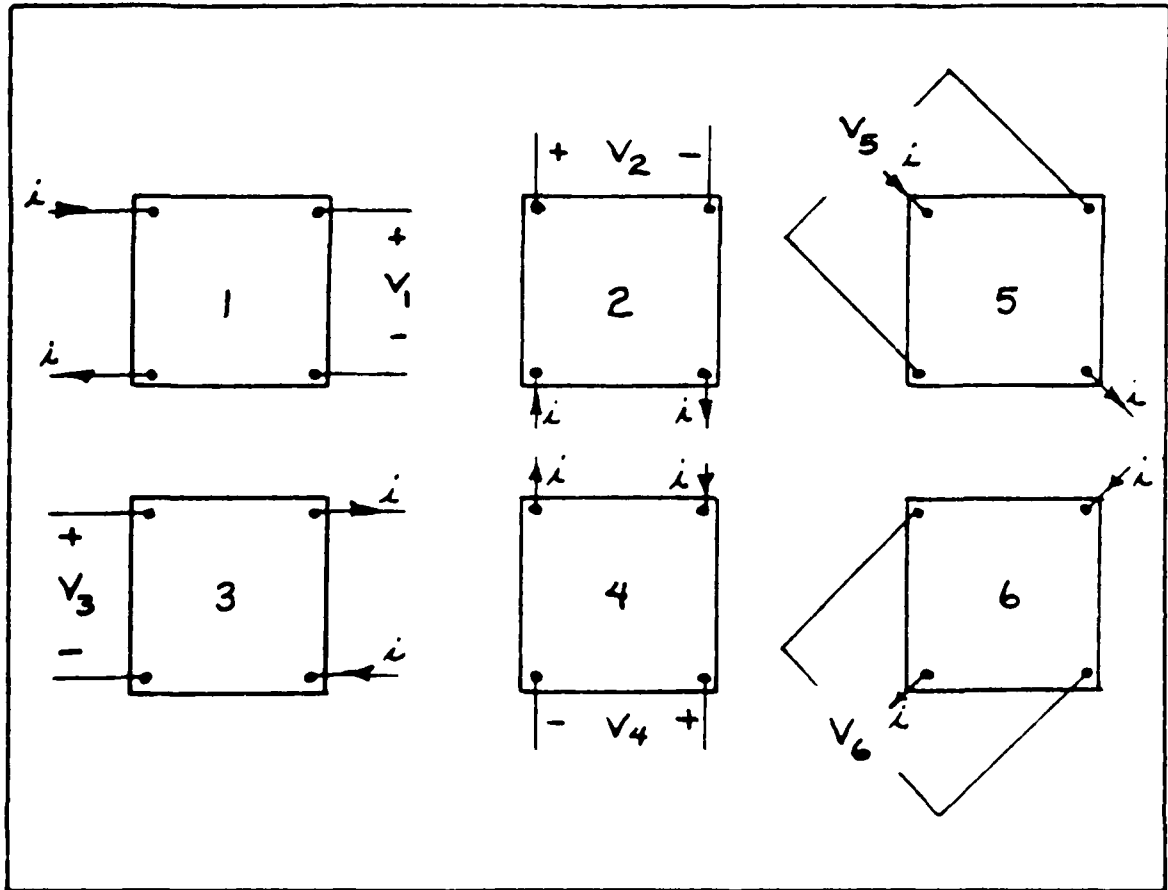


Figure 16. Van der Pauw Configurations for Hall Measurements (19:8)

should be unity. A slightly irregular sample will have some other value for the resistance ratio. This ratio should be nearly constant at all temperatures. If the ratio has a temperature dependence, it implies that the material is inhomogeneous (19:11).

The Hall coefficient,  $R_H$ , is obtained from either configurations 5 or 6. Measurements are taken over all combinations of current and magnetic field direction. Four voltage measurements are taken in all. Averaging over current direction eliminates thermoelectric effects, while averaging over magnetic field direction eliminates any magneto-resistance component due to non-symmetric voltage contacts (7:17).  $R_H$  is computed from:

$$Z = 1/2 \left\{ [R_5(+, \nearrow) + R_5(-, \nearrow)]/2 - [R_5(+, \searrow) + R_5(-, \searrow)]/2 \right\}$$

$$R_H = Zt/B \quad (\text{cm}^3/\text{coul}) \quad (24)$$

The plus or minus signs given in parenthesis after  $R_5$  refer to the current direction, while the arrows refer to the magnetic field direction.

#### The Hall Effect Systems

The equipment used in these experiments was developed by P. Hemenger (9). This system overcomes the noise problem and long time constants encountered in measuring high resistivity samples. By using high-input impedance, unity gain amplifiers between the voltage probe and the voltmeter (Hewlett-Packard 3455A DVM or equivalent), the



impedance is reduced to a level below the input impedance of the voltmeter. In addition, by using feedback from the unity gain amplifiers to drive the inner shield of the triax cables from the sample, the cable capacitance is reduced to near zero. This cancels most of the resistance-capacitance (RC) time constant which reduces noise, leakage current, and the settling time. The system uses Keithley Model 610C Electrometers as the unity gain amplifiers which are labeled, A, in Figure 17. A laboratory built switching box uses reed switches to step through all the configurations. This system is capable of measuring resistances up to  $10^{12}$  ohms.

The Hall effect system is schematically shown in Figure 18. Data was collected on two similar systems. The function of each block is identical for both systems. In each system the current is monitored by an ammeter capable of measuring current in the order of  $10^{-11}$  amps (19:5). The system referred to as Hall I can be operated manually or by computer (ADAC Corp. LSI System 100). Hall II can only be operated manually. The other differences between the systems are that Hall II uses a constant current source (Keithley 220 Programmable Current Source) where Hall I uses a DC voltage power supply (Hewlett-Packard 6299A) to provide sample current and that the gaussmeters are made by different manufacturers.

The computer that is used to automatically operate Hall I is not shown in Figure 18. The computer controls the

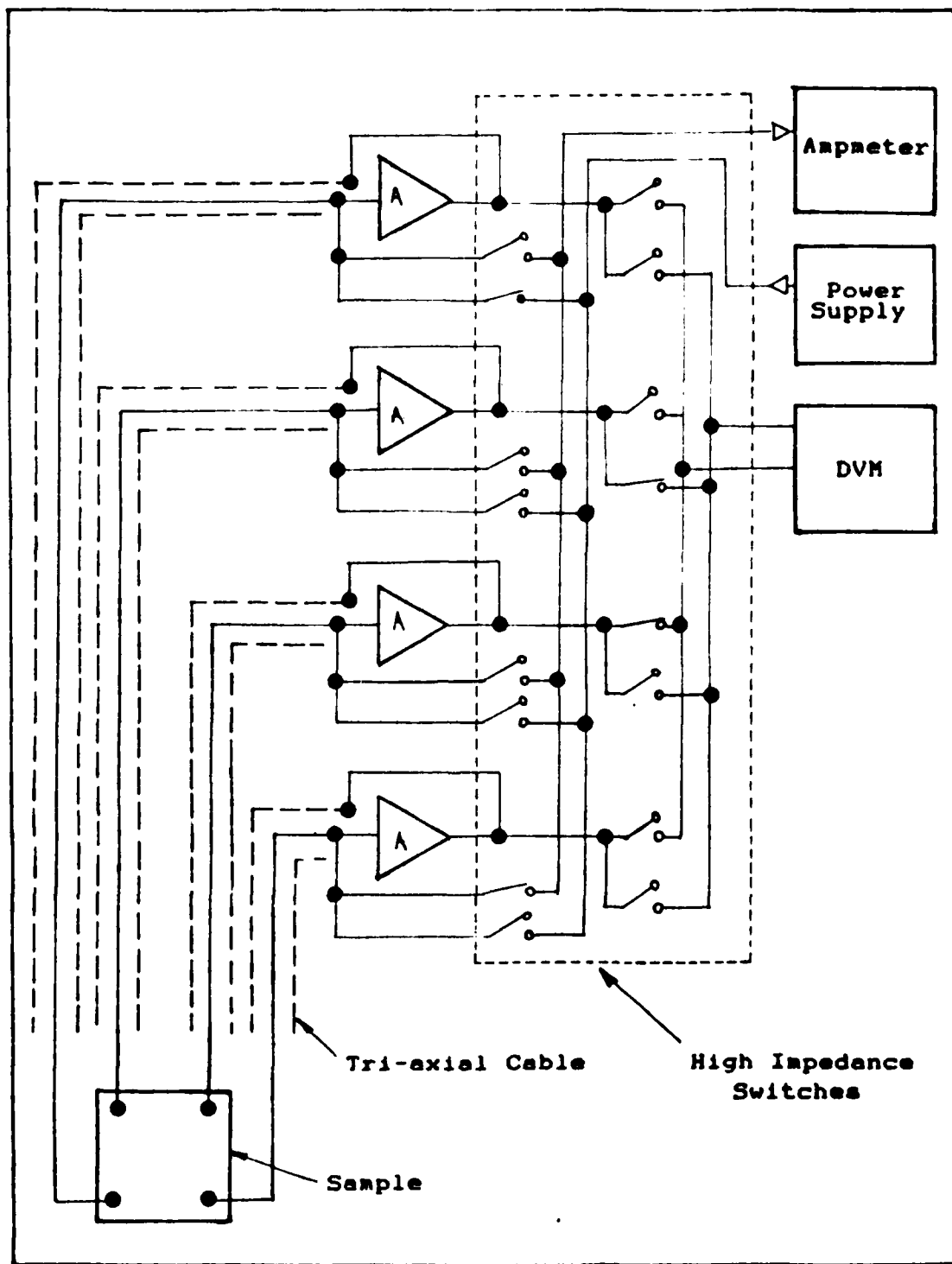


Figure 17. Schematic Diagram of Guarded Hall System

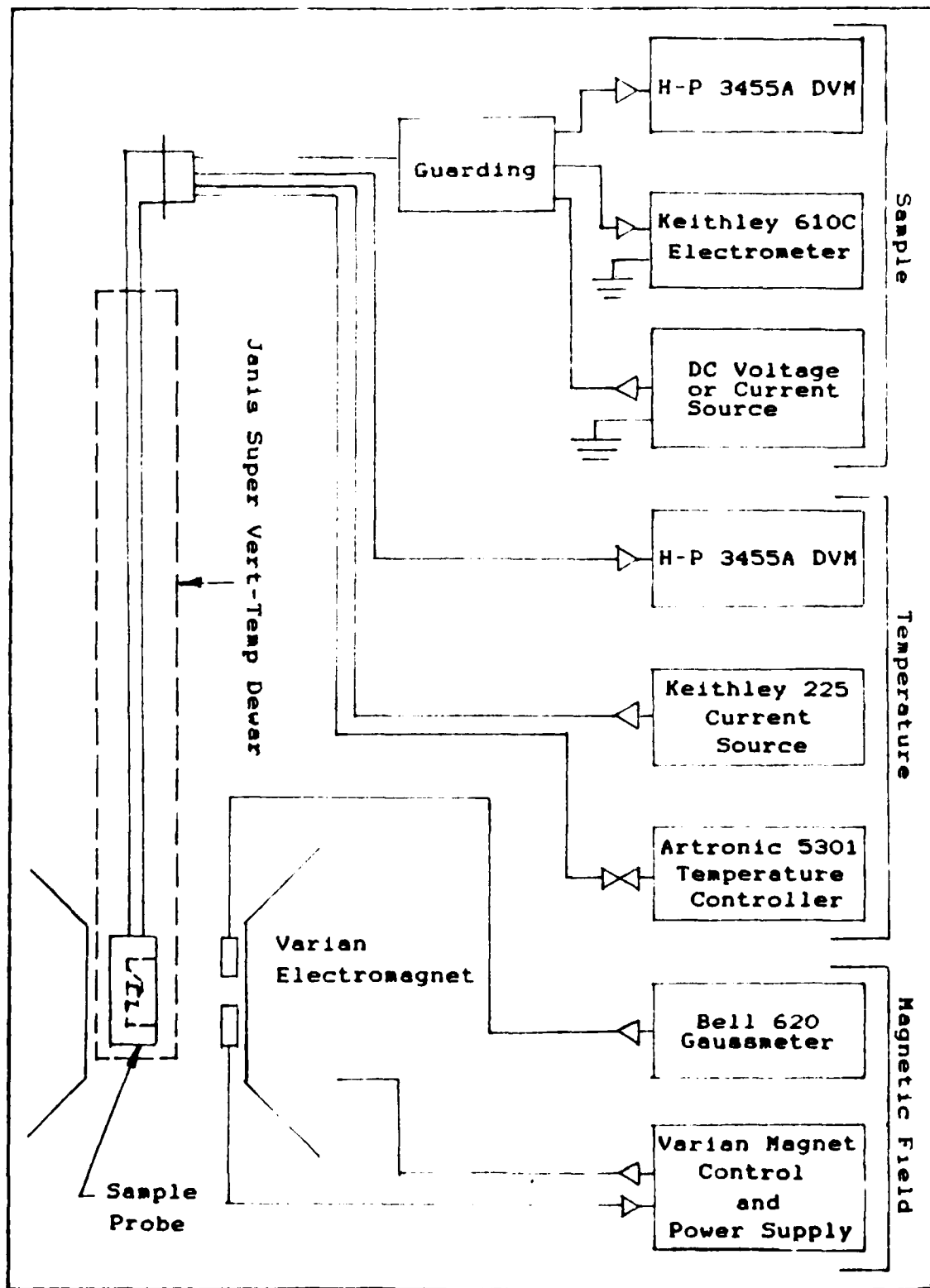


Figure 18. Schematic Diagram of the Hall Effect System

temperature, magnet, the configuration of the sample by setting the reed switches on the Van der Pauw Box, and collecting the data by reading the meters. When operated automatically, Hall I collects data over all resistivity and Hall configurations, taking 16 measurements in all.

The temperature of the sample is determined by measuring the voltage drop across a reverse biased silicon diode thermometer (Lake Shore Cryogenics Model DT500). The voltage drop across the diode is read by a Hewlett-Packard 3455A Digital Voltmeter. The temperature is determined by referencing the voltage/temperature calibration data provided by the manufacturer.

The sample probe is mounted in a Janis Super Veri-Temp helium vapor dewar. The dewar is filled with liquid helium. The helium flows through a needle valve at the bottom of the dewar then vaporizes. This allows cold helium vapors to flow around the sample holder. The sample holder (Fig. 19) is a block of copper which acts as a heat sink and is covered by a thin cylinder of copper as a radiation shield. The sample is mounted on a beryllium oxide (BeO) pad and held in place by a non-magnetic spring with a thin sheet of teflon in between for electrical insulation. BeO electrically insulates the sample from the copper sample holder while keeping in thermal contact with the silicon diode thermometer. BeO is an unusual material that has high thermal conductivity but very low electrical conductivity. The silicon diode thermometer is directly underneath and in contact with the BeO pad.

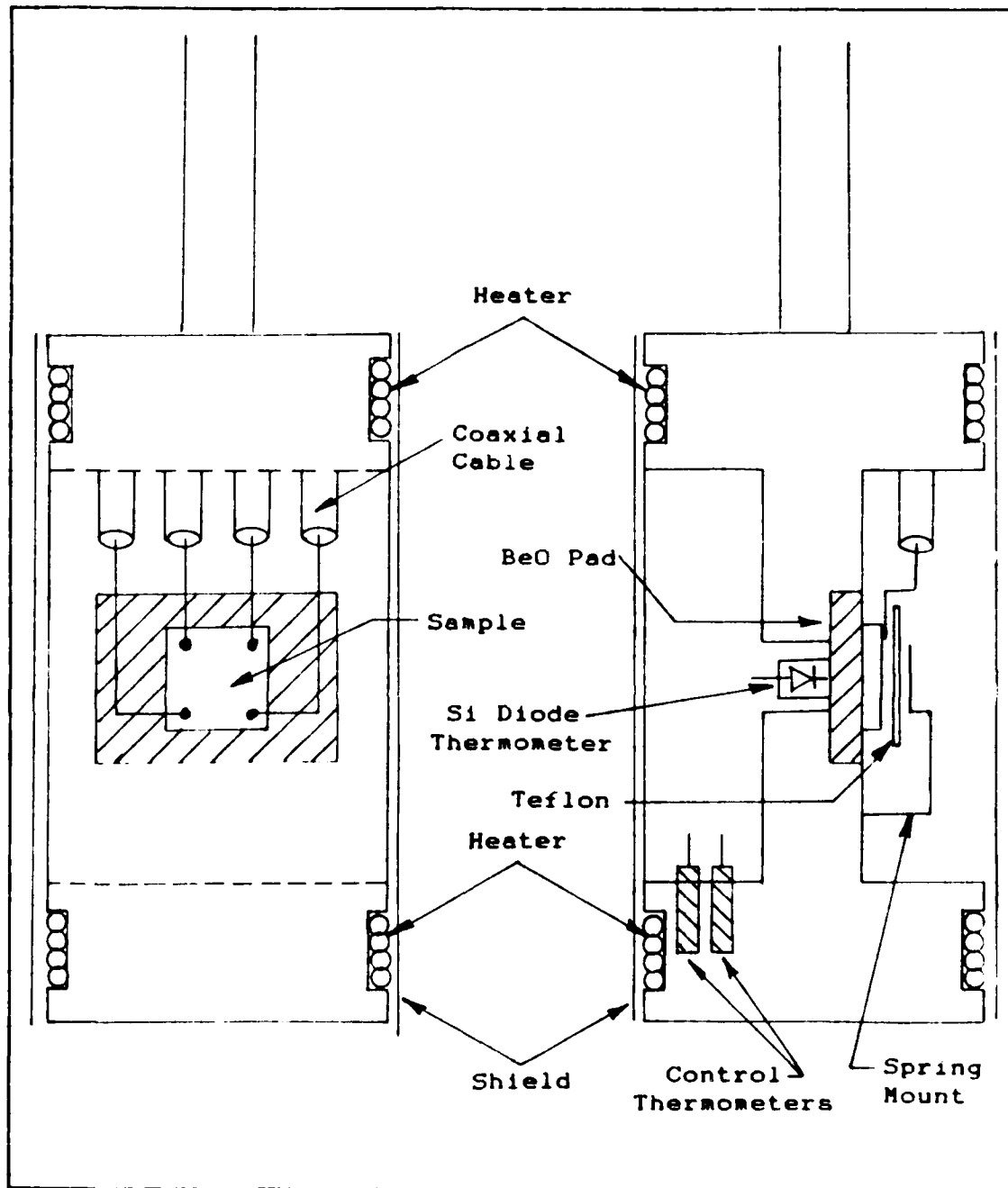


Figure 19. Schematic Diagram of Sample Probe

To raise the sample temperature above liquid helium temperature, two heater coils are positioned at each end of the sample holder. The heater coils are wound in opposite directions to reduce magnetic fields (7:29). When taking data manually on either system, sample temperature is maintained by an Artronix Instrumentation Model 5301 temperature controller. The controller senses temperature through one of the two thermometers near the bottom of the sample holder. The carbon-glass thermometer used for temperatures between 4 to 30 K while the platinum thermometer is used for temperatures 30 K and above. These thermometers unlike the Si diode thermometer are insensitive to magnetic fields in these temperature regions. The temperature controller drives the heater coils. When automatically taking data, Hall I uses a laboratory built temperature controller that is under computer control. The automatic temperature controller uses the same controlling thermometers in the sample holder.

The magnetic field is supplied by a Varian electromagnet which monitored by a Walker Magnametric Model MG-3D gaussmeter (Hall I) or Bell Model 620 gaussmeter (Hall II). The sample probe is mounted in the dewar so that the magnetic field is normal to the sample surface.

#### Sample Preparation

After the samples are cut, they must be prepared for annealing. Contacts must be put on the corners and then

mounted on the sample holder. Each step requires care to prevent contamination.

Prior to annealing the samples are rinsed successively in trichloroethylene, acetone, then methanol. Next they are placed in a solution of ammonium hydroxide, hydrogen peroxide, and water (1:1:5) at 60 °C for 15 minutes. After this they are placed in a solution of hydrochloric acid, hydrogen peroxide, and water (1:1:6) at 60 °C for 15 minutes. The samples are rinsed in de-ionized water and allowed to soak for 30 minutes or more.

The boat used for annealing the samples is high purity polycrystalline silicon. Wafers of the same material are placed between the samples to prevent possible contamination during annealing. Before annealing the boat and the wafers are cleaned using a similar procedure. During annealing, argon gas is allowed to flow through the furnace.

The first two samples were annealed at 900 °C using a quartz furnace tube. Unfortunately, the tube broke during cooling. Fiberglass was used to pack the furnace tube to keep it from losing too much heat. The fiberglass may have contracted faster than the quartz tube causing it to fracture (23). After this a polycrystalline silicon furnace tube was used, but the temperature could not be set above 830 °C.

To make ohmic contacts on the corners of the samples, a pulsed Nd:YAG laser is used to melt a 1 mm spot while

driving in dopant material. The samples were immersed in a solution of spin-on phosphorus dopant. The laser pulse melts a small localized area which incorporates phosphorus into the lattice as it recrystallizes. The result is a degenerately doped area suitable for an ohmic contact. To remove the phosphorus spin-on from the surface of the samples, they were placed in a solution of ammonium hydroxide, hydrogen peroxide, and water (1:1:5) at 60 °C for 15 minutes, then rinsed in distilled water.

After cleaning, copper leads are soldered on using indium solder. The samples are mounted to the holder by soldering the leads to the center wire of the shielded cables on the sample probe with indium solder. The probe is ready for mounting in the Hall equipment.

As a check before each data run, the sample is tested for ohmic contacts. A current is applied to the sample and the resulting voltages are read for each of the resistivity configurations 1 through 4 in both current directions. The voltage at each configuration should be the same for both current directions. If not, one or more contacts are not ohmic. Increasing the current should result in a proportional increase in the voltage. This test will also reveal broken or shorted wires.



## V. Results

The Hall effect measurements were performed on three different types of silicon: phosphorus doped CZ silicon, nitrogen doped FZ silicon, and neutron transmuted (NTD) nitrogen doped FZ silicon. All of the nitrogen doped samples, including the NTD samples, came from the same boule. The CZ was used as an example for comparison with the FZ Si:N samples, while a high purity FZ NTD sample (NT2-07-5N) that had been analyzed by W. C. Mitchel was used to compare results from the NTD Si:N samples (23). The Si:N samples were annealed for one hour at different temperatures to show the effects of annealing. Table II lists the sample identification number, silicon type, doping, and annealing temperature as a summary of the experiments performed. The magnetic field strength was 0.50 Tesla for all experiments except FZ0001 which was 0.10 Tesla. Due to surface contamination, sample 0274-0802 and 0274-802-1426 were recleaned in the ammonium hydroxide, hydrogen peroxide, and water solution and the experiments repeated.

### Electrical Data at 300 K

Since most electrical devices are designed to operate at room temperature, Table III gives the Hall coefficient,  $R_H$ ; resistivity,  $\rho_r$ ; and Hall mobility,  $u_H$ , at

Table II

## List of Samples on Which Experiments Were Performed

Name	ID#	Type	Doping Element	Annealing Temperature
CZ-AN-001	0124-1399-1312	CZ	P	900 °C
FZ0002	0274A-1581-1395	FZ (NTD)	N P	800 °C
FZ0003	0274A-1581-1396	FZ (NTD)	N P	800 °C
FZ0001 FZ0001-A	0274-0802 0274-0802	FZ FZ	N N	900 °C 900 °C
FZ0004 FZ0004-A	0274-802-1426 0274-802-1426	FZ FZ	N N	800 °C 800 °C
FZ0005	0274-802-1422	FZ	N	830 °C
FZ0006 SI-N800C	0274-802-1427 0274-802-1427	FZ FZ	N N	unannealed 800 °C

Table III

## Electrical Parameters at 300 K

Sample & Temp.	$R_{II}$ $\text{cm}^3/\text{coul}$	$\rho_r$ $\text{ohm-cm}$	Carrier Conc. $\text{cm}^{-3}$	$\mu_{II}$ $\text{cm}^2/\text{V-sec}$
Annealed Si:N Samples				
FZ0006 unannealed	$1.62 \times 10^6$	1180	$3.85 \times 10^{12}$	1380
SI-N800C 800 °C	$2.10 \times 10^5$	302	$2.97 \times 10^{13}$	696
FZ0004-A 800 °C	$8.60 \times 10^5$	652	$7.26 \times 10^{12}$	1320
FZ0005 830 °C	$4.76 \times 10^5$	801	$1.31 \times 10^{13}$	593
FZ0001-A 900 °C	$6.49 \times 10^5$	600	$9.62 \times 10^{12}$	1080
Phosphorus Doped CZ Sample				
CZ-AN-001 900 °C	$2.20 \times 10^3$	1.62	$2.84 \times 10^{15}$	1360
NTD Si:N Samples				
FZ0002 800 °C	$6.88 \times 10^4$	35.6	$9.07 \times 10^{13}$	1930
FZ0003 800 °C	$4.66 \times 10^5$	34.1	$1.34 \times 10^{14}$	1370
High Purity NTD FZ Sample				
NT2-07-SN 800 °C	$1.95 \times 10^5$	1281	$1.34 \times 10^{14}$	1530

300 Kelvin. The results for the phosphorus doped sample, CZ-AN-001, are within 5.3% of the expected results for resistivity and 4.6% for mobility when compared to the data in Figure 20 and 21 (37:29,32). It should be recalled that although drift mobility is equal to conductivity mobility where one conduction species (either electrons or holes) dominates, the Hall mobility is equal to the conductivity mobility only when the r-factor,  $r$ , is equal to one. Thus, conclusions about conductivity mobility derived from the Hall mobility data should not be made too quickly.

Assuming for the moment that in these experiments  $r = 1$ , Table IV gives a comparison of the experimental values for carrier concentration and mobility with values taken from the graphs in Figures 20 and 21. Resistivity data was used to determine the carrier concentration because it is directly measured. Most of the samples have carrier concentrations in the range of  $10^{12}$  to  $10^{13}$  electrons/cm<sup>3</sup> which is below the range given in Fig. 21. At low concentrations impurity scattering is negligible and the mobility is entirely determined by phonon scattering (21:308-317;23). From the graph of Figure 21 this limit is reached around an impurity concentration of  $10^{15}$  cm<sup>-3</sup>. The limiting value is 1500 cm<sup>2</sup>/V-sec. However, the mobility of the Si:N NTD samples vary as much as 28.6% while the high purity sample (NT2-07-SN) varies by 8.7%.

The Si:N samples should not be compared with the resistivity/concentration graph in Fig. 20, as this graph

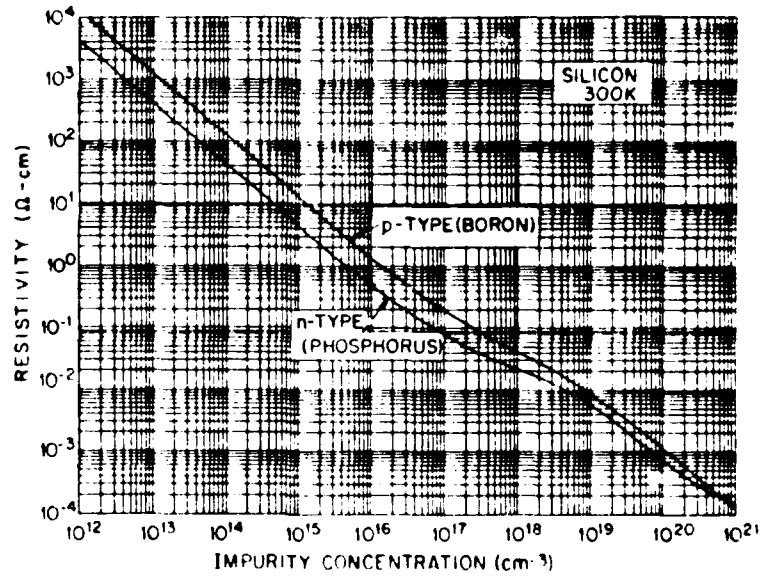


Figure 20. Resistivity versus Impurity Concentration for Silicon at 300 K (37:32)

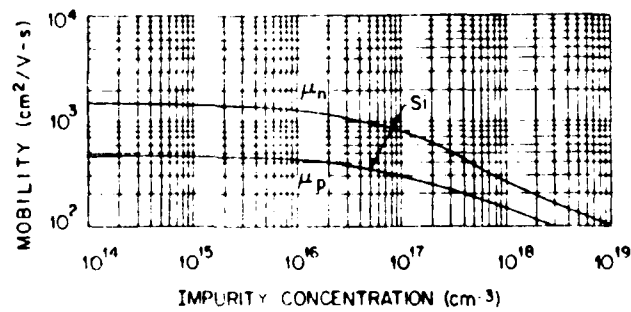


Figure 21. Drift Mobility of Silicon versus Impurity Concentration at 300 K (37:29)

Table IV

Comparison of Experimental Data with Values from  
Figures 20 and 21

Sample	$\rho_r$ ohm-cm	Carrier Conc. $\text{cm}^{-3}$	Mobility $\text{cm}^2/\text{V-sec}$
Experiment: CZ-AN-001 Sze's data: Deviation:	1.62	$2.84 \times 10^{15}$ $3 \times 10^{15}$ 5.3%	1360 1500 9.3%
Experiment: FZ0002 Sze's data: Deviation:	35.6	$9.07 \times 10^{13}$ $9 \times 10^{13}$ 0.7%	1930 1500 28.6%
Experiment: FZ0003 Sze's data: Deviation:	34.1	$13.4 \times 10^{13}$ $13 \times 10^{13}$ 3.1%	1370 1500 6.7%
Experiment: NT2-07-SN Sze's data: Deviation:	128	$3.21 \times 10^{13}$ $3 \times 10^{13}$ 7.0%	1520 1500 1.3%

was generated from phosphorus doped silicon data. The generalized resistivity curves for n and p type silicon published by Irvin gives data for material doped in the range of  $10^{14}$  to  $10^{21} \text{ cm}^{-3}$  (14). Irvin's curve for n-type material was compiled from various Four-point probe resistivity and Hall experiments performed on silicon material doped with group V donors, but not nitrogen (14:388-391). However, if the electron mobility is assumed to be about  $1500 \text{ cm}^2/\text{V-sec}$ , then the data in Table III shows that the Si:N samples have much lower than expected mobilities. Resistivity and mobility is the highest for the unannealed sample, FZ0006, but its concentration is the lowest. This is consistent with Fig. 21, which shows that

mobility decreases with increasing concentration. At 1380  $\text{cm}^2/\text{V-sec}$  the mobility of FZ0006 is nearly the same as CZ-AN-001 at 1360  $\text{cm}^2/\text{V-sec}$ , but the concentration differs by 1000. After FZ0006 was annealed, the sample name was changed to SI-N800C in order to keep the data files separate. Table III shows that resistivity, carrier concentration, and mobility all decreased. Although Table III lists Si:N samples with increasing annealing temperatures, no clear trend is established, but it appears that annealing does affect the material.

#### Comparison of Electrical Data from 20 to 380 K

The Hall experiments were performed at temperatures ranging from 20 to 380 K. The plots of temperature dependent data give more information as to the nature of the material. Comparisons are made by plotting various samples on the same graph. Plots were made of the carrier concentration, Hall coefficient, resistivity, and Hall mobility versus temperature.

Figures 22 through 23 plot the data for the Si:N samples: FZ0001-A, FZ0006, and SI-N800C. FZ0006 is the unannealed Si:N sample, while SI-N800C is the same sample annealed at 800°C. FZ0001-A was annealed at 900°C. Data below 40 K could not be obtained for FZ0006. Resistivity above  $10^3$  ohm-cm, resulted in excessively long settling time.

The Hall coefficient, which is a directly measured

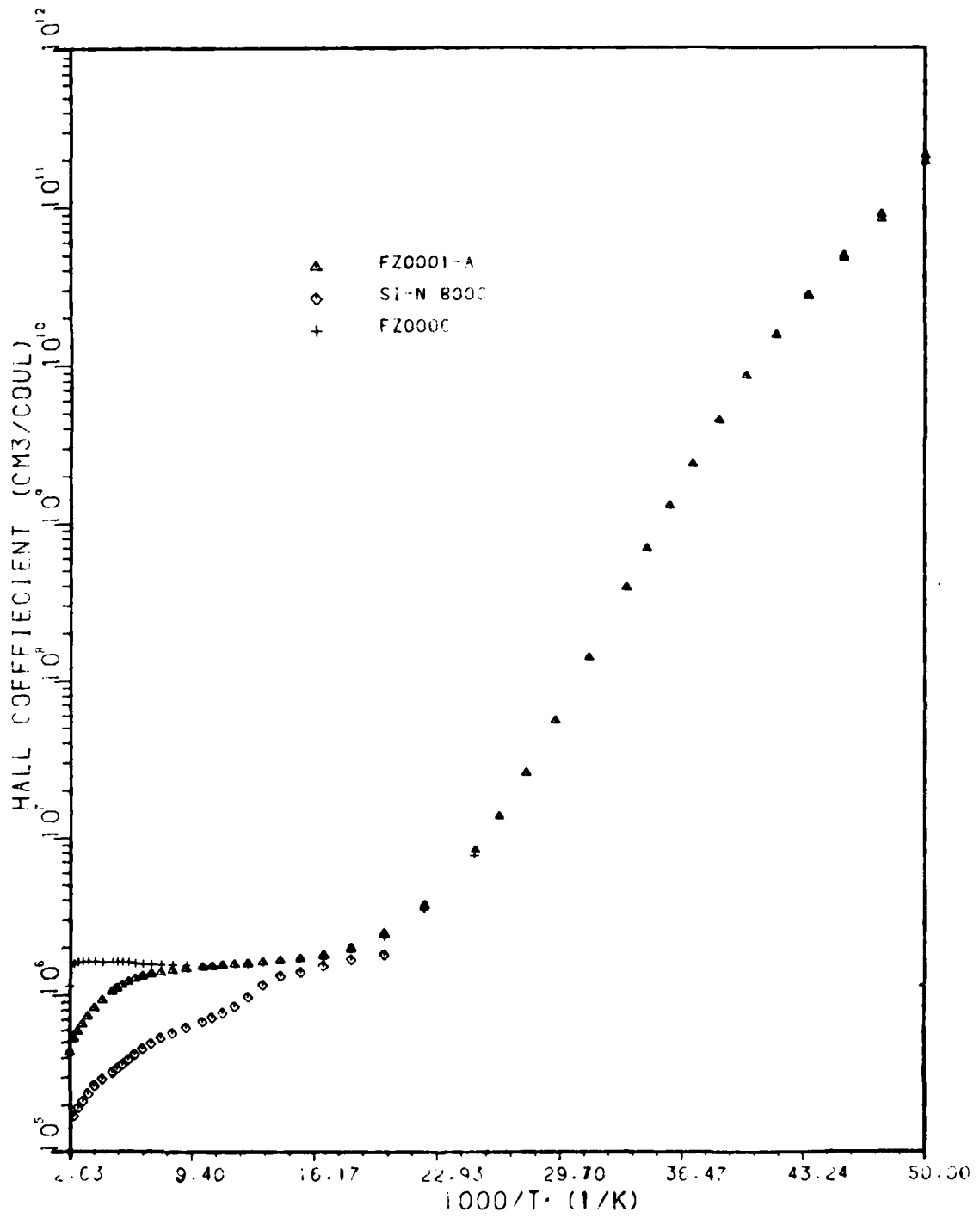


Figure 22. Hall Coefficient of Three Si:N Samples versus Inverse Temperature



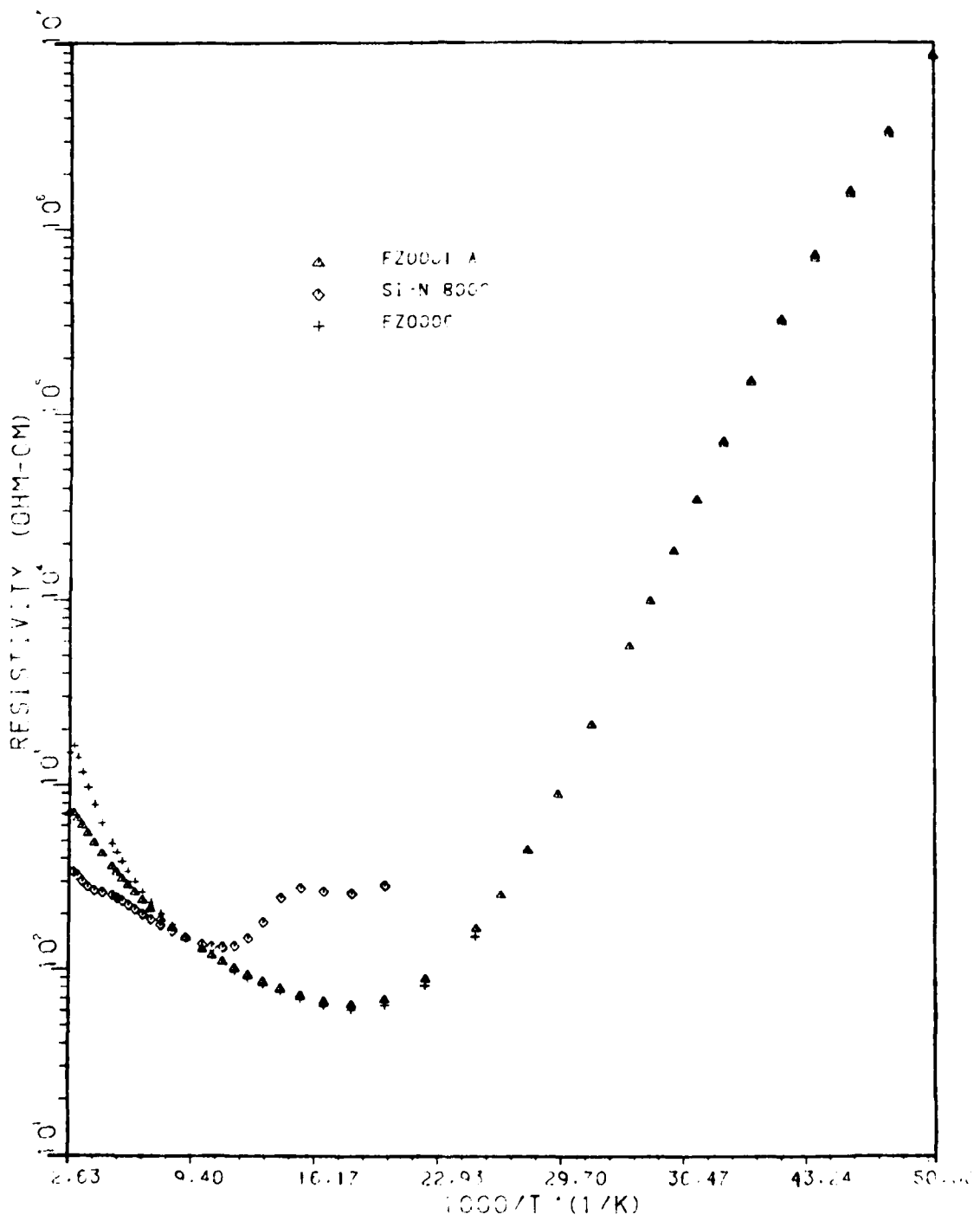


Figure 23. Resistivity of Three Si:N Samples versus Inverse Temperature

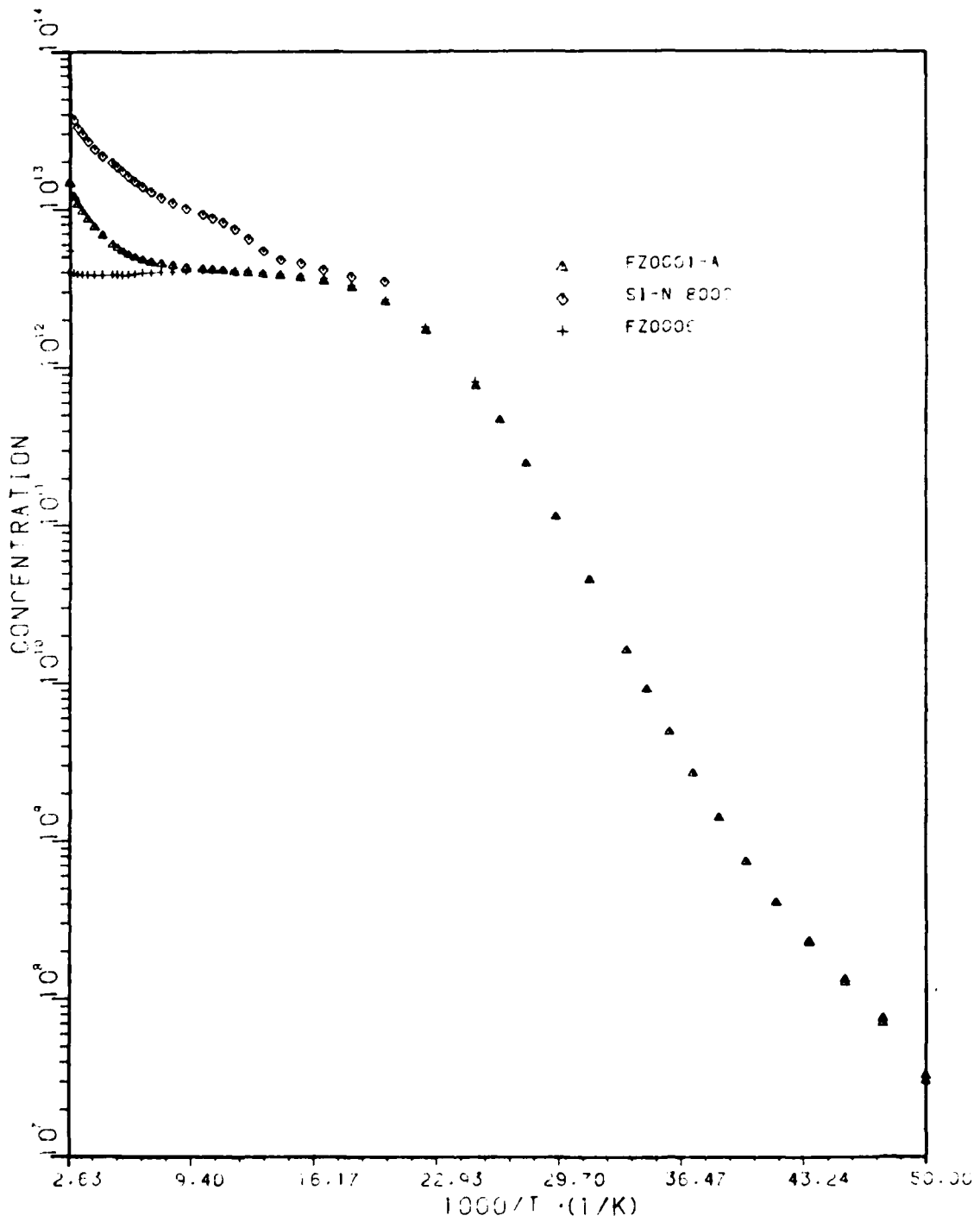


Figure 24. Carrier Concentration of Three Si:N Samples versus Inverse Temperature

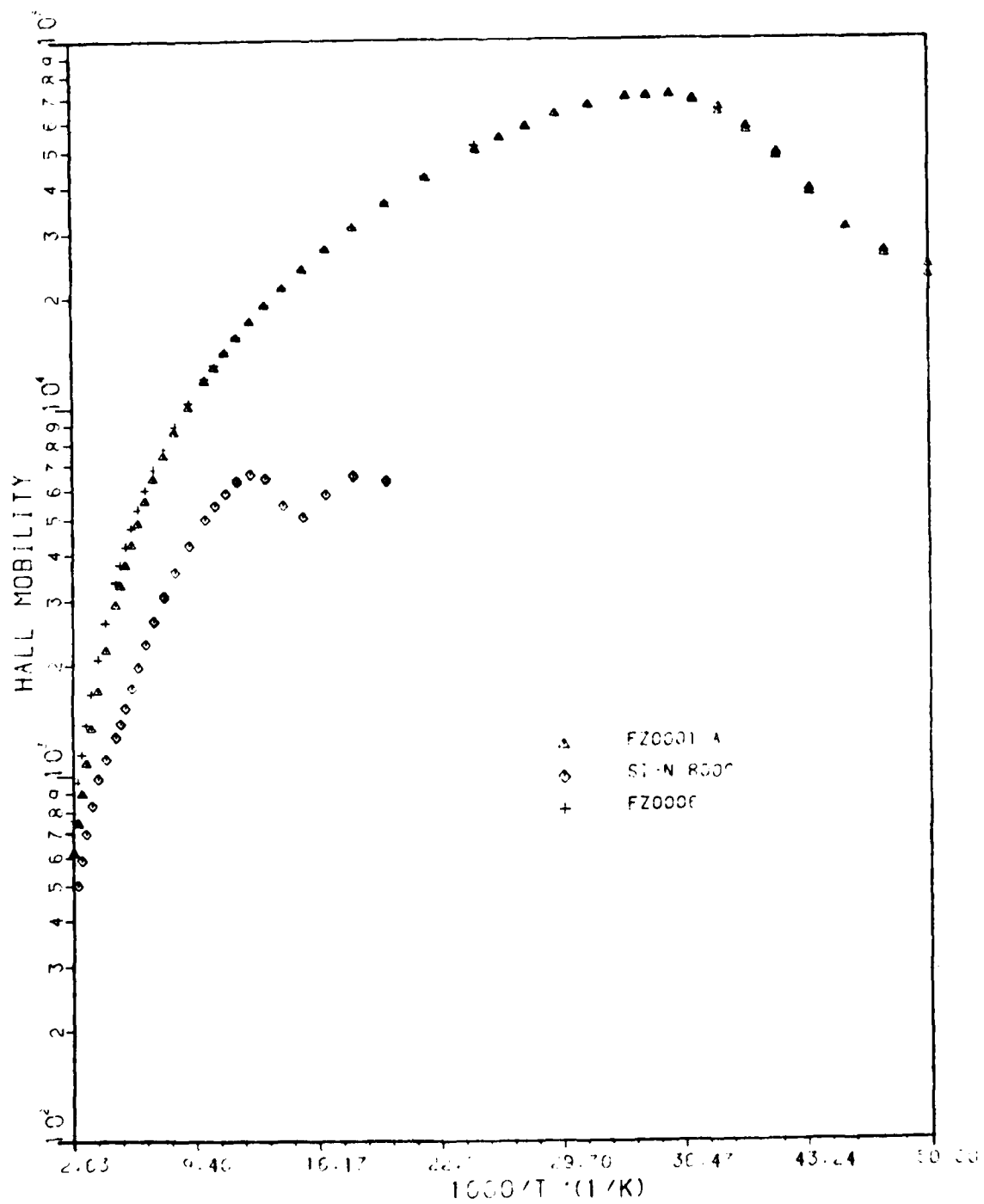


Figure 25. Hall Mobility of Three Si:N Samples versus Inverse Temperature

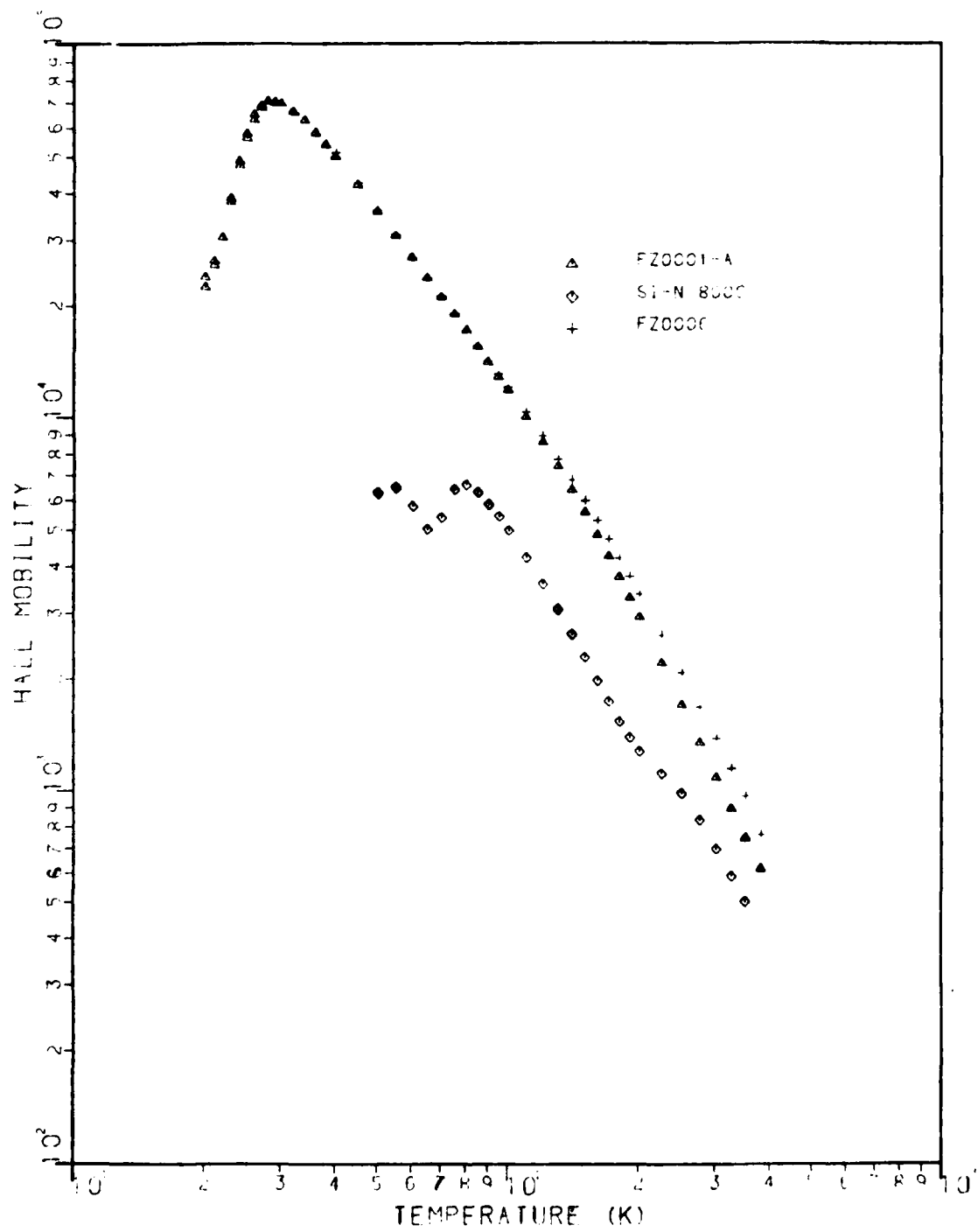


Figure 26. Hall Mobility of Three Si:N Samples versus Temperature

parameter, is plotted with inverse temperature (Fig 22). After annealing at 800°C, the unannealed sample (FZ0006) has changed considerably in the high temperature region (SI-N800C). It does not track the unannealed FZ0006 or the 900°C sample (FZ0001-A). FZ0006 and FZ001-A track each other well in the low temperature regions but start to separate above 106 K.

The other directly measured parameter is resistivity. Resistivity is also plotted against inverse temperature (Fig 23). The plot of SI-N800C appears to be highly irregular compared to the other samples and FZ0006. In fact, FZ0001-A and FZ0006 are typical resistivity plots. Above 55 K, in the resistivity plots of FZ0001-A and FZ0006, resistivity increases with temperature. At this temperature all of the donors are ionized and the increase in resistivity is from phonon scattering (21:277-281, 308-317). Below 55 K, carrier concentration decreases so resistivity increases. The concentration versus inverse temperature plot, Figure 24, shows that the carrier concentration is saturated at 55 K.

Carrier concentration which is computed from Eq. 9 assumes an  $r$ -factor of one. Thus, the carrier concentration is inversely proportional to  $R_H$ . The concentration versus temperature curve in Fig. 24 shows that the carrier concentration levels off at high temperatures for the unannealed sample, FZ0006, but annealing causes a change in the material so that

concentration starts to increase again. FZ0001-A exhibits the same behavior in the high temperature region. This implies that deep levels are activated by high temperature annealing, but it appears that increasing the temperature does not result in the proportional increase in carriers.

For the readers convenience, Hall mobility is plotted both with inverse temperature and temperature in Figures 25 and 26. Hall mobility varies proportionally with  $R_H$  and inversely with  $p_r$  (Eq. 11). For FZ0001-A mobility peaks at about  $7 \times 10^4$  cm<sup>2</sup>/V-sec at 30 K. SI-N800C has a peculiar decrease and increase below 85 K and is displaced upwards at 225 K. This is actually not so peculiar in that the resistivity and the Hall coefficient curves were not typical. What is peculiar is that a sample that produced typical data has an anomalous  $p_r$  after annealing, but another sample annealed at a higher temperature behaves quite well.

The next set of figures show the phosphorus doped CZ sample is plotted with an FZ sample, FZ0001-A. These were both annealed at the same time at 900 °C. The Hall coefficient plot, Fig. 27, shows that the  $R_H$  of the phosphorus doped CZ sample, CZ-AN-001, decreases slightly as the temperature decreases in the 380 to 200 K region then starts to increase as the temperature decreases. However, Fig. 28 shows a well behaved resistivity plot. The carrier concentration plot, Fig. 29, shows the carrier concentration of CZ-AN-001 decreasing at above 200 K.

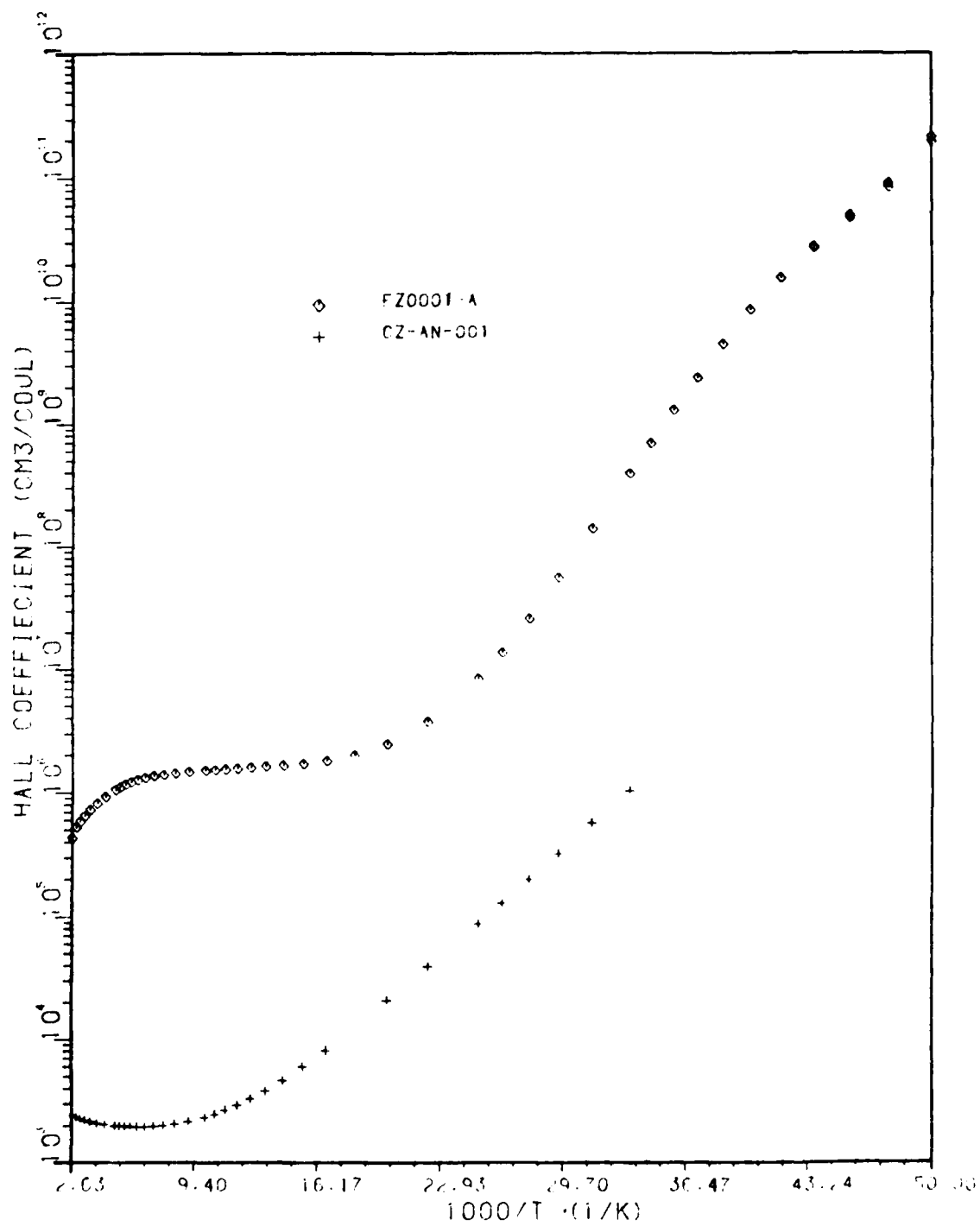


Figure 27. Hall Coefficient of CZ and Si:N Samples Annealed at 900 °C

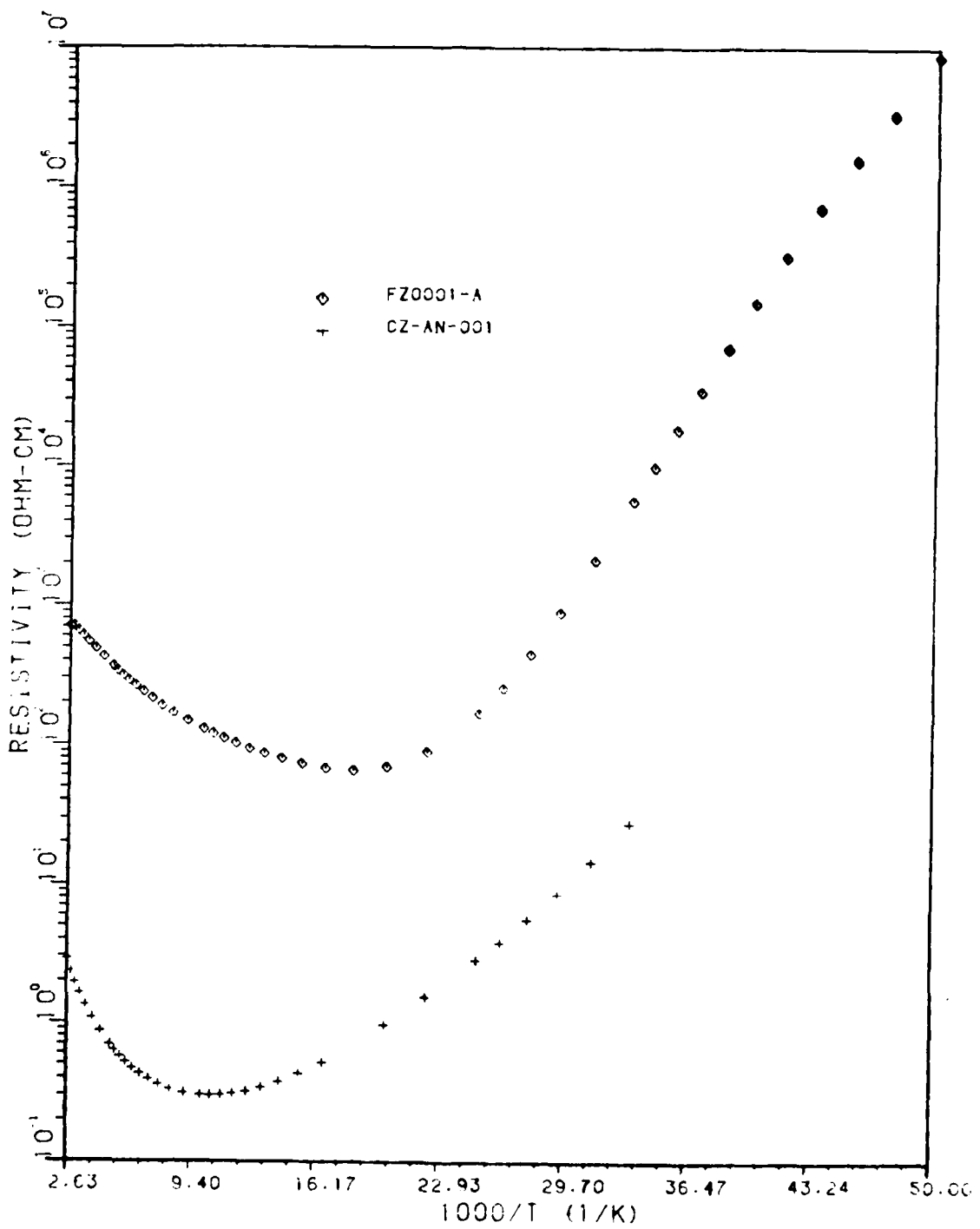


Figure 28. Resistivity of CZ and Si:N Samples Annealed at 900 °C



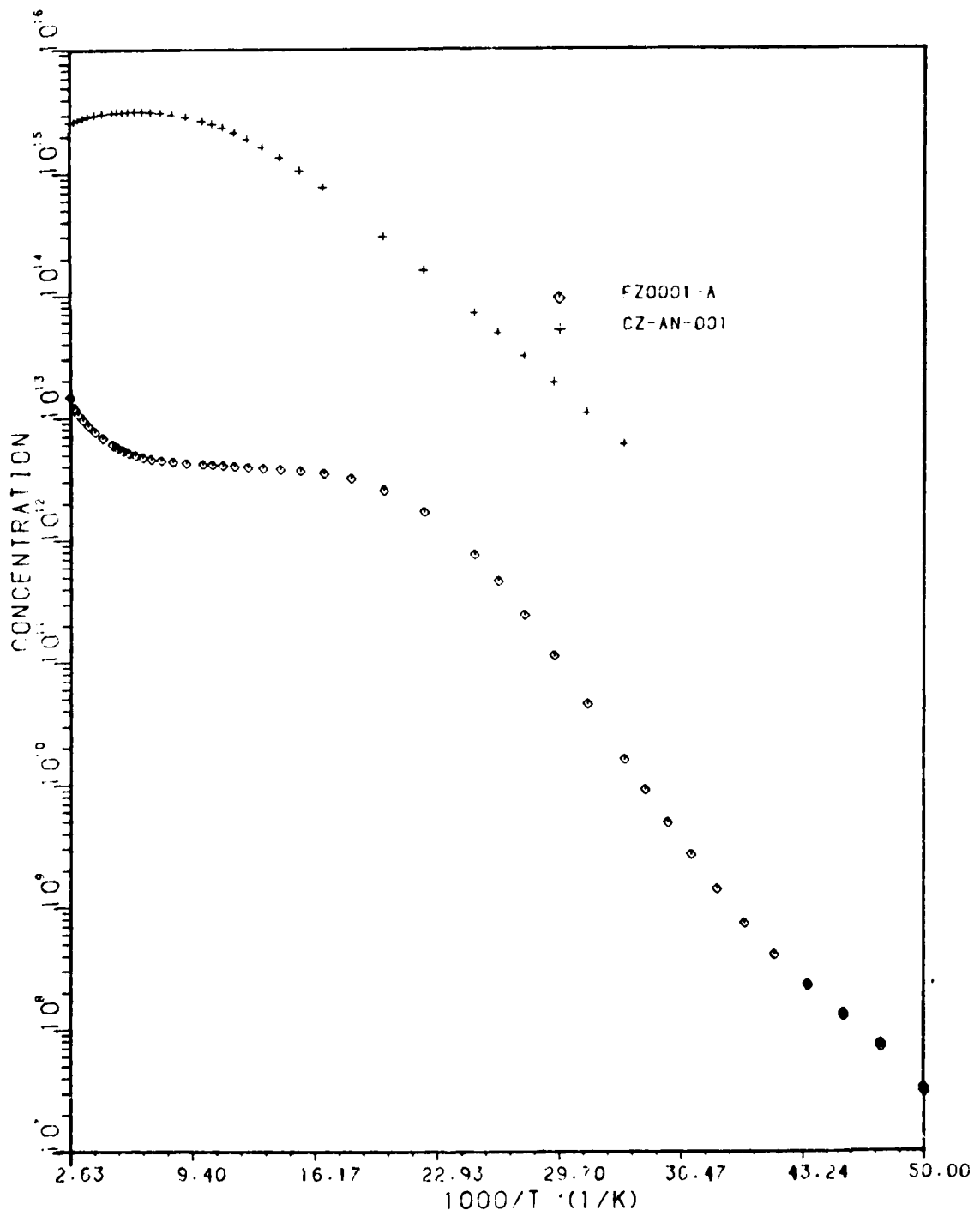


Figure 29. Carrier Concentration of CZ and Si:N Samples Annealed at 900 °C

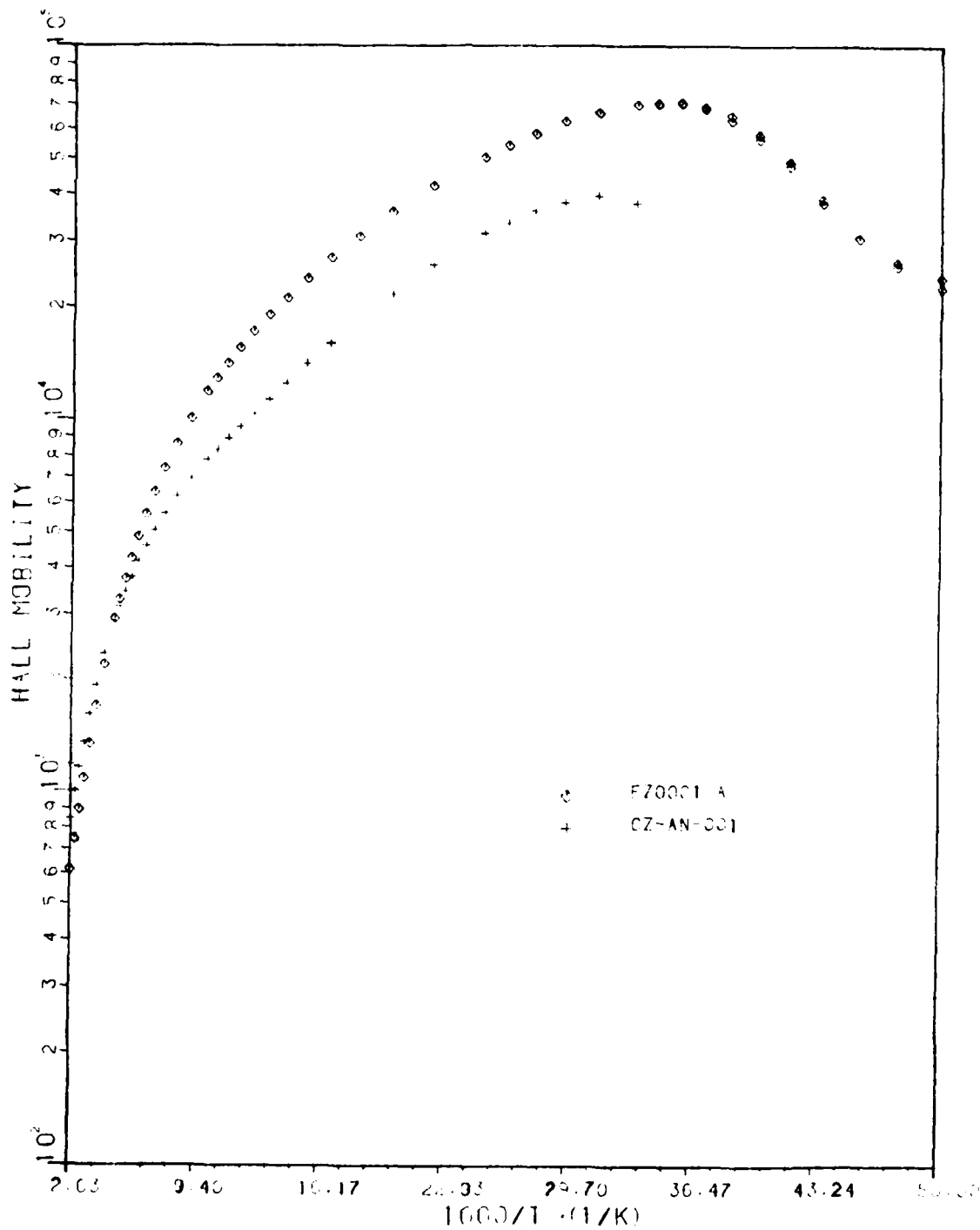


Figure 30. Hall Mobility of CZ and Si:N Sample Annealed at 900 °C versus Inverse Temperature

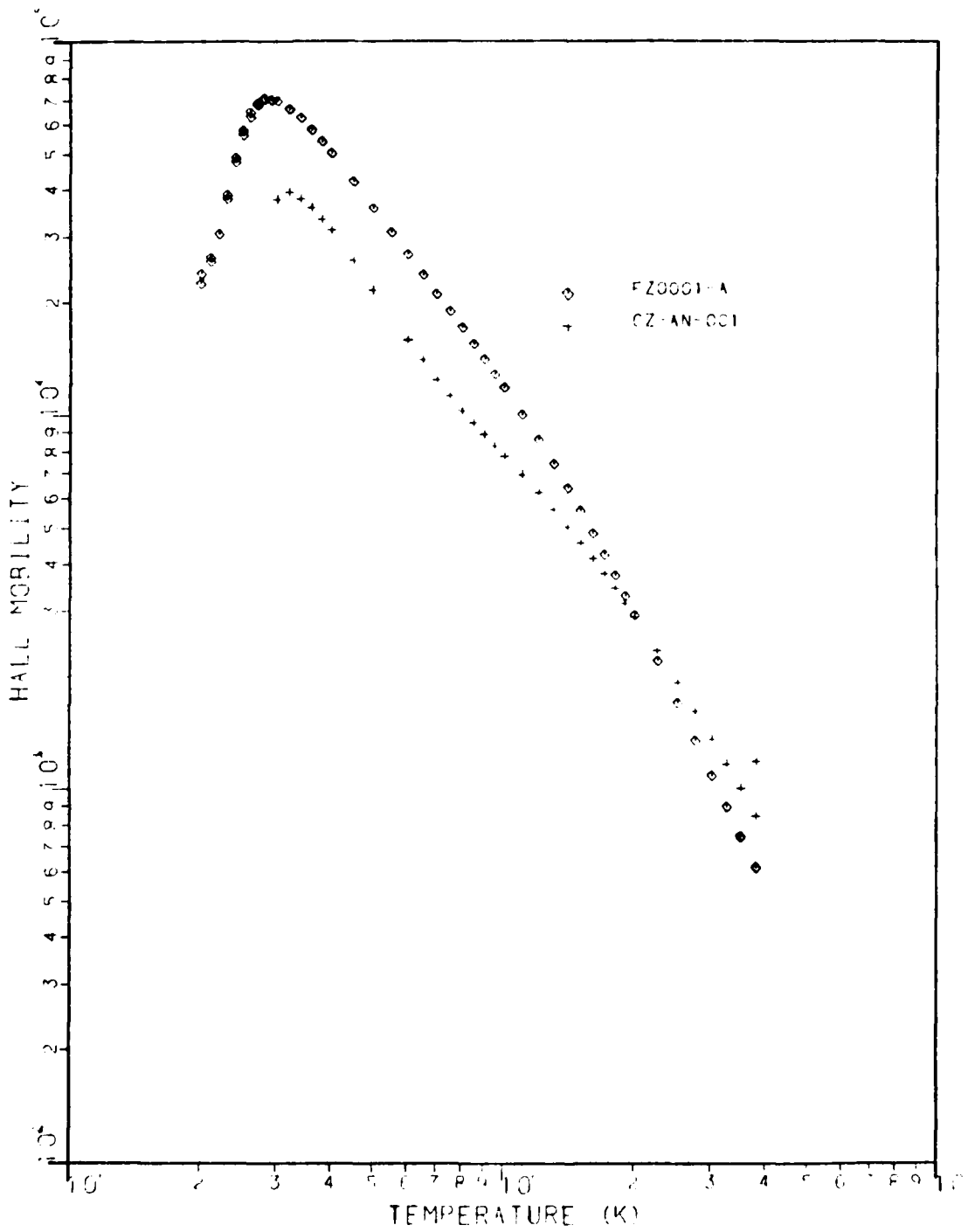


Figure 31. Hall Mobility of CZ and Si:N Samples Annealed at 900 °C versus Temperature

The dip in  $R_H$  in at the 200 to 300 K region is due to temperature dependence in the scattering mechanism. Scattering effects are included in the r-factor which was assumed to be unity at all temperatures. Although very difficult to compute, the r-factor is known to have some temperature dependence (19:66,67). This also explains the decrease in carrier concentration above 200 K. The carrier concentration is calculated from Eq. 9, which is restated here:

$$n = \frac{r}{eR_H} \quad (\text{cm}^{-3}) \quad (9)$$

becomes

$$n = r(T)n_0 \quad (\text{cm}^{-3}) \quad (25)$$

where  $n_0$  is the experimental value of the concentration and  $r(T)$  is the temperature dependent r-factor. A careful re-examination of FZ0006 in Fig. 24 shows a slight decrease in concentration at high temperatures. However, the activation of deeper energy levels in Si:N by annealing seems to overcome the pulling down of the concentration by the r-factor.

Hall mobility is computed using Eq. 11 and the r-factor appears in the Hall coefficient, but the effect of the r-factor is not clear in the Hall mobility plots (Fig. 30 and 31) of CZ-AN-001. The decrease in  $R_H$  may be offset by the resistivity. It is interesting to note that CZ-AN-001 has higher mobility than FZ0001-A, but only above 200 K. FZ0001-A has higher Hall mobility below this temperature. However, because of the r-factor problem, it

is unwise to say that the conduction mobility is exactly equal to the Hall mobility.

Combining the results of the NTD samples into one set of graphs (Figures 32 to 36) show the Si:N samples differ from the high purity sample (NT2-07-5N) mainly in the amount of phosphorus doping. All three track each other well in the Hall coefficient (Fig. 32) and resistivity (Fig. 33) graphs. The figures show that FZ0002 is not as well behaved as the other samples. FZ0002 was performed manually on Hall II while FZ0003 and NT2-07-5N were performed automatically on Hall I. Thus, the slightly erratic behavior of FZ0002 may be due to increased experimental uncertainty. Again there is a slight increase in  $R_H$  at high temperatures in all three plots indicating an r-factor problem. The concentration graph, Figure 34, also has the same decrease in concentration at high temperatures as CZ-AN-001 for all three plots. However, the Hall mobility graphs (Figures 35 and 36) show that FZ0002 and FZ0003 have the same type behavior at low temperatures as seen in SI-N800C (Fig. 25 and 26).

The carrier concentration graph (Fig. 34) shows that at very low temperatures, less than 28 K, the FZ0002 and FZ0003 plots appear to bend away from the NT2-07-5N plot on the concentration graph. This bending outward at low temperatures also appears in Fig. 24 in the plot of FZ0001-A. This may indicate an energy level shallower than phosphorus in the Si:N material. However, there are other

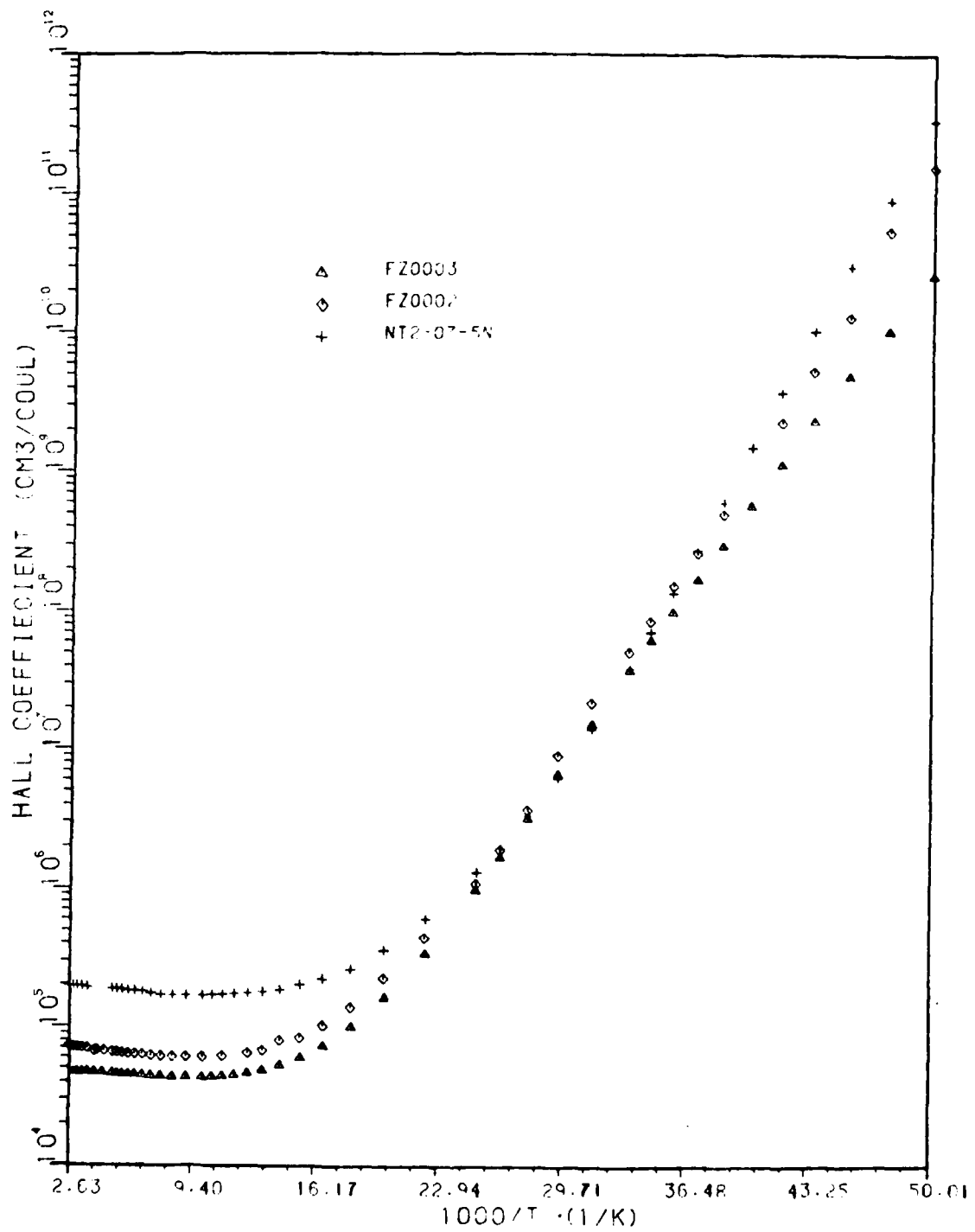


Figure 32. Hall Coefficient of Si:N NTD and High Purity FZ NTD Samples

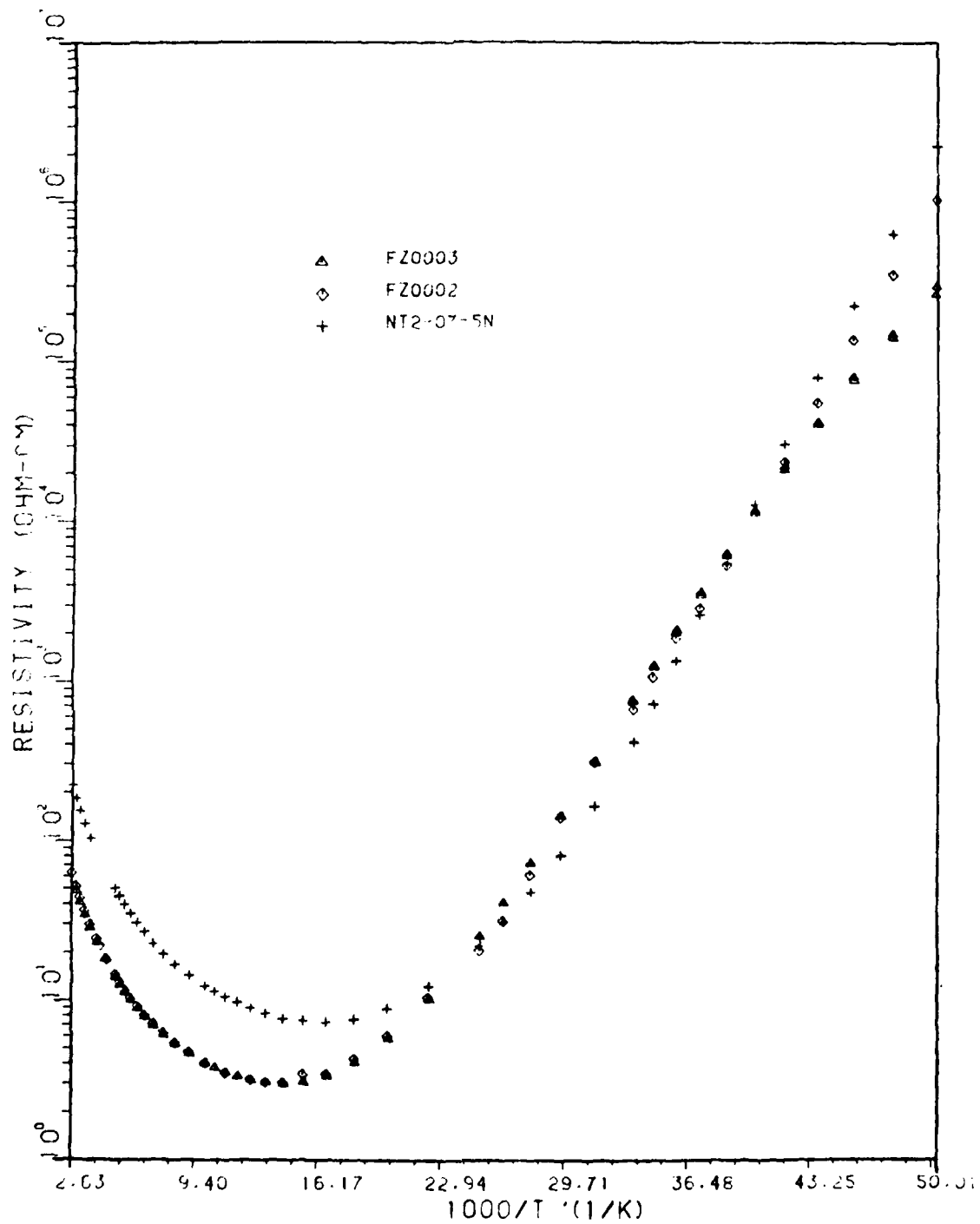


Figure 33. Resistivity of Si:N NTD and High Purity FZ NTD Samples

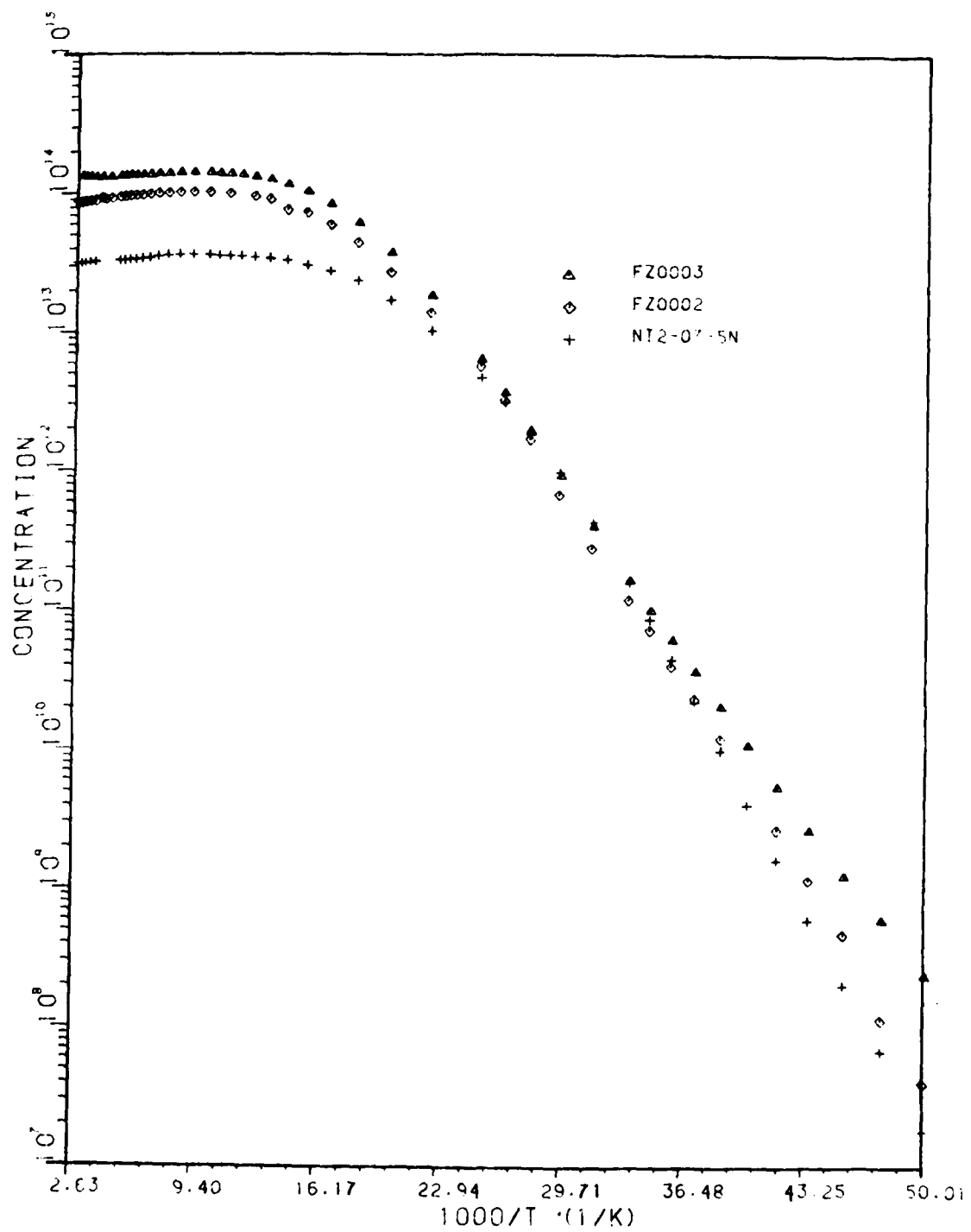


Figure 34. Carrier Concentration of Si:N NTD and High Purity FZ NTD Samples



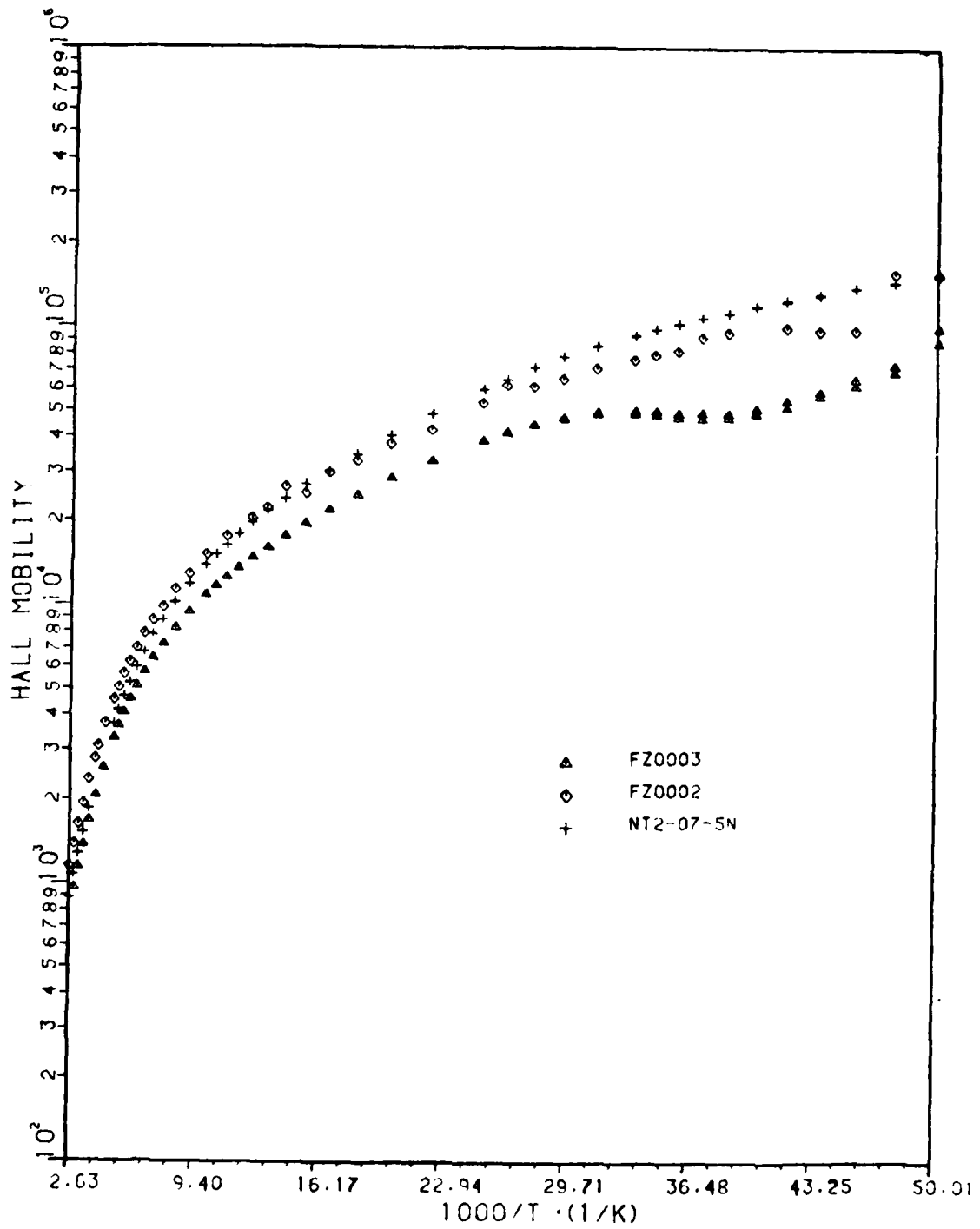


Figure 35. Hall Mobility of Si:N NTD and High Purity FZ NTD Samples versus Inverse Temperature

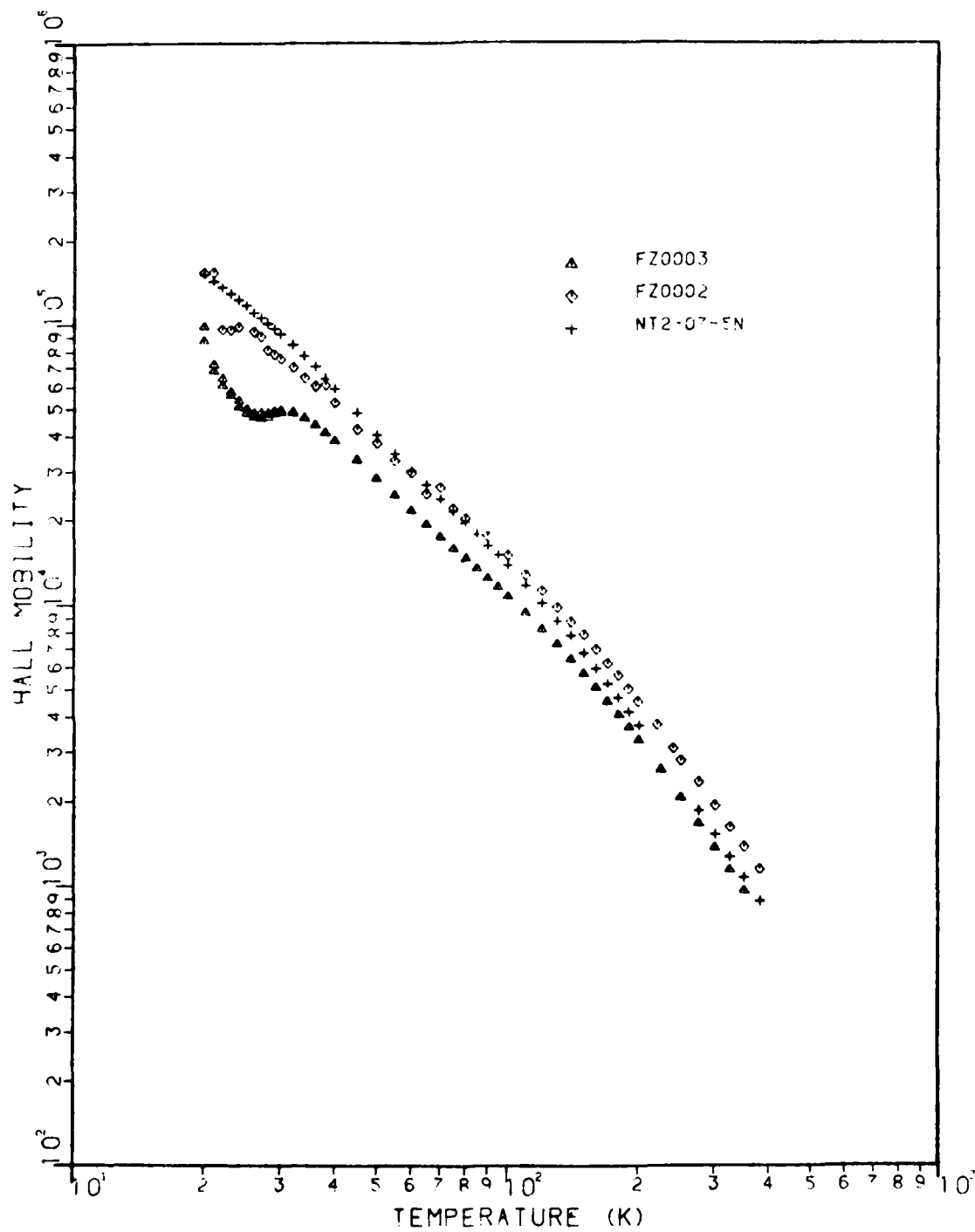


Figure 36. Hall Mobility of Si:N NTD and High Purity FZ NTD Samples versus Temperature

parameters to be considered before any statement can be made.

#### Temperature Dependence of $R_1/R_2$

In Chapter IV it was shown that resistivity as given by van der Pauw (Eq. 22) has an  $f(R_1/R_2)$  term which should be constant over all temperatures, if not, inhomogeneity is implied. This parameter is calculated for every data point in the experiment. It is not unusual to see some temperature dependence at low temperatures.

This was the case for CZ-AN-001, the phosphorus doped CZ sample. Below 30 K there is some temperature dependence in  $R_1/R_2$  as seen in Fig. 37. Figures 38 through 40 plot the CZ-AN-001 data from 30 to 380 K; however, the experimental data started at 20 K. Figures 38 and 39 show a decrease in the Hall coefficient and an increase in concentration below 30 K. This is believed to be due to surface conduction across the sample, because the resistivity does not go above 400 ohm-cm, as seen in Fig. 39. This phenomenon disappears at 30 K as conduction through the sample takes over. The simplest way to deal with this is to eliminate the data below 28 K. In any event, data in this region should not be relied on. This is why Figures 27 through 31 were plotted without the low temperature points.

If temperature dependence is seen over the entire range, then the sample is inhomogenous. Thus, a necessary

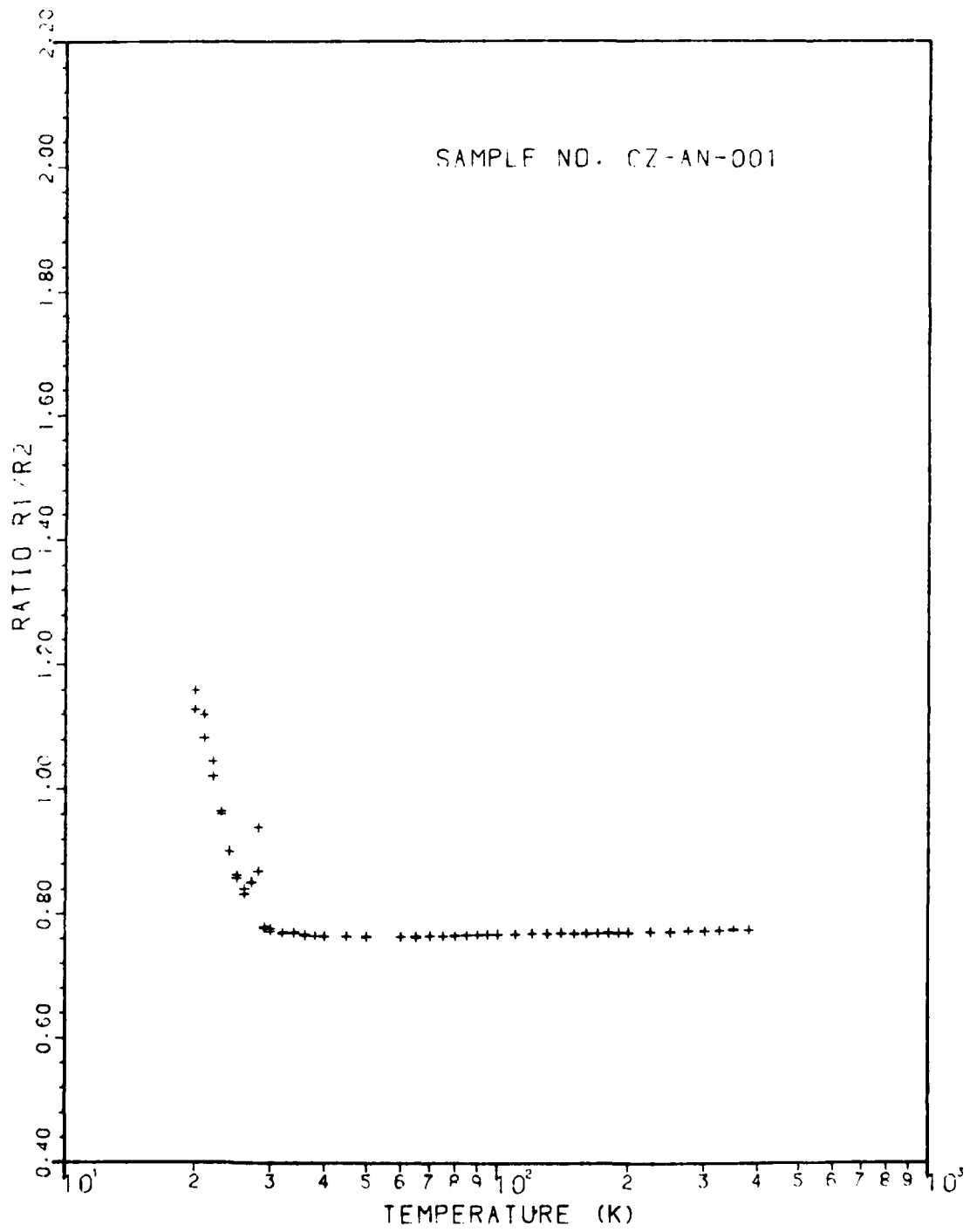


Figure 37.  $R_1/R_2$  Ratio of CZ-AN-001

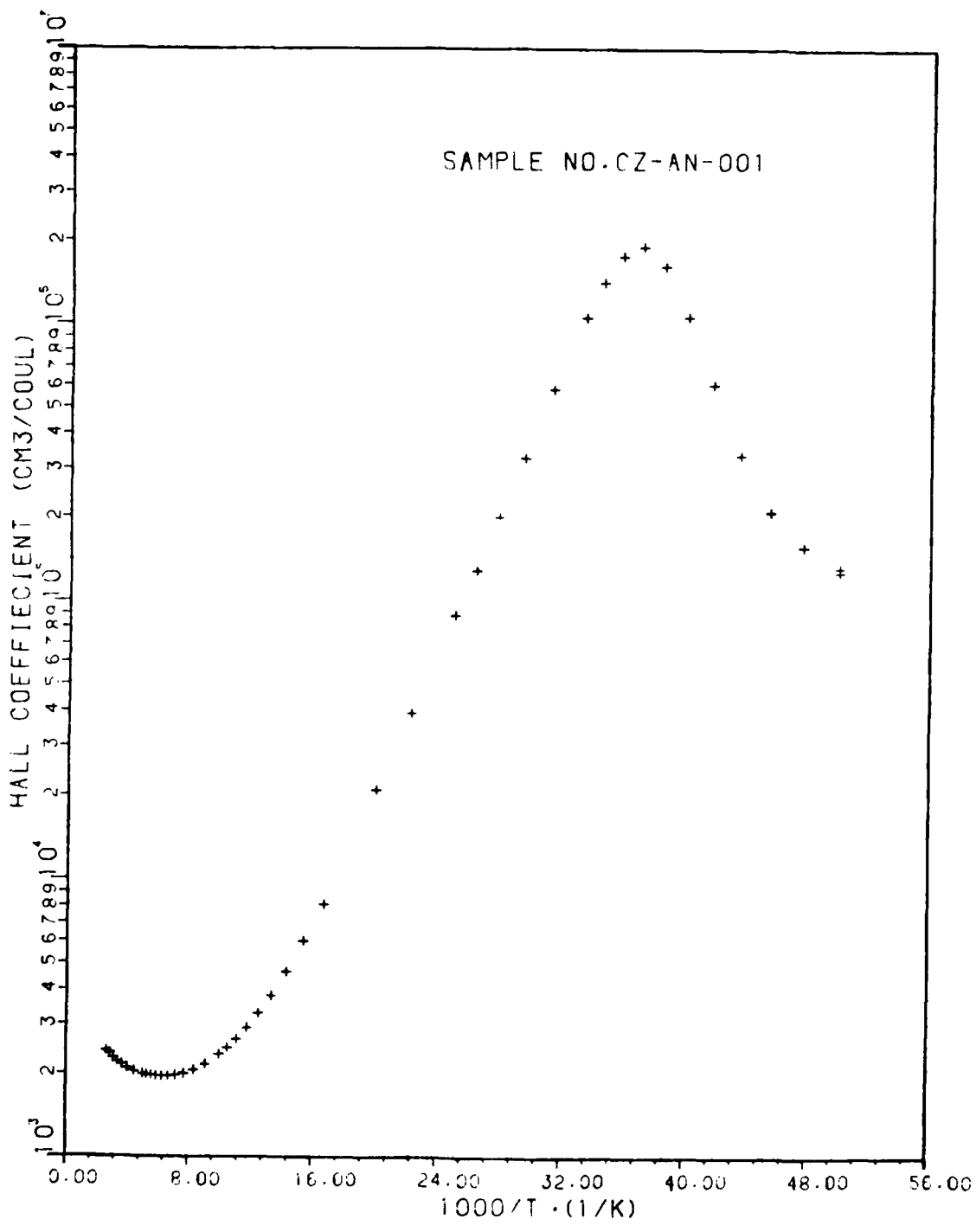


Figure 38. Hall Coefficient of CZ-AN-001 from 20 - 380 K

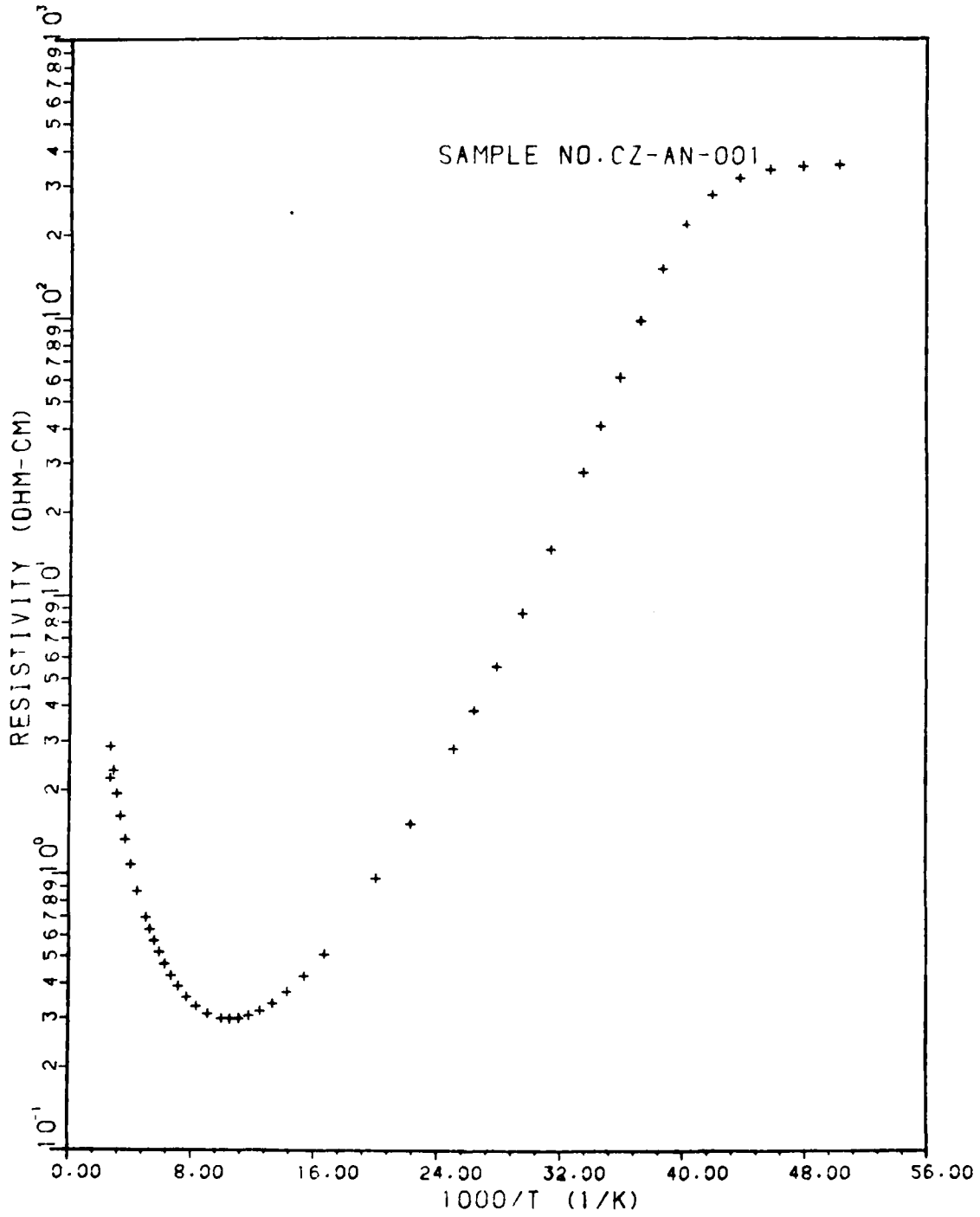


Figure 39. Resistivity of CZ-AN-001 from 20 - 380 K

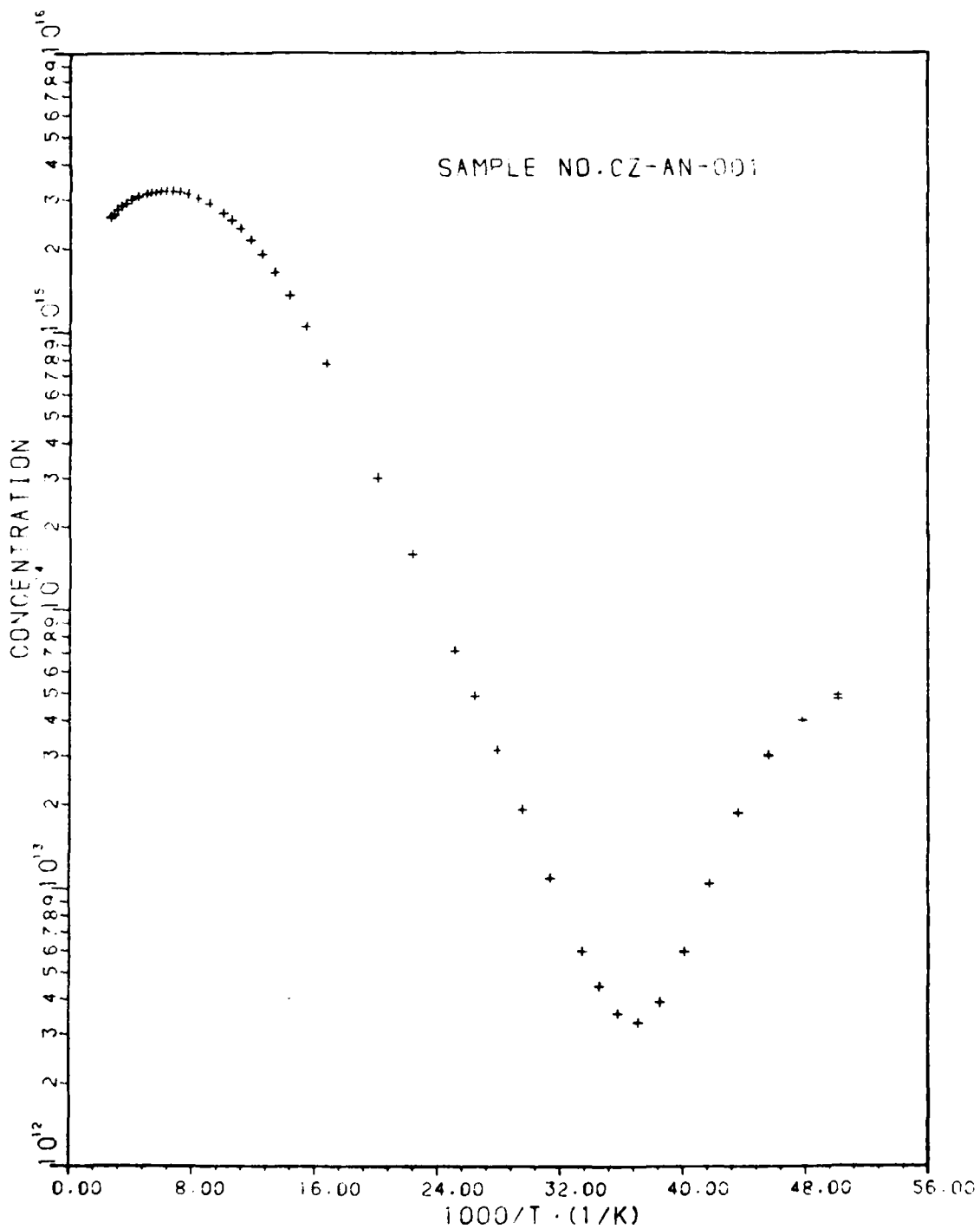


Figure 40. Carrier Concentration of CZ-AN-001 from 20 - 380 K

condition of the experiment has failed. Not only is the resistivity data questionable, but the Hall coefficient data is also unreliable due to the unknown effect of inhomogeneity on the scattering mechanism (r-factor). Unfortunately, this was the case for FZ0004-A and FZ0005 as seen in Figures 41 and 42. Sample 0274-802-1426 (experiment FZ0004 and FZ0004-A) was annealed at 800 °C and sample 0274-802-1422 (experiment FZ0005) was annealed at 830 °C. The data for the first experiment on 0274-802-1426 (FZ0004) showed a temperature dependent  $R_1/R_2$  and anomalous  $R_H$ ,  $\rho_r$ ,  $u_H$ , and concentration plots. It was thought that surface contamination was responsible so the sample was cleaned in a solution of ammonium hydroxide, hydrogen peroxide, and water and new leads soldered on. The results of the second experiment were no better. FZ0005 also had a temperature dependent  $R_1/R_2$ . The graphs of the data for FZ0004-A and FZ0005 are given in Appendix B.

Of the Si:N samples, FZ0001-A and FZ0006 have acceptable  $R_1/R_2$  ratios, but SI-N800C does not. FZ0006 and SI-N800C are the same sample. Before it was annealed FZ0006 had an acceptable  $R_1/R_2$  ratio (Figure 43). Figure 44 shows that after annealing the sample (renamed SI-N800C) is temperature dependent over its entire range and that the difference between the highest and lowest points is 0.36. This indicates that annealing produced a change in the sample that caused it to become



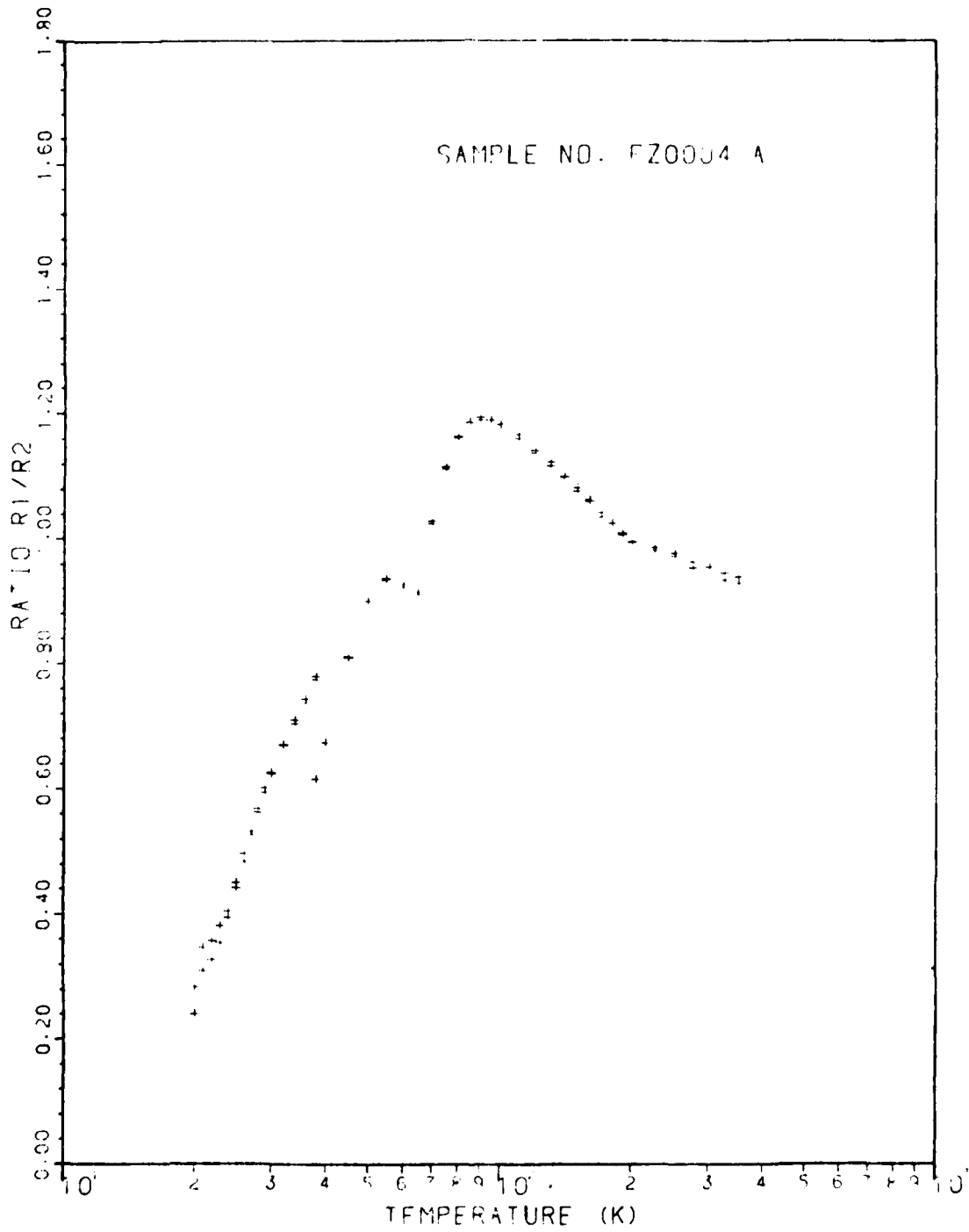


Figure 41. R<sub>1</sub>/R<sub>2</sub> Ratio of Si:N Sample Annealed at 800 °C

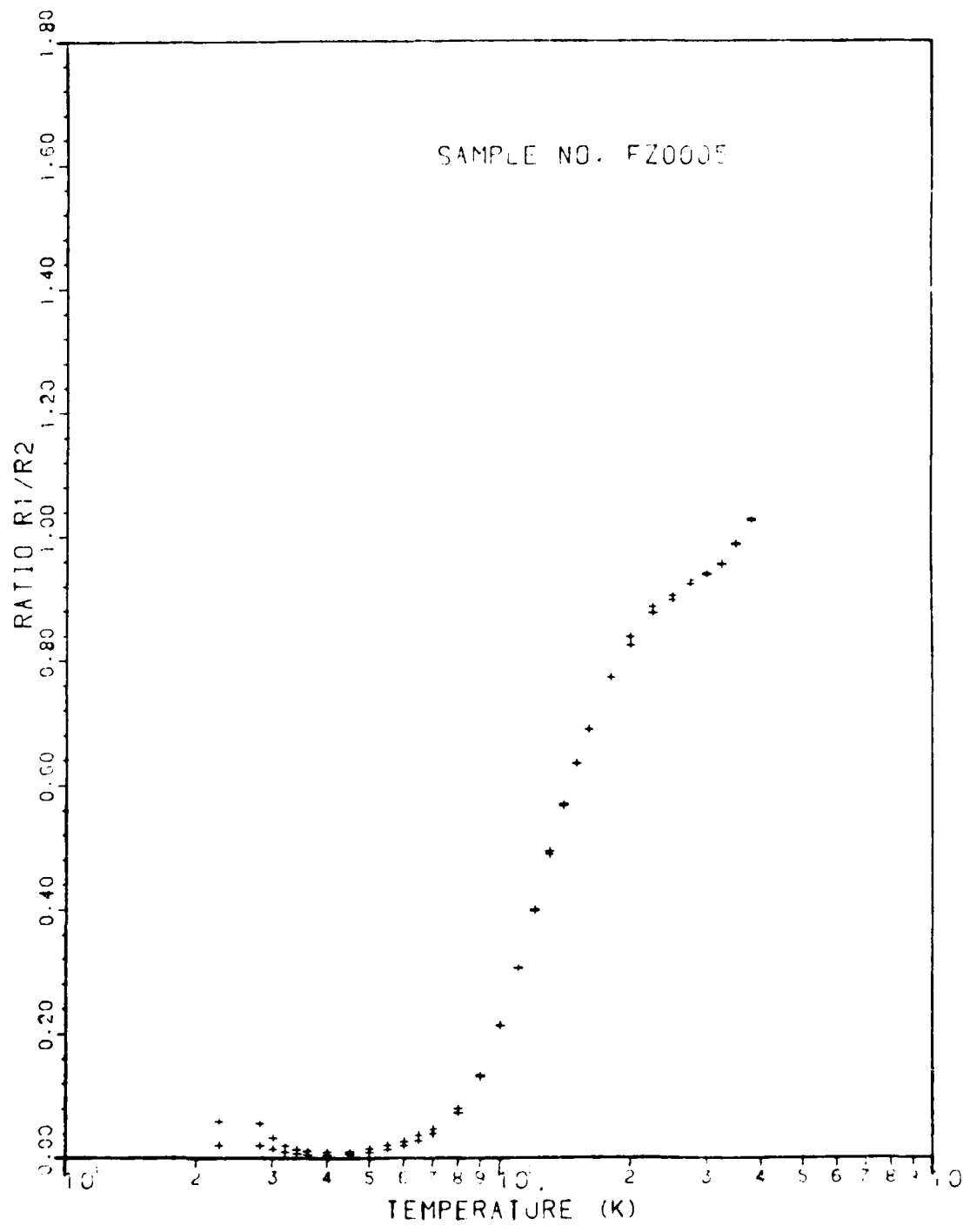
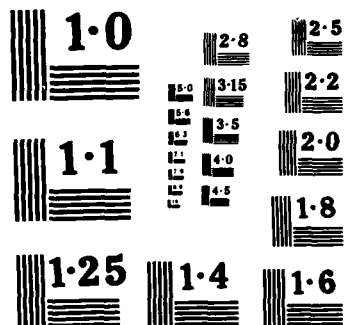


Figure 42.  $R_1/R_2$  Ratio of Si:N Sample Annealed at 830 °C





NATIONAL BUREAU OF STANDARDS  
MICROCOPY RESOLUTION TEST CHART

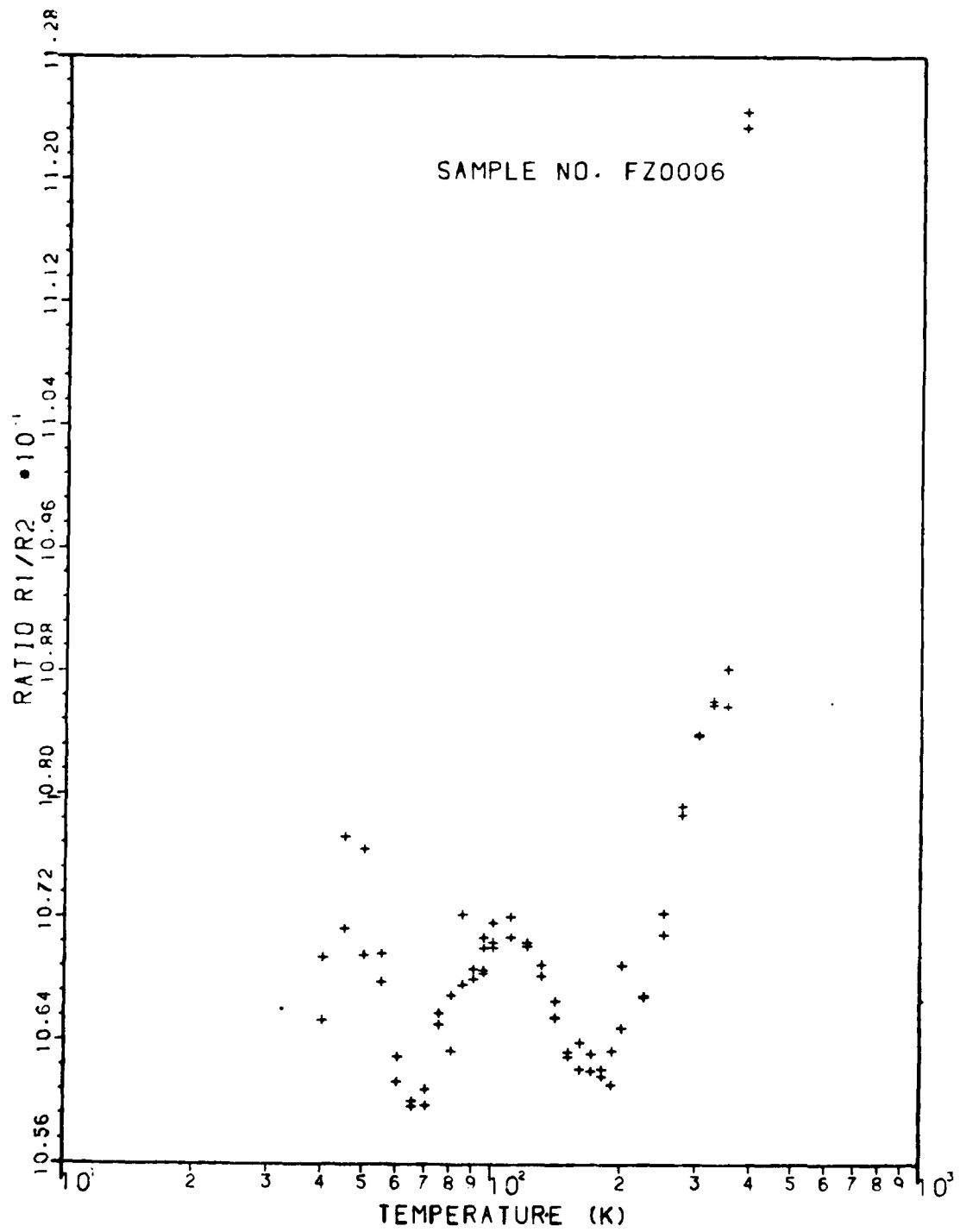


Figure 43.  $R_1/R_2$  Ratio of Unannealed Si:N Sample

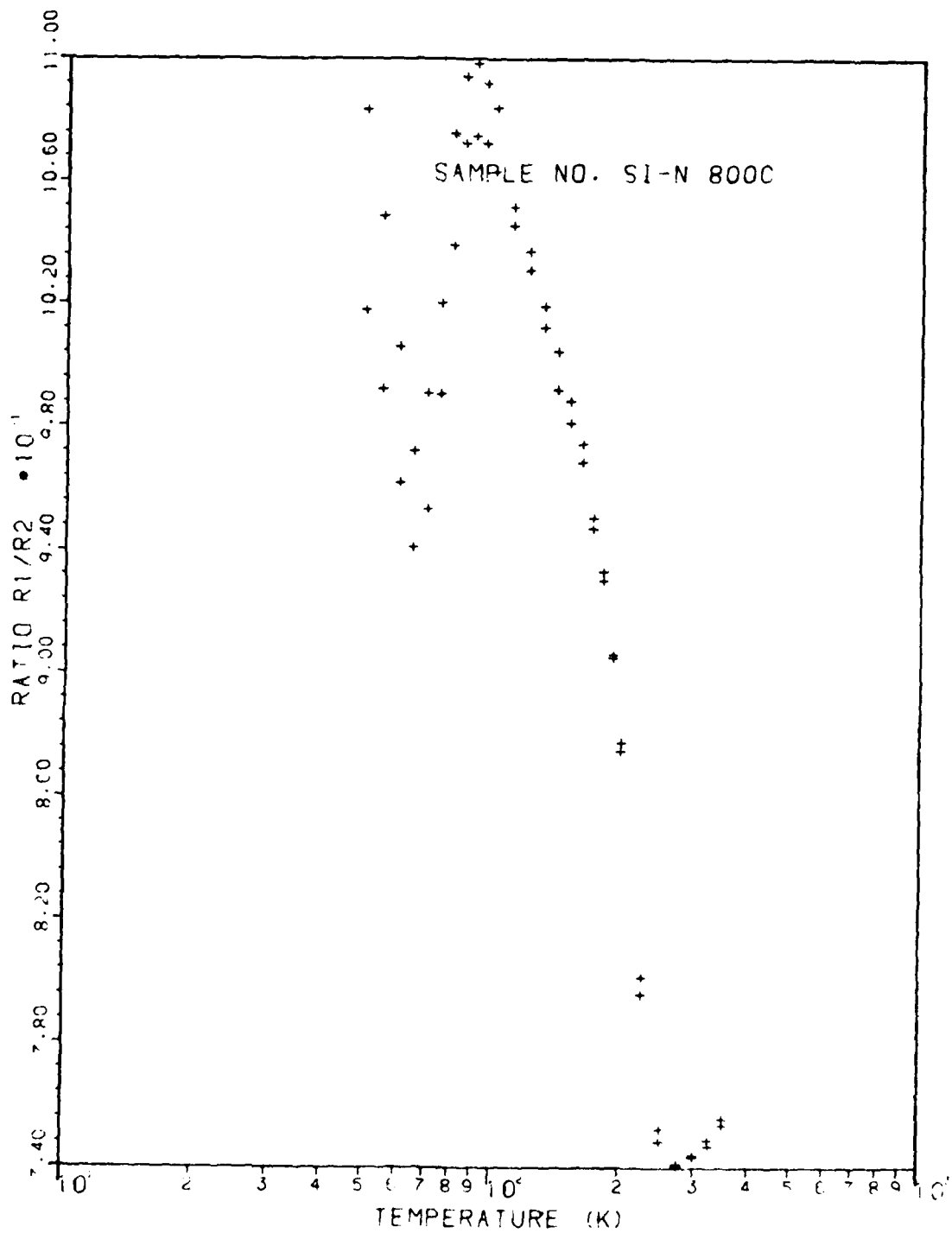


Figure 44.  $R_1/R_2$  Ratio of Si:N Sample Annealed at 800 °C (SI-N800C)

inhomogeneous. FZ0001-A has a pronounced temperature dependence in  $R_1/R_2$  at low temperatures as seen in Fig. 45. If the points below 27 K are eliminated, then the difference between the highest and lowest point is 0.16.

Some temperature dependence in  $R_1/R_2$  is not surprising in the NTD samples. The NTD process damages the lattice; however, almost all of the damage is repaired by annealing (23). The residual damage results in slightly inhomogeneous material. Figure 46 shows the  $R_1/R_2$  plot for NT2-07-5N. The ratio is temperature dependent but has a variation of 0.136. The  $R_1/R_2$  ratio in FZ0002 appears to have a strong temperature dependence in  $R_1/R_2$  below 45 K and above 45 K the  $R_1/R_2$  plot seems to become a straight line (Figure 47). However, the variation of  $R_1/R_2$  at temperatures from 45 to 380 K have a variation of 0.4. This experiment was performed manually and may have more experimental uncertainty. The data points display a random pattern in this region rather than a smooth upwards or downward trend. Thus, this  $R_1/R_2$  is marginally acceptable above 40 K. The last sample, FZ0003, also shows a strong temperature dependence at low temperatures and then levels out (Fig. 48). The total variation in  $R_1/R_2$  is 0.80 over the entire temperature range, but above 40 K the variation is 0.12. This means that the  $R_1/R_2$  in FZ0003 is acceptable at temperatures above 40 K.

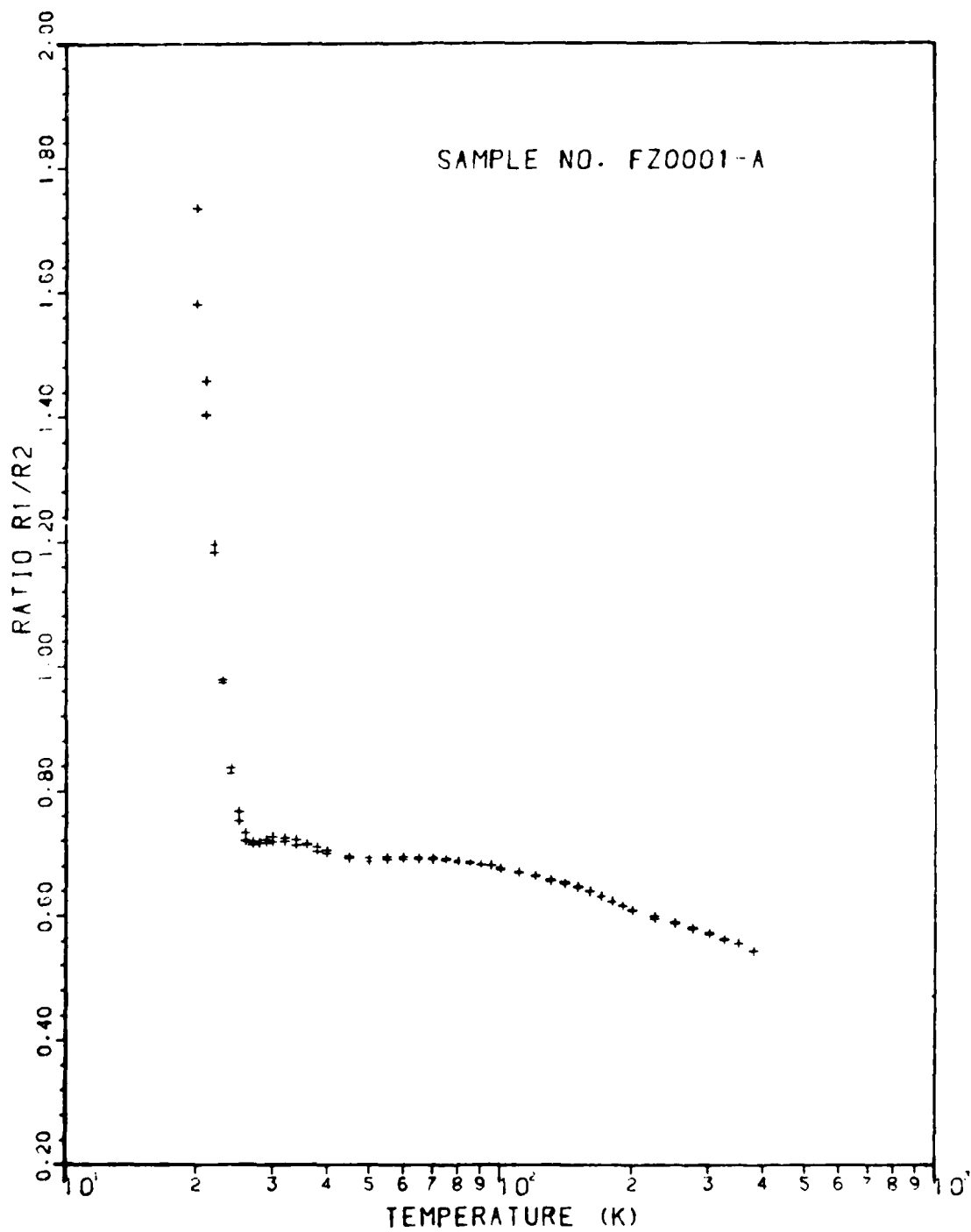


Figure 45.  $R_1/R_2$  Ratio of Si:N Sample Annealed at 900 °C



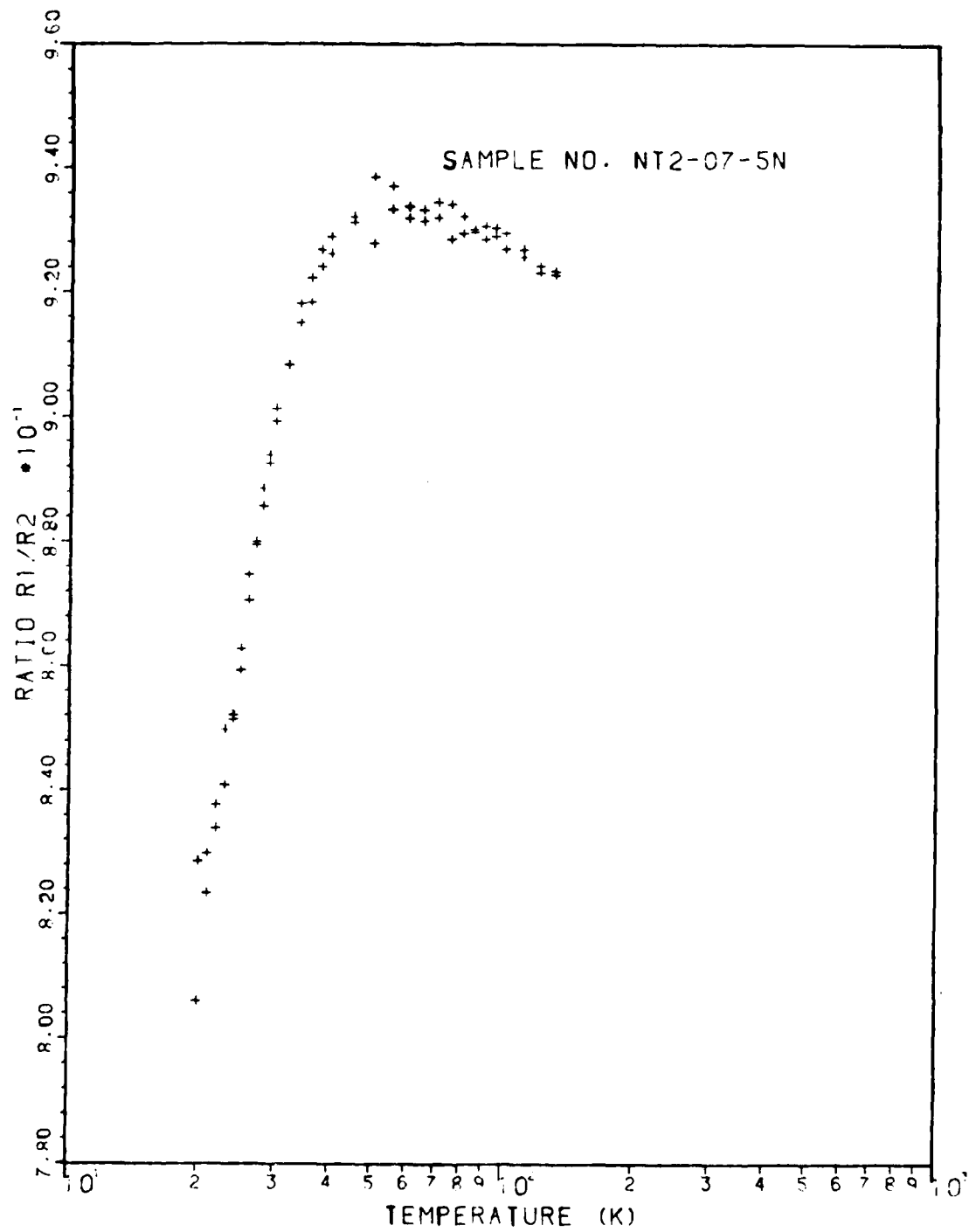


Figure 46.  $R_1/R_2$  Ratio of High Purity FZ NTD Sample

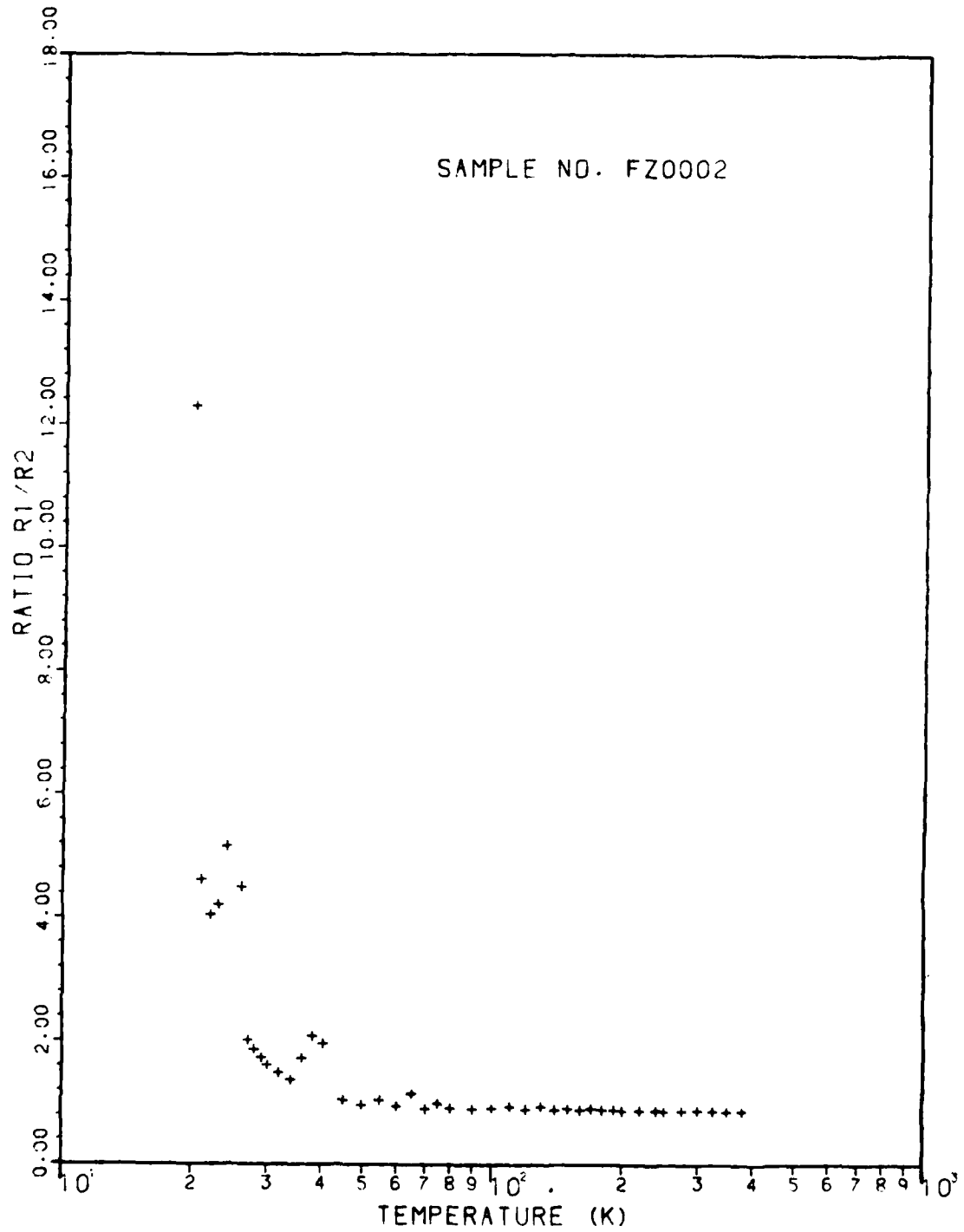


Figure 47.  $R_1/R_2$  Ratio of Si:N NTD Sample (FZ0002)

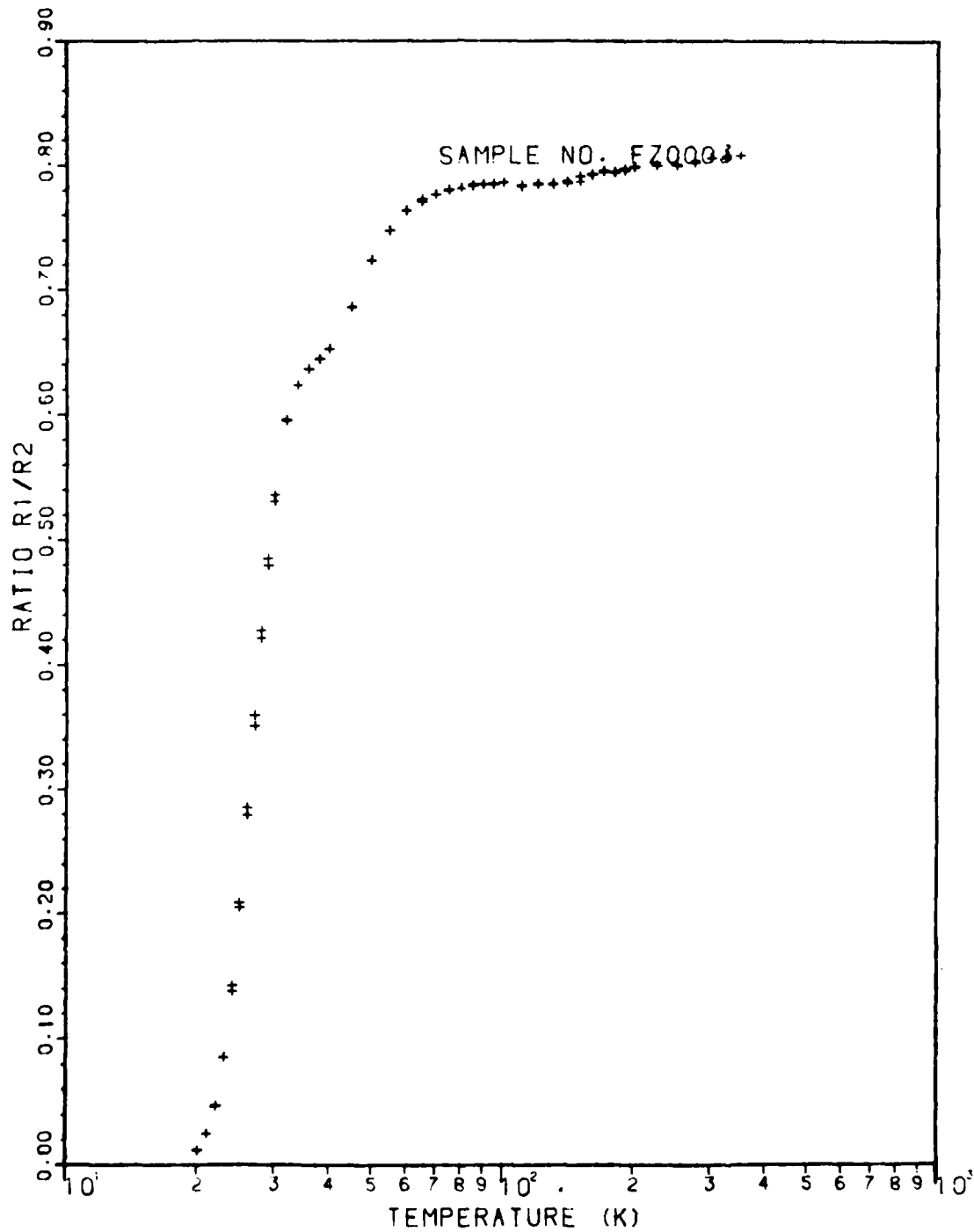


Figure 48. R<sub>1</sub>/R<sub>2</sub> Ratio of Si:N NTD Sample (FZ0003)

### Curve Fitting of Experimental Data

Attempts to use the curve fitting computer program were hindered by the r-factor problem and the temperature dependent  $R_1/R_2$  ratio at low temperatures in the samples. Because the data is unreliable where  $R_1/R_2$  is temperature dependent, these data points are eliminated. The r-factor problem effects every data point, but has the most obvious effect at high temperatures. Eliminating the points where the carrier concentration is decreasing with temperature helps generate a better fit. Nevertheless, there will still be an error in the activation energy and the concentration of the donors (19:36-38). Due to the r-factor problem, if the goodness of fit parameter, Chi-squared per degree of freedom, is less than three it can be considered as the best fit (23).

The phosphorus doped CZ sample, CZ-AN-001, had a temperature dependent  $R_1/R_2$  at low temperatures and an apparent r-factor problem at high temperatures. Eliminating points above 200 K and below 30 K still left enough data points to generate a good curve fitting function. The results as seen in Fig. 15 give a Chi-squared value of 0.39, which is an excellent fit. The donor was identified from the activation energy as phosphorus and the donor concentration was given as  $3.19 \times 10^{15} \text{ cm}^{-3}$ . Because of the r-factor the phosphorus concentration should be given as about  $3 \times 10^{15} \text{ cm}^{-3}$ .

The NTD samples also exhibited an obvious r-factor

problem at high temperatures. Curve fitting the high purity NTD FZ sample, NT2-07-5N, was accomplished by eliminating points above 140 K. The best fit had a Chi-squared of 4.05 as seen in Figure 49. Table 5 gives the results for the NTD samples. For NT2-07-5N the number of donors is  $3.68 \times 10^{13} \text{ cm}^{-3}$  and the activation energy is 0.0456 eV. This means that the sample was doped with phosphorus at a concentration of about  $4 \times 10^{13} \text{ cm}^{-3}$ . The curve fitting program cannot give any information about the number of acceptors other than the concentration. It is likely that the acceptors are boron atoms. The segregation coefficient (ratio of the concentration in solid silicon to the concentration in melted silicon) of boron is close to unity so that it is virtually impossible to zone refine a boule of silicon to have a concentration of boron less than  $10^{11} \text{ cm}^{-3}$  (23).

Due to the r-factor problem, points above 120 K were deleted from the Si:N NTD samples. The  $R_1/R_2$  ratio in these samples was very temperature dependent at low temperatures, so points below 32 K were also eliminated. The curve fitting program resulted in Chi-squared values of 1.38 for FZ0002 and 3.67 for FZ0003. Figures 50 and 51 give the resulting curves. Again the activation energy is affected by the r-factor, but it is close enough to be identified as phosphorus. Clearly the Si:N NTD samples are dominated by the phosphorus and behave similarly to the high purity FZ NTD sample.

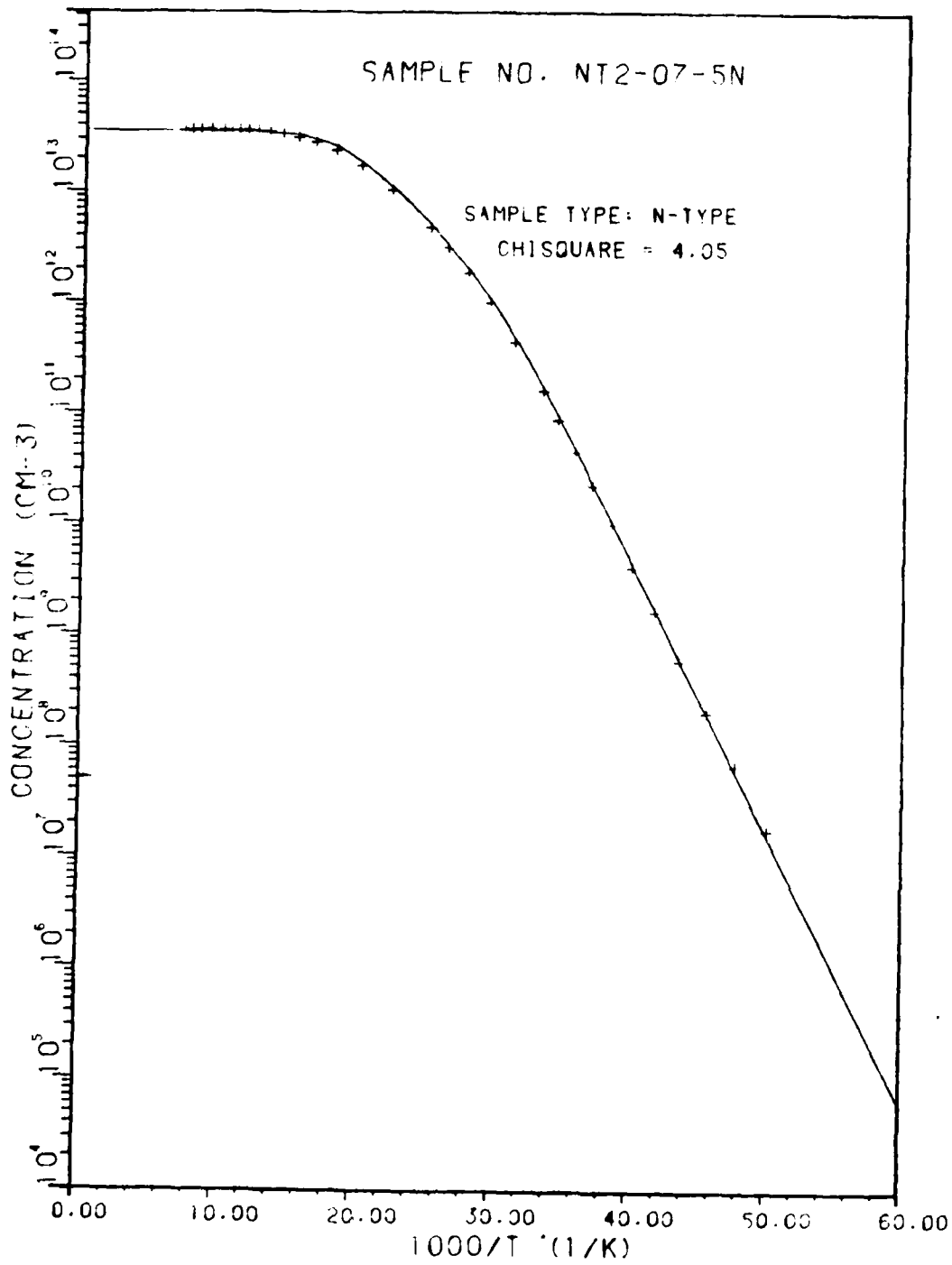


Figure 49. Least Squares Fit of Carrier Concentration of High Purity FZ NTD Sample

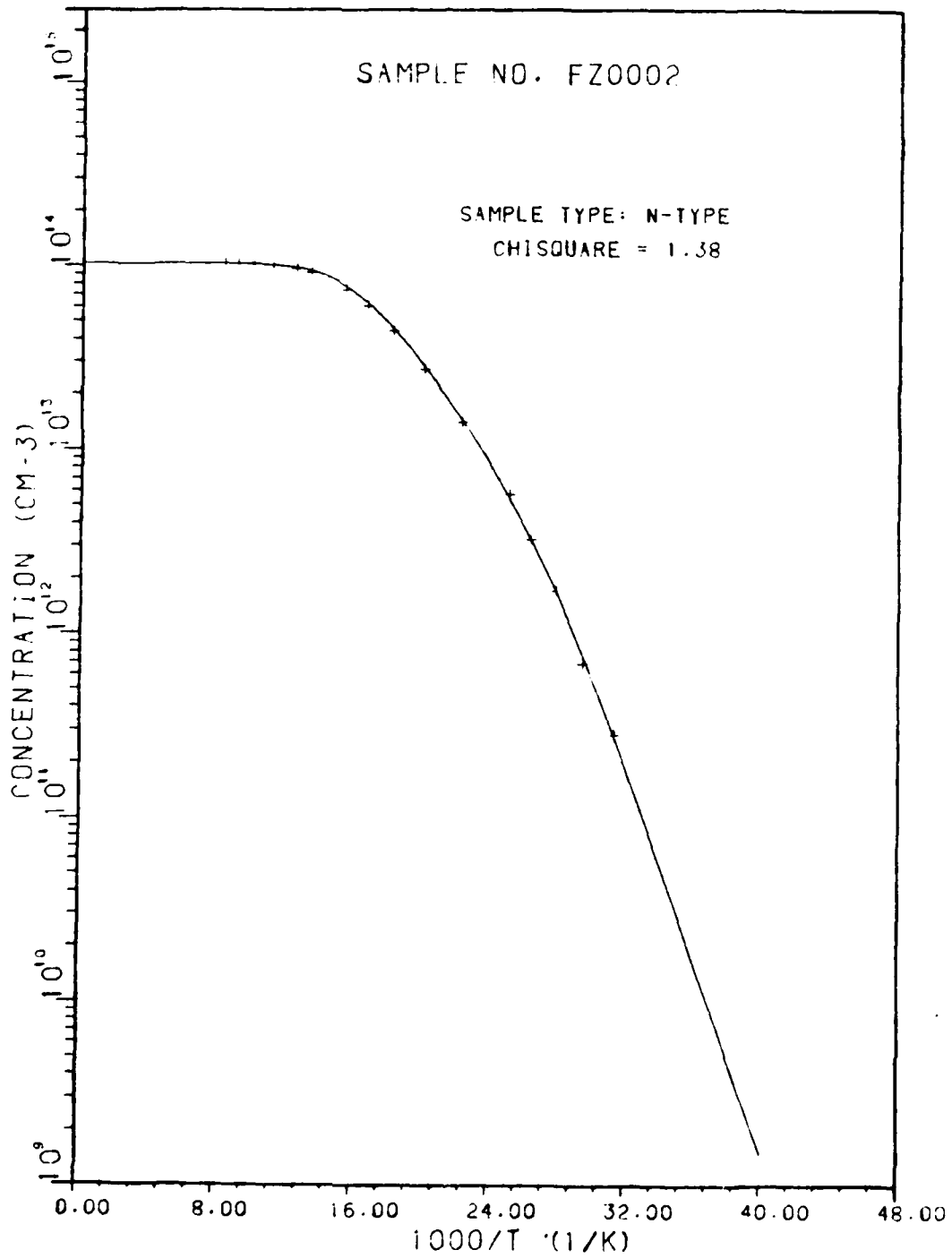


Figure 50. Least Squares Fit of Carrier Concentration of Si:N NTD Sample (FZ0002)

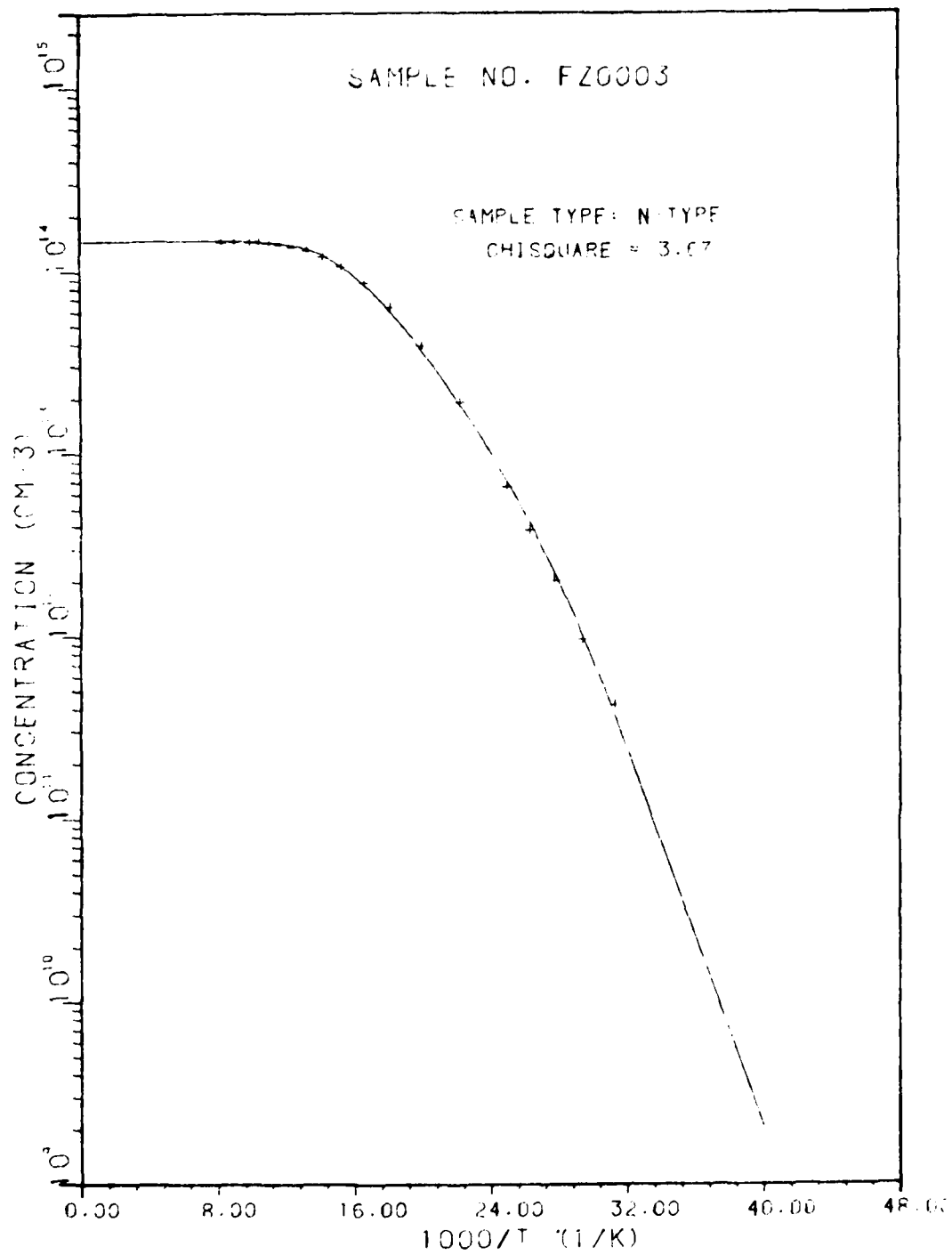


Figure 51. Least Squares Fit of Carrier Concentration of Si:N NTD Sample (FZ0003)



Table V

## Results of Curve Fitting NTD Samples

Sample	Acceptor Conc. $\text{cm}^{-3}$	Donor Conc. $\text{cm}^{-3}$	Activation Energy eV	$\chi^2$
NT2-07-5N	$1.69 \times 10^{12}$	$3.68 \times 10^{13}$	0.0456	4.05
FZ0002	$3.85 \times 10^{12}$	$1.06 \times 10^{14}$	0.0485	1.38
FZ0003	$4.64 \times 10^{12}$	$1.51 \times 10^{14}$	0.0481	3.67

The concentration data was much more difficult to computer fit for the rest of the Si:N samples. It was impossible to try to fit FZ0004-A, FZ0005, and SI-N800C because of the anomalous carrier concentration plots and more importantly because of the temperature dependence in  $R_1/R_2$  over all temperatures. This left the unannealed Si:N sample, FZ0006, and the 900 °C annealed Si:N sample, FZ0001-A, for curve fitting.

A one level fit was performed on FZ0006, resulting in a solution of  $4.58 \times 10^{10} \text{ cm}^{-3}$  acceptors,  $4.02 \times 10^{12} \text{ cm}^{-3}$  donors, and an activation energy of 0.053 eV. Chi-squared was 3.48. Next, a two level fit was attempted in order to generate a better fit (Figure 52). The deeper energy level turned out to be 0.50 eV at  $2.13 \times 10^{12} \text{ cm}^{-3}$ ; however, this level is probably indicates the onset of intrinsic conduction. At high temperatures there is enough thermal energy to start ionizing silicon atoms (27:106-109). Thus a sharp rise in concentration is seen at high temperatures. The lower energy level was 0.052 eV

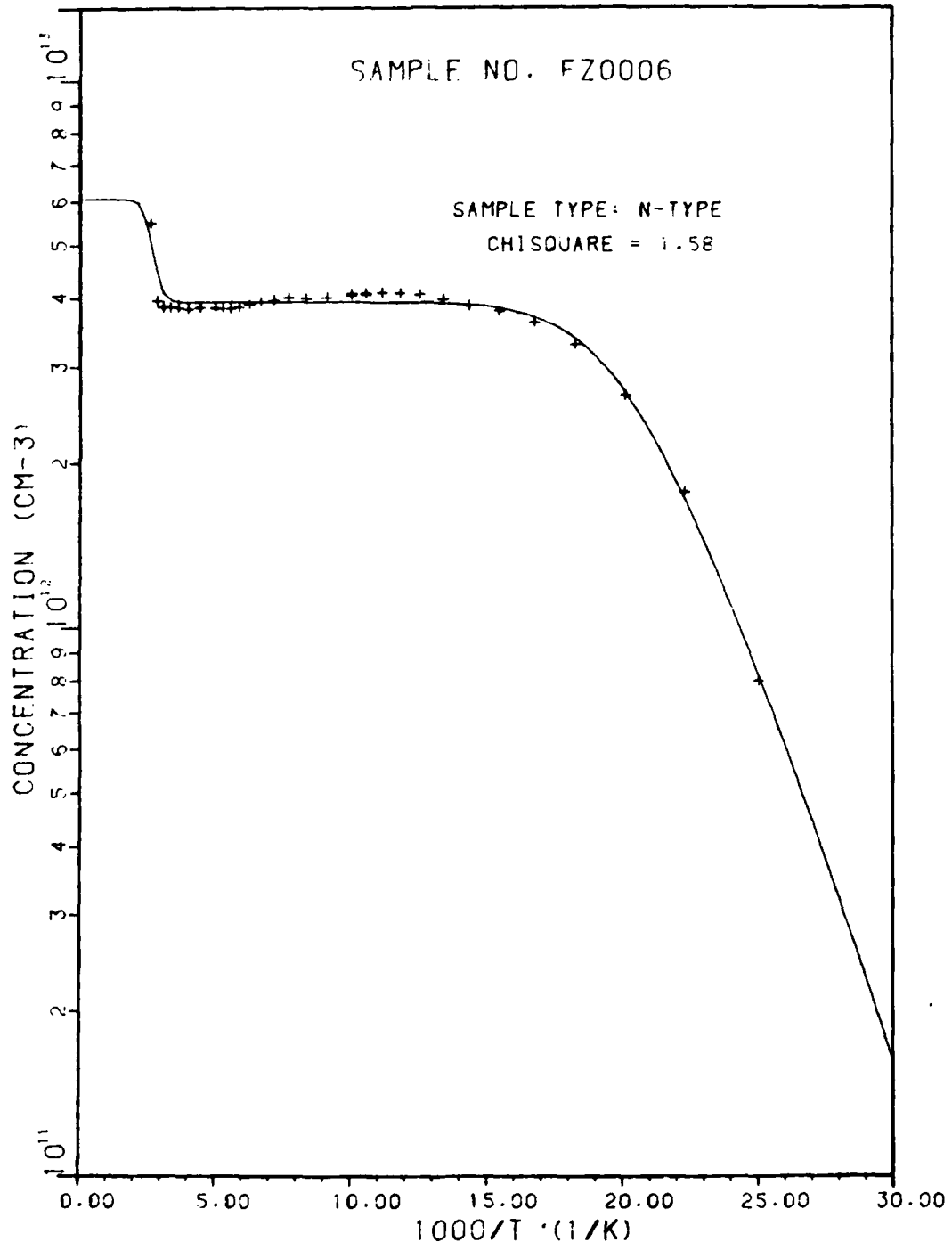


Figure 52. Two Level Least Squares Fit of Carrier Concentration of Unannealed Si:N Sample

at  $3.96 \times 10^{10} \text{ cm}^{-3}$  and the acceptor concentration was  $3.41 \times 10^{10} \text{ cm}^{-3}$ .

The only sample with an acceptable  $R_1/R_2$  ratio after annealing was FZ0001-A. Points below 28 °K were eliminated as  $R_1/R_2$  was temperature dependent in this region. The best one level fit on data from 28 to 380 K gave a Chi-squared of 73.48 (Fig. 53). Most of the error appears to be in the high temperature region. In this case it can be said that deep levels have been activated in the sample because the increase in carrier concentration at the high temperatures gives a smooth curve rather than the abrupt jump that is seen in Figure 52. In the one level fit the activation energy was 0.0537 eV with a donor concentration of  $4.76 \times 10^{12} \text{ cm}^{-3}$  and an acceptor concentration of  $9.13 \times 10^{10} \text{ cm}^{-3}$ .

In order to fit the deep energy level, a two level fit was tried. Although Chi-squared was reduced to 8.73, the fit resulted in unrealistically large values for the acceptor and shallow donor energy level concentrations. The acceptor concentration was reported to be  $6.66 \times 10^{13} \text{ cm}^{-3}$  while the shallow donor was  $7.07 \times 10^{13} \text{ cm}^{-3}$  with an energy level of 0.0369 eV. Because the two level fit was unsuccessful, a three level fit was tried. The best fit, Fig. 54, gave a Chi-squared of 7.25 with an acceptor concentration of  $1.32 \times 10^{11} \text{ cm}^{-3}$ . The shallowest energy level was 0.0525 eV with a concentration  $4.14 \times 10^{12} \text{ cm}^{-3}$ . The next higher donor energy level

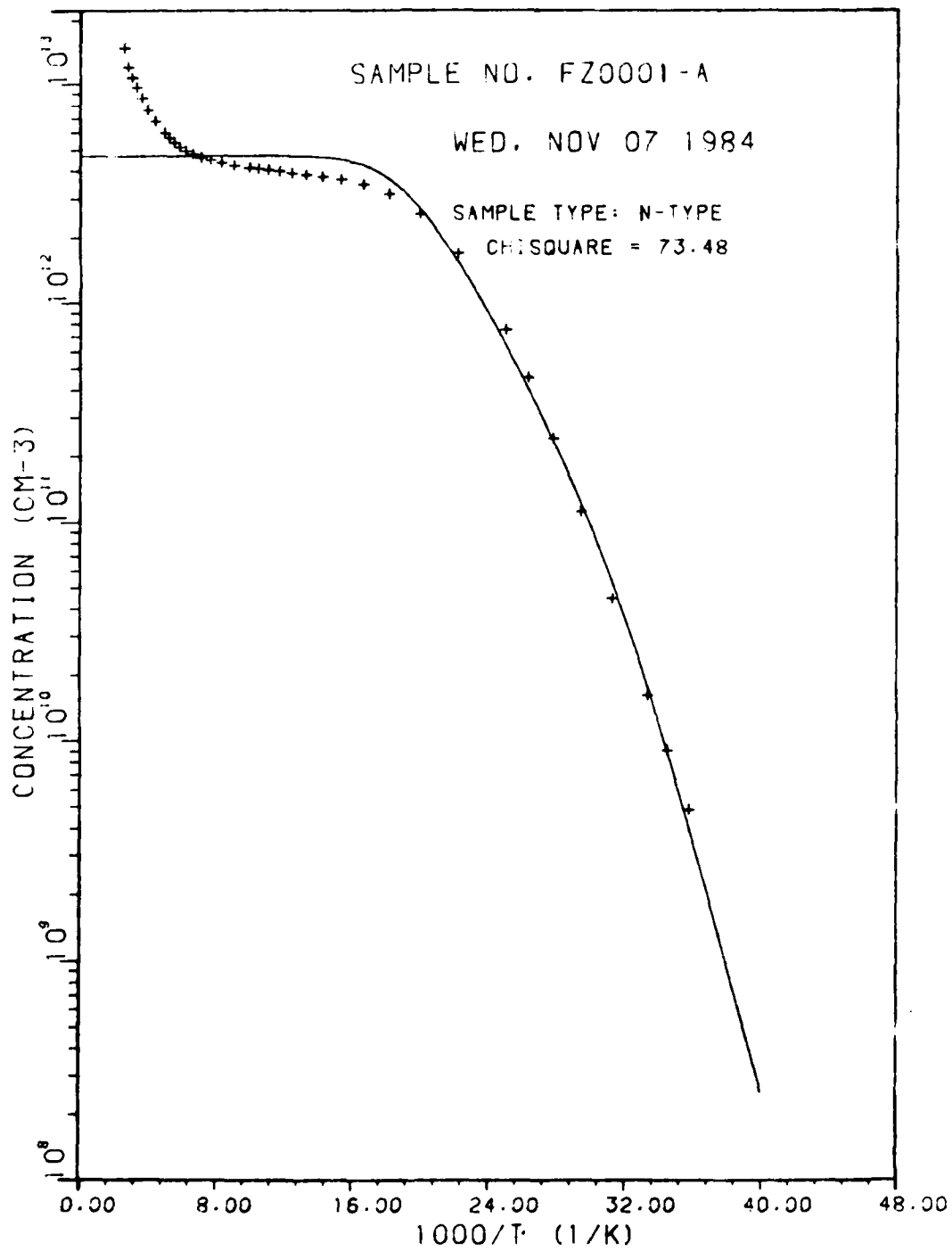


Figure 53. One Level Least Squares Fit of Carrier Concentration of Si:N Annealed at 900 °C

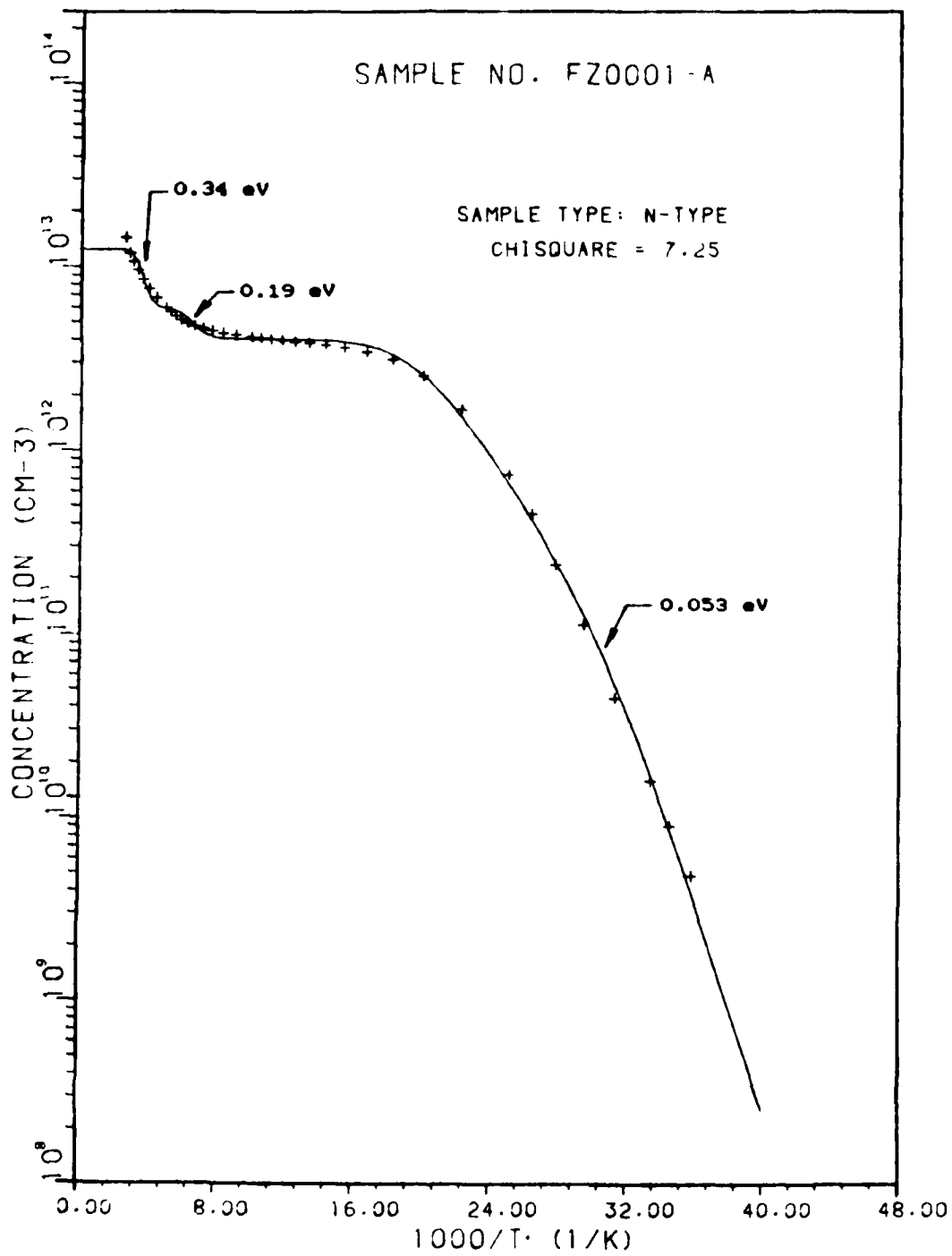


Figure 54. Three Level Least Squares Fit of Carrier Concentration of Si:N Annealed at 900 °C

was 0.1856 eV at  $1.91 \times 10^{12}$  cm<sup>-3</sup> and the deepest donor level was 0.348 eV at  $6.51 \times 10^{12}$  cm<sup>-3</sup>. Although the 0.19 eV energy level was reported by Tokamaru, this appears to be a coincidence. An examination of Fig. 54 shows that this energy level just does not fit the data. The deepest level does not fit the data very well either.

The shallow level in the three level fit; however, is consistent with the one level fit of the FZ0001-A and the one level fit of the unannealed sample, FZ0006. It appears that this boule of nitrogen doped FZ silicon has a donor with an energy level of about 0.052 to 0.054 eV at a concentration of  $4 \times 10^{12}$  cm<sup>-3</sup>. This energy level is not precise due to the r-factor problem; however, it should still be close enough to identify the donor.

## VI. Analysis

The results of these experiments show that nitrogen doped silicon is not as well behaved as silicon doped with other group V atoms. All of the samples had some temperature dependence in  $R_1/R_2$  at low temperatures. Some samples, FZ0004-A, FZ0005, and SI-N800C, were temperature dependent over the entire temperature range. Because of the requirement that  $R_1/R_2$  must have a constant value with temperature, it means that these samples are inhomogeneous. The carrier concentration data from the Si:N samples that were homogenous enough for curve fitting could only be resolved for the shallowest energy level. The Si:N NTD samples were dominated by the phosphorus doping and this was the only energy level found in the data.

The Hall experiment does not give a precise activation energy level. The r-factor problem distorts the energy level even more. The average donor energy level, 0.0483 eV, found in the Si:N NTD samples was close enough to phosphorus to identify it as the doping atom even though the energy was higher than the accepted value of 0.045 eV (37:21). The shallow energy level of 0.052 to 0.054 eV found in the Si:N samples could be: arsenic which has an accepted donor energy value of 0.054 eV, phosphorus, or nitrogen. The donor atom is unlikely to be arsenic as no

arsenic was found in the NTD samples. This leaves phosphorus or nitrogen as the probable donor species.

Although Zorin reported the activation energy of ion implanted nitrogen in silicon as 0.045 eV, no one has duplicated this result. Zorin's experiments were conducted from 100 to 250 K (44). Mitchell repeated the Hall experiment on ion implanted nitrogen, but extended the temperature range from 20 to 250 K (25). It is probable that Zorin did not find an activation energy for nitrogen at all and that his samples were contaminated with phosphorus.

Mitchell reported a shallow energy level of 0.017 eV (25). Curve fitting was attempted using this energy level on Si:N and Si:N NTD samples. Low temperature data down to 20 K was included in these attempts in spite of the  $R_1/R_2$  problem without success. The fitting routine kept pulling the energy up until it closed in on the 0.052 to 0.054 eV level.

A photoluminescence (PL) study of unannealed samples of this boule of Si:N was performed in 1982 by David Brown of the University of Dayton Research Institute (5,6). He reported finding a 1.1223 eV line in this material. This line was reported by Tajima and is considered to be an exciton bound to substitutional nitrogen (38,39). Figure 55 is a PL plot of the intensity verses photon energy of a sample of boule number 0274 (Si:N) which was provided by David Brown (6). The 1.1223 eV bound exciton line appears



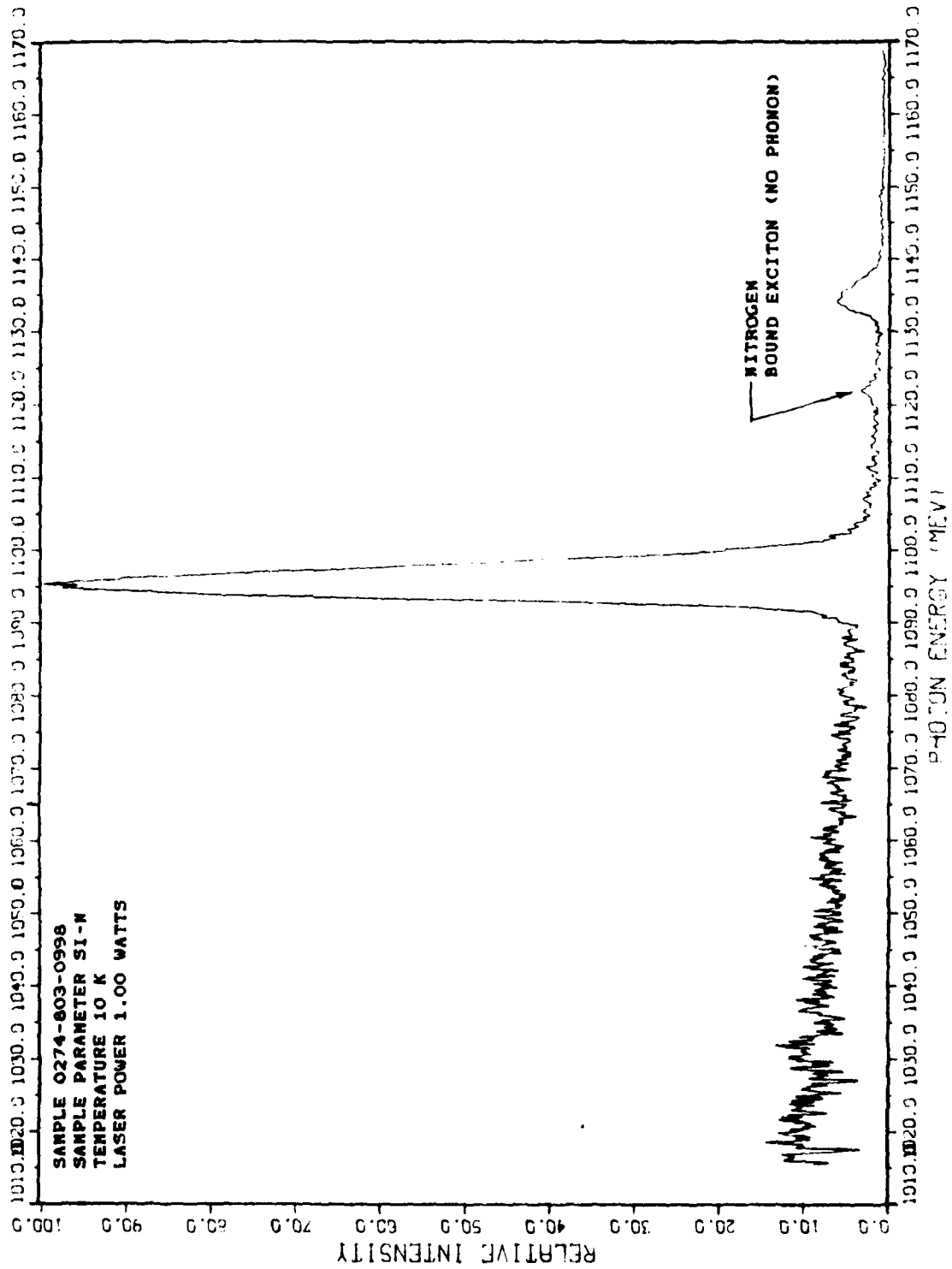


Figure 55. Photoluminescence Plot of Si:N

between the more prominent lines at 1095 and 1135 milli-eV which are free excitons emitted by the silicon. Brown also found phosphorus in the samples at levels of 1 to 2 x  $10^{12}$  cm<sup>-3</sup>. Other samples of this material were ion implanted with gallium and sent to the MIDAC Corp. of Costa Mesa, California for PL analysis using the processing infrared active dopant (PIORAD) method. They also reported finding phosphorus and the 1.1223 eV nitrogen line (6).

Brown also noted that although phosphorus is found everywhere in the samples, nitrogen may not be. When the laser is moved to another spot on the same sample the 1.1223 eV line may not appear at all. This is another confirmation that the material is inhomogeneous.

Because the PL studies found phosphorus in the samples in about the same quantity as the shallow donor in the Hall experiments, this positively identifies the shallow donor in the Si:N samples as phosphorus. A shallow activation energy level for nitrogen could not be found in these Hall experiments. It is possible that the concentration of substitutional nitrogen in bulk material is so low that it is beyond detection limits of the system or overcompensated by acceptors.

It has been shown by these experiments, that annealing activates deep levels in Si:N. However, annealing may also bring out inhomogeneities that were not present in the material before. The deep energy levels and inhomogeneous nature of the material may be due to silicon-nitrogen

complexes and precipitates (23;32:5020). Annealing could produce changes in these complexes. Ironically, it may be the clustering of silicon nitrides that lock the lattice and provides the strengthening mechanism.

## VII. Conclusions and Recommendations

The objective of this study was to determine if bulk grown nitrogen doped silicon is a suitable VLSI and VHSIC substrate material. These applications require substrates with well behaved electrical parameters. The manufacturing process requires wafers that can stand up to thermal processing without warping or developing more defects. Small quantities of nitrogen added to the boule during growth was discovered to lock dislocations, but the electrical parameters had not been investigated.

### Findings

Through the series of Hall effect experiments performed in this study it was discovered that the electrical parameters of this material are not well behaved. The experiments are listed in Table II (page 53) while Table IV (page 54) summarizes the electrical parameters at 300 K. The resistivity and the Hall mobility of the Si:N samples decreased upon annealing. The resistivity in sample FZ0006 dropped from 1180 ohm-cm to 302 ohm-cm upon annealing at 800 °C while the Hall mobility dropped from 1380 cm<sup>2</sup>/V-sec. Annealing activated more carriers in this sample. The carrier concentration went from  $3.85 \times 10^{12}$  cm<sup>-3</sup> to  $2.97 \times 10^{13}$ . However, the decrease in resistivity and Hall mobility and increase in carrier

concentration is not a function of the annealing temperature. The sample annealed at 900 °C had higher resistivity and Hall mobility than the samples annealed at 800 °C.

The electrical parameters in the bulk grown Si:N varied considerable. In all but the unannealed sample, the Hall mobility was not as high as the phosphorus doped CZ sample. The CZ sample had a Hall mobility of 1360 cm<sup>2</sup>/V-sec while the annealed Si:N samples varied from 583 cm<sup>2</sup>/V-sec to 1320 cm<sup>2</sup>/V-sec.

The Si:N NTD samples had similar resistivity and carrier concentrations at 300 K, but not the Hall coefficient or Hall mobility. One Si:N NTD sample had a Hall mobility of 1930 cm<sup>2</sup>/V-sec and the other sample was 1370 cm<sup>2</sup>/V-sec. The high purity FZ NTD sample had a Hall mobility of 1530 cm<sup>2</sup>/V-sec which is near the mobility limit 1500 cm<sup>2</sup>/V-sec which is due to phonon scattering.

The Hall effect data was taken over a wide temperature range: 20 to 380 K. Examination of the carrier concentration plots of the phosphorus doped CZ sample, the unannealed Si:N sample, and the NTD samples shows that the concentration decreases at high temperatures. This indicates that the r-factor or "r", is temperature dependent and the assumption that it is equal to one for all temperatures is not justified. However, the assumption that r = 1 is the best that can be done for now, because the computation of the temperature dependent r-factor in

n-type material has not been worked out in detail (23).

A necessary condition for the accuracy in the resistivity and Hall coefficient measurements is that the sample must be homogeneous. The  $R_1/R_2$  ratio was found to be temperature dependent in several samples. This means that these samples are inhomogeneous. Three out of four Si:N samples were found to be inhomogeneous after annealing. The unannealed sample, FZ0006, became inhomogeneous after annealing. The only sample that was homogeneous after annealing was FZ0001-A which was annealed at the highest temperature, 900 °C. The Si:N NTD samples were annealed at 800 °C but were homogeneous. It is possible that these samples were so dominated by the phosphorous doping that this overcame any inhomogeneities.

The inhomogeneous nature of Si:N make it a poor choice for a VLSI or VHSIC substrate. The inhomogeneity implies that the electrical parameters will not be uniform across the substrate. This leads to device problems such as non-uniform signal propagation time, different gains in transistors, variations in resistors, and host of other problems. The material may be acceptable for discrete and power devices, as these devices are large enough to average out electrical parameters across the substrate.

Exactly what happens to the nitrogen in a silicon lattice cannot be determined by the Hall effect experiments. The inhomogeneities brought out by annealing may be due to silicon-nitride complexes and possible

precipitates. It was also concluded by examining the concentration plots that annealing activated deep energy levels. This was seen in all the annealed Si:N samples including; the inhomogeneous samples, but not the unannealed sample, FZ0006.

Attempting to curve fit the carrier concentration data to find the donor activation energies and species concentrations was clearly impossible for the inhomogeneous samples. However, curve fitting was done on the Si:N NTD samples and the two homogeneous bulk Si:N samples (FZ0001-A and FZ0006). The activation energy of the deep level in the annealed Si:N sample, FZ0001-A, could not be resolved. The only shallow energy level that could be resolved in any of the samples was phosphorus. A shallow level that unambiguously identified nitrogen was not found. Nitrogen was identified in the Si:N boule by a photoluminescence study performed by David Brown (6). The conclusion is nitrogen does not go into substitutional sites in silicon to any appreciable extent.

#### Recommendations

Based on these experiments it appears that nitrogen doped silicon is not a suitable VLSI or VHSIC substrate material due to its inhomogeneous nature. However, the Hall effect experiments on the Si:N NTD samples show that it is may be possible to overcome this problem.

It is recommended that these experiments be repeated.

The Hall experiment should be performed on each sample before and after annealing to get a better understanding of the effects of annealing. However, to determine exactly what happens to nitrogen in a silicon lattice a Transmission Electron Microscope (TEM) study may be undertaken.

The experiments undertaken in this work gave data on the electron mobility of nitrogen doped silicon. The mobility of holes in this material can be determined by ion implanting a p-type material into Si:N, then performing the Hall effect experiment. The details of this type of experiment are given in Appendix A.

It is also recommended that the temperature dependent r-factor in n-type silicon material be determined if n-type material is to be studied in the future. One of the results of this would be more accurate curve fitting, thus donor concentrations and activation energies would be determined more accurately.



## Appendix A

### Hall Effect Experiment with Bulk Grown Nitrogen Doped Silicon Ion Implanted with Gallium

In order to study the mobility of holes in n-type silicon, it is possible to implant p-type ions into the n-type silicon lattice. By reverse biasing the p-type implanted layer with respect to the n-type substrate, the depletion region electrically isolates the ion implanted p-layer and the Hall effect experiment can be performed (39:336). As long as the reverse bias leakage current is less than 1 or 2% of the source current, the rest of the current is confined to the ion implanted p-type layer and data can be taken (36:69-72).

Leakage and sample current has to be measured at each temperature. Leakage current increases with temperature, so it is likely that the temperature range of this type of experiment would be limited. Excessive leakage current is the reason Zorin had to stop his Hall effect experiments on ion implanted nitrogen in p-type silicon at 250 K (44:111).

Wafers of phosphorus doped CZ silicon, Si:N, and Si:N NTD were ion implanted with gallium at the Avionics Laboratory (AFWAL). Square samples were made from the wafers. Four contacts, one in each corner, were made on

the ion implanted surface. Contacts were formed by ion implanting boron to degenerately dope the contact area with a p-type material. Ion implanting is for making contacts instead of using a laser and spin on dopant because the laser pulse penetrates the ion implanted layer. In order reverse bias the pn-junction a contact had to be put on the back of the sample on the n-type substrate. Unfortunately, this contact was put on the wrong surface on eleven out of the twelve samples.

Leads were soldered on the remaining sample which was Si:N ion implanted with gallium. The sample was mounted in the sample holder and tested at room temperature in a Hall effect system that had been modified. At room temperature the leakage current may be excessive, but the test showed that the leakage current was small compared to the sample current.

The system, Hall II, was modified to include a power supply to reverse bias the pn-junction and an extra ammeter. Figure 56 shows a schematic illustration of the modified system. The high side of the current source (Keithley 220) is connected to the high side of ammeter A (one channel of the Keithley 619 DVM) and the low side of the power supply. Ammeter A measures the current through the ion implanted layer. Ammeter B measures the total current through the current source. The leakage current is determined by subtracting current through ammeter A (sample current) from the current in ammeter B (total source current). The ground on the switching box is the path for

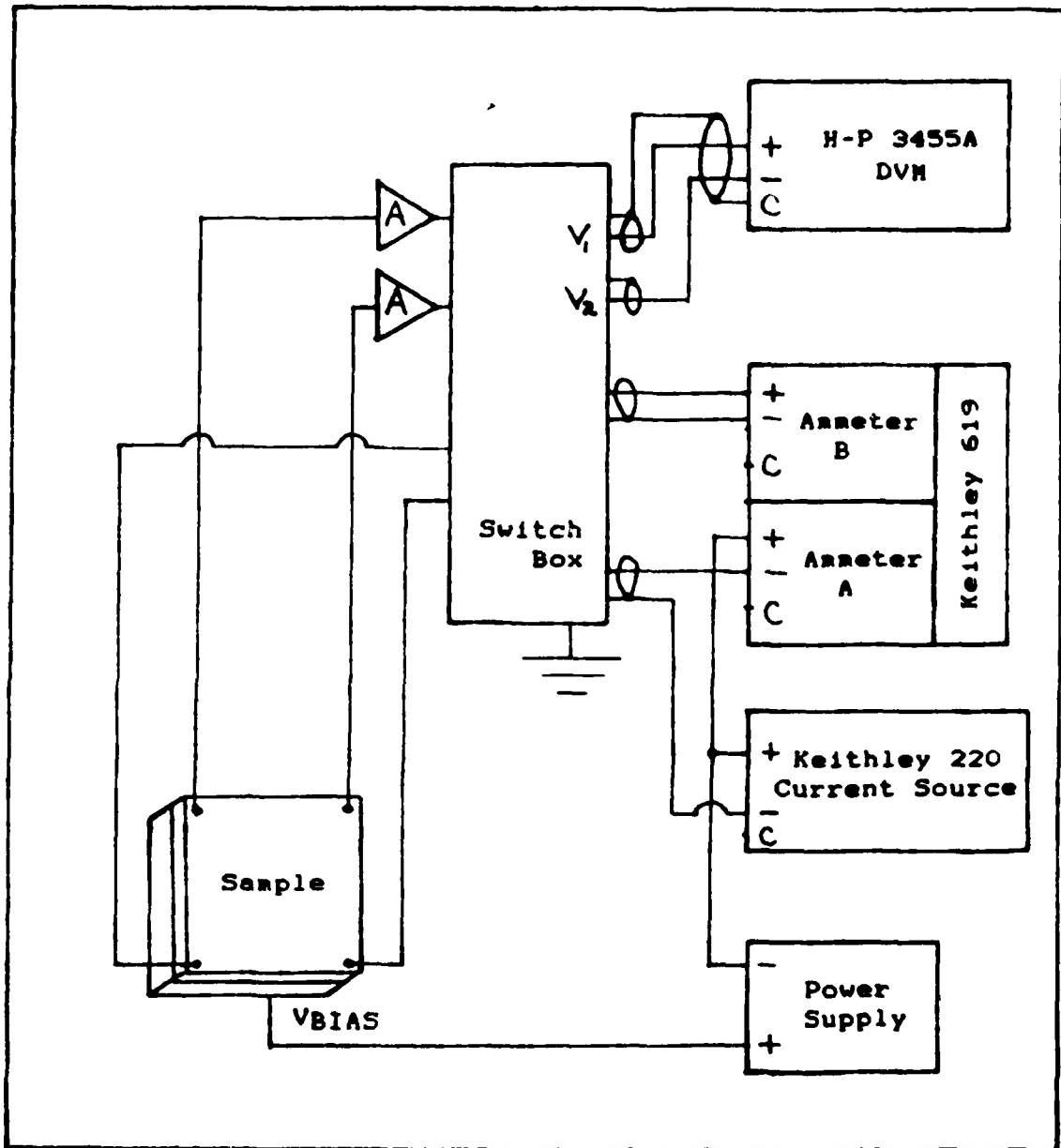


Figure 56. Schematic of the Hall Effect System Modified for an Ion Implanted Sample (23)

the return currents. The sample voltage is measured in the same way as described in Chapter IV for a bulk sample. The voltage signal goes through high impedance unity gain amplifiers, A, then through the switching box to the digital voltmeter (H-P 3455A).

The Hall II system is not difficult to modify and the room temperature test of the Si:N gallium implanted sample indicates that an analysis of a p-type ion in Si:N would be feasible. There are sufficient quantities remaining of gallium implanted Si:N and Si:N NTD to make more samples. Because a study of the electrical properties of a p-type ion implanted layer in nitrogen doped silicon has not been done, this could be a fruitful thesis topic.

## Appendix B

### Graphs of Experiments FZ0004-A and FZ0005

The following figures are the plots of the temperature dependent electrical parameters of FZ0004-A and FZ0005. In both cases these samples had temperature dependent  $R_1/R_2$  ratios. This means that these samples are inhomogeneous. The plots are included to show the results of Hall effect experiments with inhomogeneous samples.

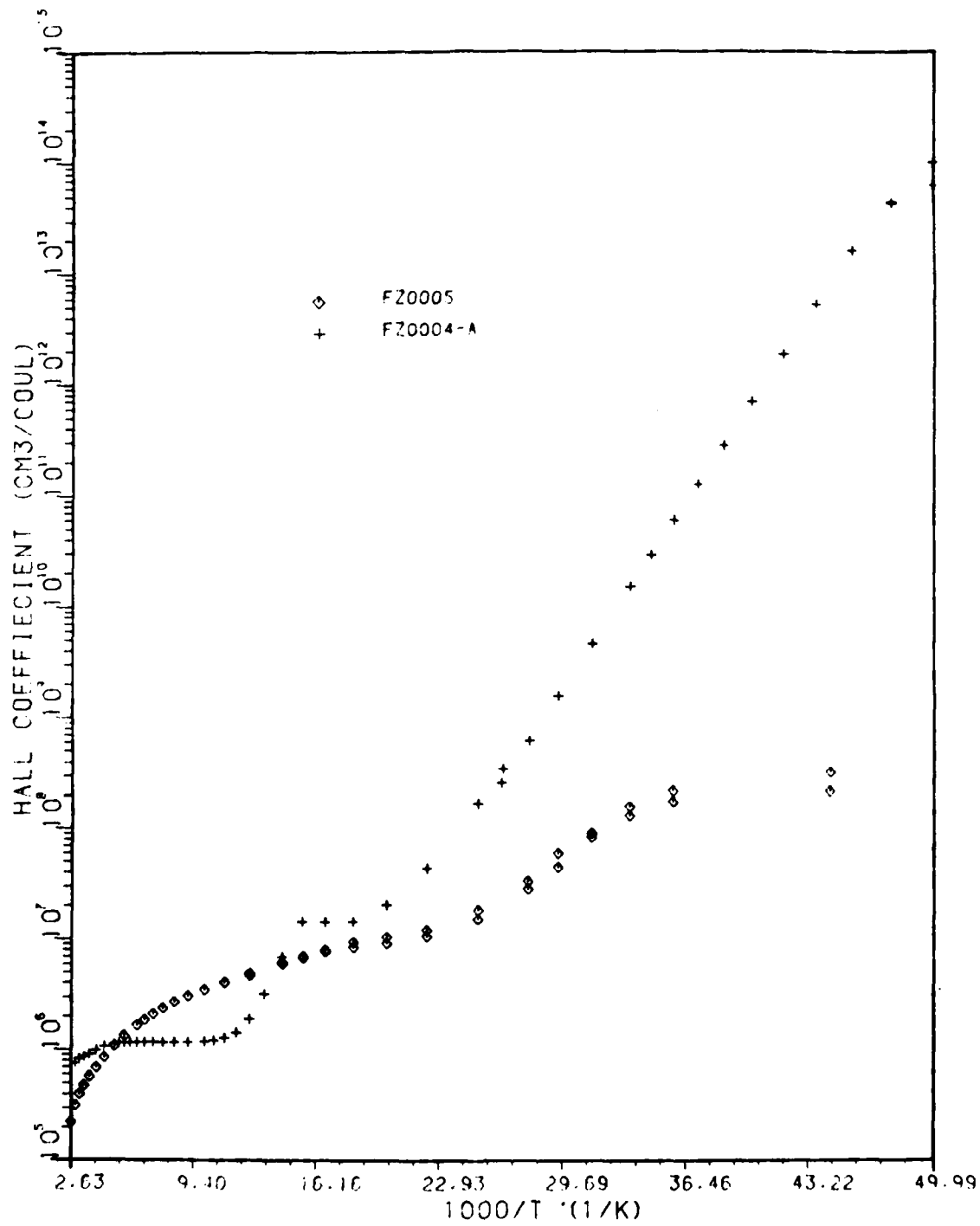


Figure 57. Hall Coefficient of FZ0004-A and FZ0005 versus Inverse Temperature

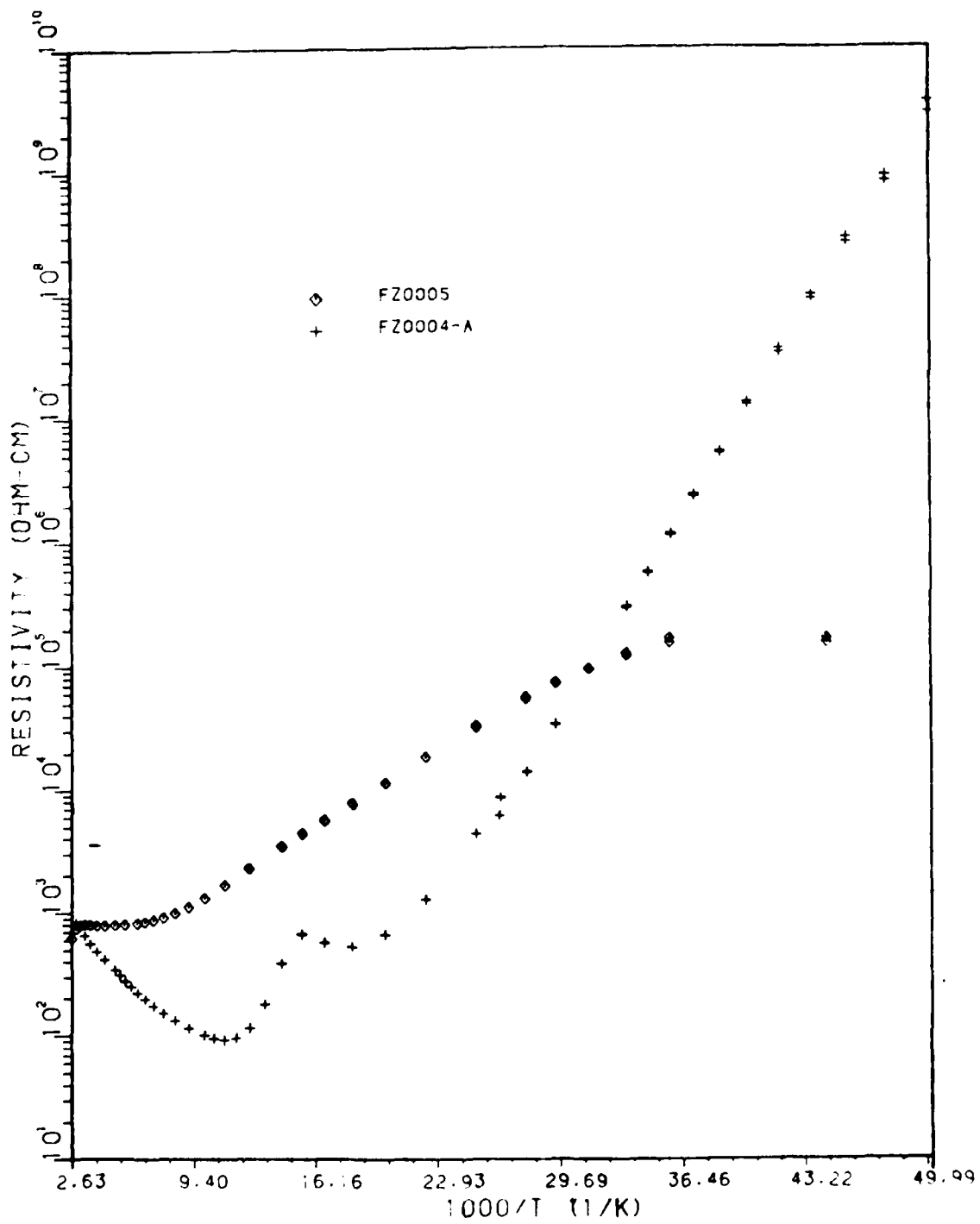


Figure 58. Resistivity of FZ0004-A and FZ0005 versus Inverse Temperature

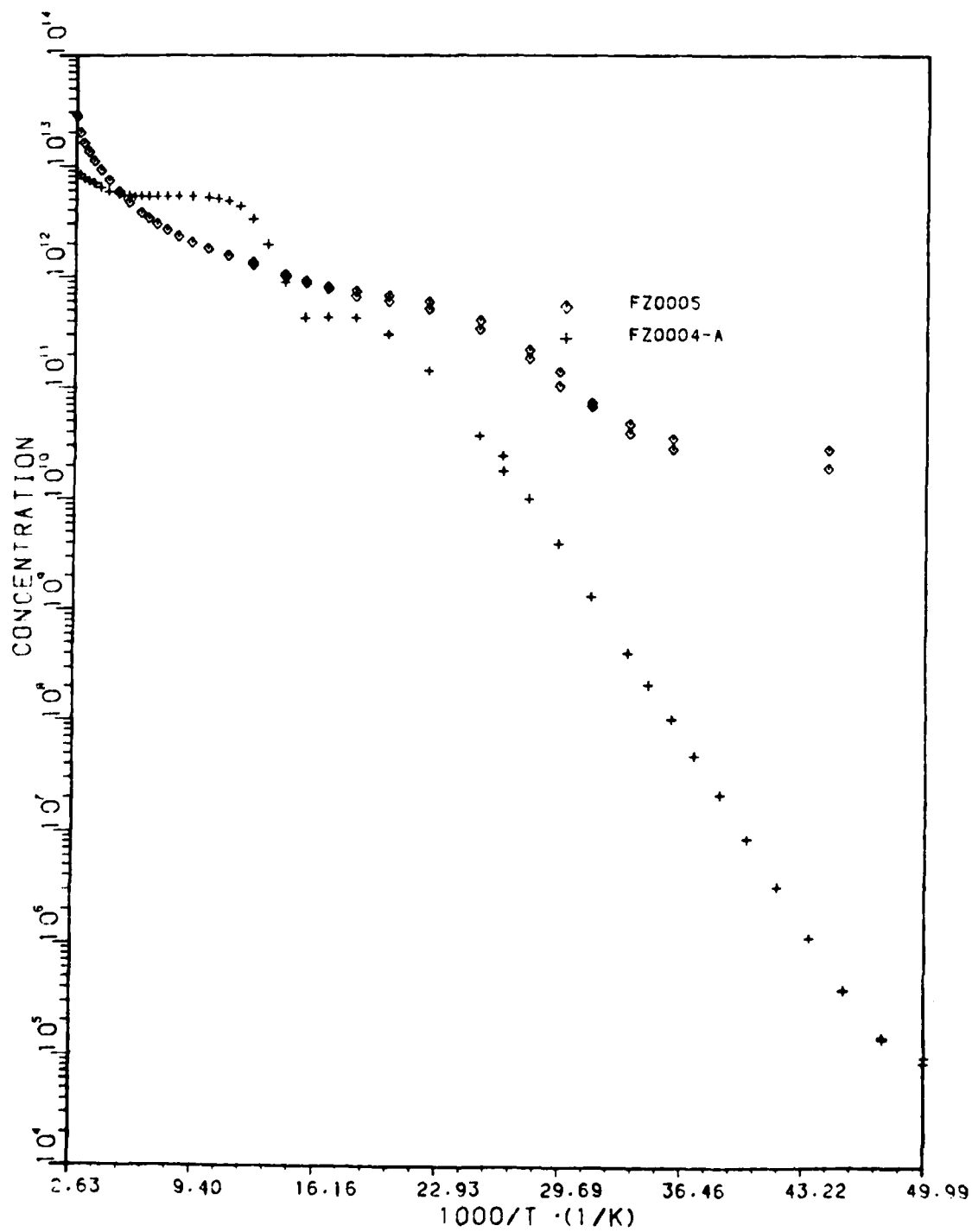


Figure 59. Carrier Concentration of FZ0004-A and FZ0005 versus Inverse Temperature



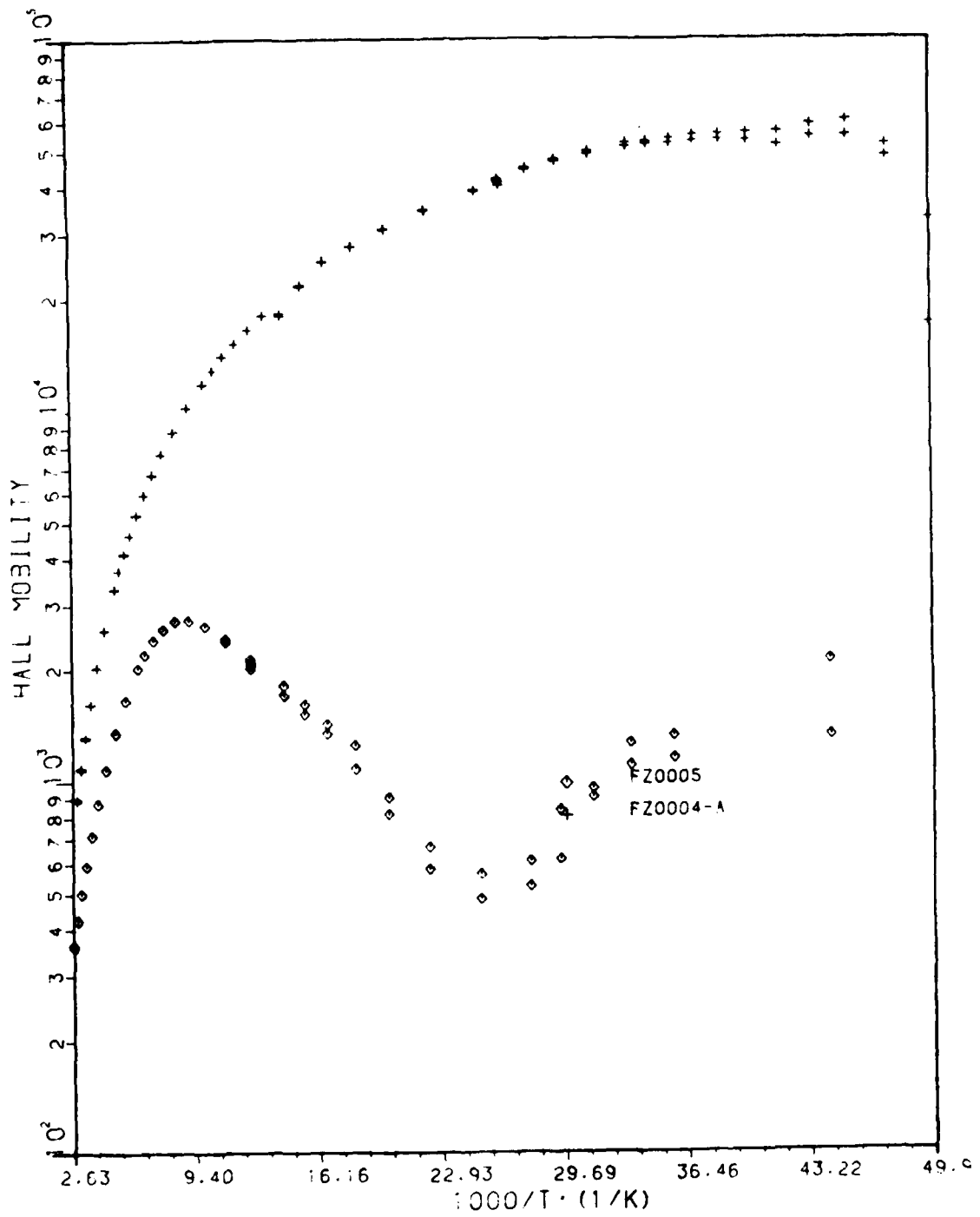


Figure 60. Hall Mobility of FZ0004-A and FZ0005 versus Inverse Temperature

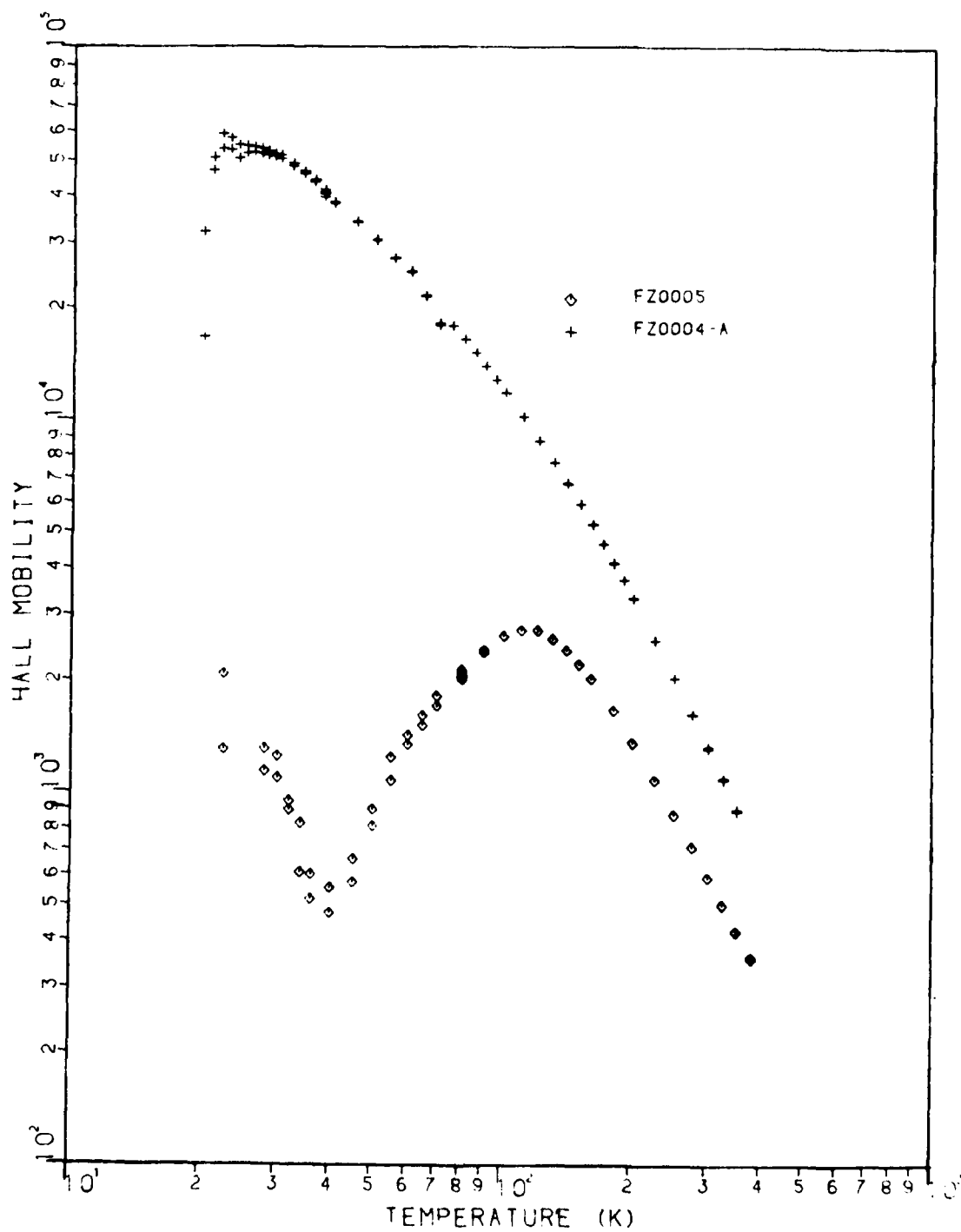


Figure 61. Hall Mobility of FZ0004-A and FZ0005 versus Temperature

## Bibliography

1. Abe, T., S. Kikuchi, S. Shirai, and S. Muraoka. "Impurities in Silicon Single Crystal - A Current View," Semiconductor Silicon 1981, Proceedings of the Fourth International Symposium on Silicon Materials Science and Technology: 54-71. The Electrochemical Society, Inc., Pennington, NJ, 1981.
2. Abe, Takao and Hirofumi Harada. "Microdefects and Impurities in Dislocation-Free Silicon Crystals," Defects in Semiconductor Silicon, II, Materials Research Society Symposium Proceedings, Vol. 14 (Boston, MA, Nov 82): 1-17. Elsevier Publishing Co., Inc. (1983).
3. Alt, H. Ch. and L. Tapfer. "Photoluminescence Study of Nitrogen Implanted Silicon," Applied Physics Letters, Vol. 45, No. 4: 426-428. American Institute of Physics (August 1984).
4. Brower, Keith L. "Jahn-Teller-Distorted Nitrogen Donor in Laser-Annealed Silicon," Physical Review Letters, Vol. 44, No. 24: 1627-1629 (16 July 1980).
5. Brown, David, Physicist. Private Communication. University of Dayton Research Institute, Dayton, OH, 2 October 1984.
6. Brown, David, Physicist. Private Communication. University of Dayton Research Institute, Dayton, OH, 25 October 1984.
7. Gassman, Richard A. and W. C. Mitchel. A Study of Defects in Neutron Transmutation Doped Silicon: Gallium by Hall Effect Analysis. Interim Technical Report, OCT 82 through Oct 83 (AFWAL-TR-83-4158), Laser and Optical Materials Branch, Electromagnetic Materials Division, Materials Laboratory, Air Force Wright Aeronautical Laboratories (AFSC), Wright Patterson AFB.
8. Grove, A. S. Physics and Technology of Semiconductor Devices. New York: John Wiley and Sons, 1967.
9. Hemenger, P. M. "Measurement of High Resistivity Semiconductors Using the van der Pauw Method," Review of Scientific Instruments, Vol. 44, No. 6: 698-706 (June 1973).
10. Huber, Diethard and Joeseeph Reffle. "Precipitation Process Design for Denuded Zone Formation in CZ-Silicon Wafers," Solid State Technology, Vol. 26(8): 137-143 (August 1983).

11. Huff, Howard R. "Chemical Impurities and Structural Imperfections in Semiconductor Silicon, Part I," Solid State Technology: 89-95 (February 1983).
12. Huff, Howard R. "Chemical Impurities and Structural Imperfections in Semiconductor Silicon, Part II," Solid State Technology: 211- 222 (April 1983).
13. Imai, Matsato and Koji Sumino. "In-situ X-Ray Topographic Study of the Dislocation Mobility in High-Purity and Impurity-doped Silicon Crystals," Philosophical Magazine A, Vol. 47, No. 4: 599-621 (1983).
14. Irvin, John C. "Resistivity of Bulk Silicon and of Diffused Layers in Silicon," The Bell System Technical Journal, Vol. XLI (41), No. 2: 387-410 (March 1962).
15. Kaiser, W. and C. D. Thurmond. "Nitrogen in Silicon," Journal of Applied Physics, Vol. 30, No. 3: 427-431 (March 1959).
16. Kane, Phillip F. and Graydon B. Larrabee. Characterization of Semiconductor Materials. New York: McGraw- Hill Book Company, 1970.
17. Kramer, Horst G. "Float-Zoning of Semiconductor Silicon: A Perspective," Solid State Technology: 137-142 (January 1983).
18. Lang, Joseph E., Physicist. Private communication. University of Dayton Research Institute, Dayton, OH, July 1984.
19. Lang, J. and P. M. Hemenger. Computer Assisted Analysis of Electronic Transport Data. Version 12 of unpublished technical report (June 1984).
20. Madarasz, Frank L., Joseph E. Lang, and Patrick M. Hemenger. "Effective Masses for Nonparabolic Bands in P-type Silicon," Journal of Applied Physics, Vol. 52, No. 7: 4646-4648 (July 1981).
21. McKelvey, John P. Solid State and Semiconductor Physics. New York: Harper and Row, 1966.
22. Meese, J. M., D. L. Cowen, and M. Chandrasekhar. "A Review of Transmutation Doping in Silicon," IEEE Transactions on Nuclear Science, Vol. N5-26, No. 6 (December 1979).
23. Mitchel, W. C., Physicist. Private Communication. Laser and Optical Materials Branch, Electromagnetic Division, Materials Laboratory, Air Force Wright Aeronautical Laboratories, Wright-Patterson AFB, OH, June through October 1984.

24. Mitchell, J. B., P. P. Pronko, J. Shewchun, and D. A. Thompson. "Nitrogen-implanted Silicon. I. Damage Annealing and Lattice," Journal of Applied Physics, Vol. 46, No. 1: 332-334 (January 1975).
25. Mitchell, J. B., J. Shewchun, and D. A. Thompson. "Nitrogen-implanted Silicon. II. Electrical Properties," Journal of Applied Physics, Vol. 46, No. 1: 335-343 (January 1975).
26. Ohmer, Melvin C. "Visits to Semiconductor Materials Research Groups in Japan, the 1982 Symposium on VLSI Technology, and the International Conference on Solid State Devices," Scientific Bulletin Department of the Navy Office of Naval Research Far East, Vol. 8 No. 2 (NAVSO P-3580): 64-66 (reprint April to June 1983).
27. Putley, E. H. The Hall Effect and Semiconductor Physics. London: Dover Publications, 1960.
28. Schwuttke, G.H. "Crystal Defect Problems," Sixteenth IEEE Photovoltaic Conference - 1982: 327-331. Institute of Electrical and Electronics Engineers, Piscataway, NJ (1982).
29. Smith, Robert Allen. Semiconductors. Great Britain: Cambridge University Press, 1978.
30. Sumino, Koji, Hirofumi Harada, and Ichiro Yonenaga. "The Origin and the Difference in the Mechanical Strengths of Czochralski Grown Silicon and Float Zone Grown Silicon," Japanese Journal of Applied Physics, Vol. 19, No. 1: L49-L52 (January 1980).
31. Sumino, Koji. "Interaction of Dislocations with Impurities and its Influence on the Mechanical Properties of Silicon Crystals," Defects in Semiconductor Silicon, II, Materials Research Society Symposium Proceedings, Vol. 14 (Boston, MA, Nov 82): 307-321. Elsevier Science Publishing Co., Inc. (1983).
32. Sumino, Koji, Ichiro Yonenaga, Masato Imai, and Takao Abe. "Effects of Nitrogen on Dislocation Behavior and Mechanical Strength in Silicon Crystals," Japanese Journal of Applied Physics, Vol. 54, No. 9: 5016-5020 (September 1983).
33. Sumino, Koji and Masato Imai. "Interaction of Dislocations with Impurities in Silicon Crystals Studied by In-situ X-Ray Topography," Philosophical Magazine A, Vol. 47, No. 5: 753-766 (1983).
34. Swaroop, Robert B. "Advances in Silicon Technology for the Semiconductor Industry, Part I," Solid State Technology: 111-114 (June 1983).

35. Swaroop, Robert B. "Advances in Silicon Technology for the Semiconductor Industry, Part II," Solid State Technology: 97-101 (July 83).
36. Swenson, Capt Orven F. Luminescence and Electrical Characterization of Ion Implanted Si:Ti. PHD Dissertation, AFIT/DS/PH/82-1 School of Engineering, Air Force Institute of Technology (AU), Wright-Patterson AFB, June 1982.
37. Sze, S. M. Physics of Semiconductor Devices (Second Edition). New York: John Wiley and Sons, 1981.
38. Tajima, M., T. Masui, T. Abe, and N. Tadashi. "Photoluminescence Associated with Nitrogen in Silicon," Japanese Journal of Applied Physics, Vol. 20 (6): L423-L425 (June 1981).
39. Tajima, M. "(Invited) Recent Advances in Photoluminescence Analysis of Si: Application to an Epitaxial Layer and Nitrogen in Si," Japanese Journal of Applied Physics, Vol. 21, Supplement 21-1: 113-119 (1982).
40. Tokamaru, Yozo, Hideyo Okushi, Tsumoru Masui, and Takao Abe. "Deep Levels Associated with Nitrogen in Silicon," Japanese Journal of Applied Physics, Vol. 21 (7): L443 - L444 (July 1984).
41. van der Pauw, L. J. "A Method of Measuring the Specific Resistivity and Hall Effect of Discs of Arbitrary Shape," Philips Research Reports, Vol. 13, No. 1: 1-9 (September 1957).
42. van der Pauw, L. J. "A Method of Measuring the Resistivity and Hall Coefficient on Lamellae of Arbitrary Shape," Philips Technical Review, Vol. 20: 220-24 (1958).
43. Yatsurugi, N., N. Akiyama, Y. Endo and T. Nozaki. "Concentration, Solubility, and Equilibrium Distribution of Nitrogen and Oxygen in Semiconductor Silicon," Journal of the Electrochemical Society, Vol. 120 (7): 975-979 (July 1973).
44. Zorin, E. I., P. V. Pavlov, and D. I. Tetel'baum. "Donor Properties of Nitrogen in Silicon," Soviet Physics - Semiconductors, Vol. 2, No. 1: 111-113 (July 1968).

Vita

Mary Anne O'Leary was born on 10 JAN 47 in Saint Louis, Missouri, the daughter of John E. and Anne L. Flavin. She graduated from Horton Watkins High School in Ladue, MO in 1965. In Jan 1970, she graduated from the University of Illinois with a Bachelor of Fine Arts in Industrial Design. She held a variety of positions including Product Designer at Manning-Bowman Div. of the McGraw-Edison Co. She enlisted in the Air Force in Jun 1973. She was assigned the Instrumentation Technican Training School at Lowery AFB, CO where she was in the first class to included women. After graduation, she was assigned to Air Force Geophysics Laboratory at Hanscom AFB, MA. She entered the Airman Education and Commissioning Program in August 1977. She graduated magna cum laude with a Bachelor of Science in Electrical Engineering from the University of Lowell, Lowell, MA in May 1980. Upon commissioning after OTS (9 SEP 80), she was assigned to Aeronautical System Division, Wright-Patterson AFB, OH where she served as Visual Systems Engineer in the Simulator Division, Equipment Engineering Directorate. She entered the AFIT Graduate Electrical Engineering Program in May 1983.

Permanent Address: 13 Quailways Dr.

St. Louis, MO. 63141

REPORT DOCUMENTATION PAGE

REPORT SECURITY CLASSIFICATION <b>UNCLASSIFIED</b>		1b. RESTRICTIVE MARKINGS	
2a. SECURITY CLASSIFICATION AUTHORITY		3. DISTRIBUTION/AVAILABILITY OF REPORT Approved for public release; distribution unlimited	
2b. DECLASSIFICATION/DOWNGRADING SCHEDULE			
4. PERFORMING ORGANIZATION REPORT NUMBER(S) <b>AFIT/GE/ENG/85M-3</b>		5. MONITORING ORGANIZATION REPORT NUMBER(S)	
6a. NAME OF PERFORMING ORGANIZATION <b>School of Engineering</b>	6b. OFFICE SYMBOL (If applicable) <b>AFIT/ENG</b>	7a. NAME OF MONITORING ORGANIZATION	
6c. ADDRESS (City, State and ZIP Code) <b>Air Force Institute of Technology Wright-Patterson AFB, OH 45433</b>		7b. ADDRESS (City, State and ZIP Code)	
8a. NAME OF FUNDING/SPONSORING ORGANIZATION <b>Laser/Optical Materials Branch</b>	8b. OFFICE SYMBOL (If applicable) <b>AFWAL/MLPO</b>	9. PROCUREMENT INSTRUMENT IDENTIFICATION NUMBER	
8c. ADDRESS (City, State and ZIP Code) <b>Electromagnetic Division Materials Laboratory Wright-Patterson AFB, OH 45433</b>		10. SOURCE OF FUNDING NOS.	
		PROGRAM ELEMENT NO.	PROJECT NO.
11. TITLE (Include Security Classification) <b>See Box 19</b>		12. PERSONAL AUTHOR(S) <b>Mary A. O'Leary, Captain, USAF</b>	
12a. TYPE OF REPORT <b>MS Thesis</b>	13b. TIME COVERED FROM _____ TO _____	14. DATE OF REPORT (Yr., Mo., Day) <b>1985 March</b>	15. PAGE COUNT <b>139</b>
16. SUPPLEMENTARY NOTATION			
17. COSATI CODES		18. SUBJECT TERMS (Continue on reverse if necessary and identify by block number) <b>SILICON, NITROGEN, ELECTRICAL PROPERTIES HALL EFFECT</b>	
FIELD	GROUP		
<b>20</b>	<b>02</b>		
19. ABSTRACT (Continue on reverse if necessary and identify by block number)  Title: <b>ELECTRICAL PROPERTIES OF BULK GROWN NITROGEN DOPED SILICON</b>  Thesis Chairman: <b>Donald R. Kitchen, Captain, USAF</b>  <div style="text-align: right;">Approved for public release: IAW AFR 190-17. <i>Lynn E. Wolaver</i> 1 May 85 LYNN E. WOLAVER Edn for Research and Professional Development Air Force Institute of Technology (AIC) Wright-Patterson AFB OH 45433</div>			
20. DISTRIBUTION/AVAILABILITY OF ABSTRACT <input type="checkbox"/> UNCLASSIFIED/UNLIMITED <input type="checkbox"/> SAME AS RPT. <input type="checkbox"/> DTIC USERS <input type="checkbox"/>		21. ABSTRACT SECURITY CLASSIFICATION <b>UNCLASSIFIED</b>	
22a. NAME OF RESPONSIBLE INDIVIDUAL <b>Donald R. Kitchen, Captain, USAF</b>		22b. TELEPHONE NUMBER (Include Area Code) <b>(513)255-4960</b>	22c. OFFICE SYMBOL <b>AFIT/ENG</b>



ABSTRACT

The electrical parameters of a boule of nitrogen doped float zone silicon were studied by Hall effect analysis. Samples were annealed at temperatures ranging from 800 to 900 °C. In addition, a section of this boule was neutron transmuted (NTD) to increase the n-type doping. Samples from the NTD section were annealed at 800 °C.

Resistivity and mobility varied considerably from sample to sample, but the variation is not a function of annealing temperature. The annealed Si:N samples were found to be inhomogeneous; however, the Si:N NTD samples were homogeneous. In addition, annealing activated deep energy levels. The shallow energy levels reported in studies on ion implanted nitrogen in silicon were not found. The only shallow energy level found was phosphorus.

The conclusion is nitrogen does not go into substitutional sites in silicon to any great extent. Although what happens to nitrogen in silicon is unknown it is suggested that nitrogen may form silicon-nitride complexes and precipitates. This could be the mechanism for strengthening the lattice.

**END**

**FILMED**

**7-85**

**DTIC**